

©2014

Shuliang Zhang

ALL RIGHTS RESERVED

COMBUSTION CHARACTERIZATION AND KINETIC MODELING IN  
REACTIVE FLOW SIMULATIONS

by

SHULIANG ZHANG

A Dissertation submitted to the  
Graduate School-New Brunswick  
Rutgers, The State University of New Jersey

In partial fulfillment of the requirements

For the degree of

Doctor of Philosophy

Graduate Program in Chemical & Biochemical Engineering

Written under the direction of

Marianthi G. Ierapetritou, Ph.D.

Ioannis P. Androulakis, Ph.D.

And approved by

---

---

---

---

New Brunswick, New Jersey

MAY, 2014

**ABSTRACT OF THE DISSERTATION**  
**COMBUSTION CHARACTERIZATION AND KINETIC MODELING IN**  
**REACTIVE FLOW SIMULATIONS**

By SHULIANG ZHANG

Dissertation Directors:

Marianthi G. Ierapetritou, PhD

Ioannis P. Androulakis, PhD

The primary objective of this research is to characterize fuel combustion in reactive flow simulations using advanced kinetic modeling and mechanism reduction tools. Since incorporating detailed chemical kinetic model in the realistic reactive flow simulations is a computationally challenging task due to the large size of detailed kinetic mechanism, it is of great interest to develop approaches for simplifying the kinetic models and reducing computational costs in reactive flow simulations. In this dissertation, we first extend the previously developed on-the-fly reduction approach to the characterization of complex biodiesel combustion using detailed biodiesel surrogate mechanism. Major combustion characteristics such as ignition, emission, as well as engine performance for biodiesel compared with conventional fossil fuels are studied. Although the incorporation of detailed biodiesel combustion mechanism in complex reactive flow simulation is enabled,

the simulation is still highly time-consuming. To further alleviate the computational intensity, a hybrid reduction scheme coupling the on-the-fly reduction with global quasi-steady-state approximation (QSSA) is developed. The proposed hybrid reduction scheme is demonstrated in various reactive flow simulations including zero-dimensional PFR model, multidimensional HCCI engine CFD model, and realistic gas phase injector CFD simulations. A flux-based quasi-steady-state (QSS) species selection procedure is introduced to facilitate the demonstration of hybrid scheme. Finally, a novel computational framework integrating automated mechanism generation and on-the-fly reduction is proposed and implemented using a stepwise integration. The proposed framework is then demonstrated in methane oxidation case studies and shows a new way of conducting reactive flow simulation without having an actual mechanism before the simulation starts. The integration of automated mechanism generation and on-the-fly reduction is a promising technique to perform reactive flow simulations and has the potential to reduce the computational cost of the simulations. The work in this dissertation provides powerful tools and important insight for the incorporation of detailed chemical kinetics in the reactive flow simulations.

## **ACKNOWLEDGEMENTS**

First of all, I would like to gratefully acknowledge my advisors, Prof. Marianthi G. Ierapetritou and Prof. Ioannis P. Androulakis, for their strict supervision, insightful advice, kindly encouragement, and endless support during my Ph.D. study. They not only teach me necessary knowledge and skills for academic research, but, more importantly, also train me how to think of problems and how to ask meaningful questions instead of just answer them. They educate me to realize that “research is an active process and to a great extent requires your own self-calibration and the challenge is to figure out what we are asking”. I have learned a lot from them which I believe will always benefit my future career. I would like to express my deepest appreciation to them.

I would like to thank my research collaborators Dr. Andrea Zambon at Combustion Research and Flow Technology, Inc. for the considerable time and work devoted in this dissertation, as well as Prof. Linda J. Broadbelt and Dr. Chun-Yi Sung at Northwestern University for sharing the NetGen package and discussing all the technical details. Further, I would like to thank Dr. John T. Farrell at ExxonMobil, Prof. Nina Shapley, and Prof. Stephen D. Tse for being my committee members and providing insightful suggestions on my work.

I would like to acknowledge the funding sources which supported me throughout my graduate research career here at Rutgers. This work is financially supported by the NSF CBET Grant No. 0730582 and ONR Contract N0014-10-10440.

I would like to thank the Ierapetritou group and the Androulakis group for working together with all the help, support, and friendship throughout these unforgettable years. I would like to thank all my friends for bringing me laughter and joy during these years.

I also would like to thank my parents, parents-in-law, and all the families and friends in China for the support and care from thousands of miles away.

Finally, I would like to dedicate this dissertation to my incredible wife Chen Chen, whose love, company, support, and encouragement have made this work possible. This work is also dedicated to our newborn baby girl Carrie, who brings us so much fun and hope.

## Table of contents

ABSTRACT OF THE DISSERTATION .....	ii
ACKNOWLEDGEMENTS .....	iv
List of tables.....	viii
List of illustrations .....	ix
Chapter 1 Introduction.....	1
1.1 Kinetic model development for hydrocarbon and biodiesel combustion.....	1
1.2 Incorporation of detailed chemistry in reactive flow simulations.....	3
1.3 Element flux analysis and on-the-fly reduction .....	6
1.4 Automated mechanism generation .....	8
1.5 Motivation and outline of the dissertation.....	9
Chapter 2 Biodiesel combustion characterization using element flux analysis.....	12
2.1 Computational framework .....	12
2.2 Validation of the computational framework .....	15
2.3 Combustion characteristics and fuel comparison in HCCI engine simulations .....	20
2.4 Summary .....	29
Chapter 3 Development of the hybrid reduction scheme .....	31
3.1 Quasi-steady-state approximation.....	31
3.2 Hybrid scheme based on on-the-fly reduction and global QSSA .....	32
3.3 Demonstration of the proposed hybrid scheme.....	37

3.4 Summary .....	56
Chapter 4 Hybrid reduction scheme with flux-based QSS species selection .....	57
4.1 Selection of quasi-state-state species based on element flux .....	57
4.2 Demonstration of hybrid scheme with flux-based QSS species selection .....	59
4.3 Computational cost evaluation of hybrid reduction scheme .....	70
4.4 Summary .....	74
Chapter 5 Integration of mechanism generation and reduction.....	76
5.1 Integration of mechanism reduction during mechanism generation .....	76
5.2 Stepwise integration of mechanism generation and reduction.....	77
5.3 Case studies of the stepwise implementation.....	79
5.4 Summary .....	86
Chapter 6 Conclusions and future perspectives.....	87
6.1 Conclusions .....	87
6.2 Suggestions for future work .....	89
Bibliography .....	91

## List of tables

Table 2.1 Engine operation conditions and parameters .....	15
Table 3.1 List of the QSS species selections obtained by Montgomery et al. (2006) for methane mechanism GRI-Mech 3.0 .....	38
Table 3.2 Engine specifications and operation parameters used in KIVA .....	46
Table 4.1 QSS species selections for GRI-Mech 3.0 mechanism.....	61
Table 4.2 Selected QSS species for n-heptane mechanism at two different temperatures	67
Table 4.3 Summary of CPU time for 50 iterations in CRUNCH CFD simulations .....	73
Table 4.4 Summary of CPU time in KIVA CFD simulations for n-heptane oxidation....	73

## List of illustrations

Figure 2.1 Two-dimensional computational mesh used in KIVA engine simulations .....	13
Figure 2.2 Computational procedures integrating on-the-fly reduction in KIVA-3V .....	14
Figure 2.3 Ignition delay time validation for methyl decanoate and methyl-9-decenoate in PFR simulations. Shock tube ignition data is obtained from Herbinet et al. (2008) .....	16
Figure 2.4 Temperature and selected species profiles in KIVA simulations with methyl butanoate .....	17
Figure 2.5 Simulation time reduction for different fuels (upper figure) and mechanism reduction for methyl-9-decenoate (lower figure).....	19
Figure 2.6 Ignition timing for different fuels in HCCI engine simulations .....	21
Figure 2.7 Early formation of CO and CO <sub>2</sub> for biodiesel fuels compared with n-heptane	22
Figure 2.8 CO emissions for different fuels at different engine speeds.....	24
Figure 2.9 NO emissions for different fuels at different engine speeds .....	24
Figure 2.10 Total heat release for different fuels at different engine speeds.....	26
Figure 2.11 Work done per cycle and power output for different fuels at different engine speeds .....	27
Figure 3.1 Schematic illustration for the integration of on-the-fly reduction with QSSA	34
Figure 3.2 Summary of the steps in the hybrid reduction algorithm .....	36
Figure 3.3 Reproduced species mole fractions for different QSS species selections in PRF isothermal runs. Temperature at 1650 K and equivalence ratio 1.0. ....	39
Figure 3.4 Temperature profiles obtained by applying QSSA with different QSS species selections. Initial temperature at 1000 K and pressure at 9.6 atm, equivalence ratio is 0.5 .....	40

Figure 3.5 Species mass fractions profiles obtained in the PFR simulations with different QSS species selections. Initial temperature at 1000 K and pressure at 9.6 atm, equivalence ratio is 0.5. ....	42
Figure 3.6 Temperature profiles obtained in adiabatic PFR model with different QSS species selections. Initial temperature at 1000 K and pressure at 9.6 atm, equivalence ratio is 0.5.....	44
Figure 3.7 Ignition delay timing predicted in PFR with different QSS species selections. Initial temperature from 950 K to 1350 K, pressure at 9.6 atm (left) and 30.0 atm (right) .....	45
Figure 3.8 Temperature and pressure profiles obtained in KIVA engine simulations with 1, 7, 12, and 17 QSS species.....	48
Figure 3.9 Selected species composition profiles obtained in KIVA engine simulations with 1, 7, 12, and 17 QSS species.....	49
Figure 3.10 Number of active C-bearing and N-bearing non-QSS species identified during KIVA-3V engine simulations.....	51
Figure 3.11 Improvement of NO and NO <sub>2</sub> species concentration profiles by increasing cutoff value from 99% to 99.99% .....	51
Figure 3.12 Number of nitrogen-bearing species during the simulations with higher nitrogen flux cutoff 99.99% .....	52
Figure 3.13 Comparison of the QSSA assumption of species in nitrogen reaction network .....	53
Figure 3.14 CPU time of the hybrid reduction simulations in KIVA-3V.....	54
Figure 4.1 Maximum net flux for species.....	60

Figure 4.2 PFR simulation with application of QSSA.....	62
Figure 4.3 Net production rate with detailed mechanism for selected QSS species.....	63
Figure 4.4 Temperature and pressure profiles obtained in KIVA with application of QSSA .....	64
Figure 4.5 Temperature and pressure profiles obtained in KIVA with hybrid reduction.	65
Figure 4.6 Maximum net carbon flux for species at two different initial temperatures ...	66
Figure 4.7 Simulation results in KIVA with application of QSSA at two initial temperatures .....	68
Figure 4.8 Simulation results in KIVA with hybrid reduction at two initial temperatures .....	69
Figure 4.9 Simulation results of the generic CH <sub>4</sub> /LOX injector simulated in CRUNCH CFD with hybrid reduction scheme .....	70
Figure 4.10 Temperature at the last iteration step for different QSS species cases.....	71
Figure 5.1 A schematic illustration of the stepwise implementation of the integration of mechanism generation and reduction.....	78
Figure 5.2 Schematic illustration of two-step integration.....	80
Figure 5.3 Species concentration profiles obtained in the two-step integration.....	81
Figure 5.4 Mechanism size and reduced number of species in the two-step integration..	81
Figure 5.5 Species concentration profiles obtained in the 12-step integration.....	82
Figure 5.6 Mechanism size and reduced number of species in the 12-step integration....	83
Figure 5.7 Temperature and species concentration profiles obtained in the 13-step integration with adiabatic PFR simulation.....	84
Figure 5.8 Mechanism size evolution in the 13-step integration .....	85

## Chapter 1

### Introduction

#### 1.1 Kinetic model development for hydrocarbon and biodiesel combustion

In the background of growing global energy demands and stringent environmental regulations, combustion research and development are playing significant roles in improving the utilization of existing energy resources as well as exploring the applicability of potential alternative fuels. In combustion research, detailed chemical kinetics describing the elementary steps of the combustion reactions is essential. However, combustion kinetics for most fuels is still not fully understood since some of the detailed and transient information in the combustion process is not easily captured through experiments. In recent years, with the rapid advancement of computational capacity, kinetic modeling and reactive flow simulation have become important tools to investigate the details and fundamentals of fuel combustion process. In the computational combustion studies, establishing accurate and comprehensive combustion kinetic models for different types of fuels is essential in order to better explore the underlying details and characteristics of combustion process. In the past few decades, great efforts have been made to develop comprehensive kinetic models for various fuel combustion systems (Lai et al., 2011; Pitz and Mueller, 2011).

Detailed reaction mechanisms for a wide variety of hydrocarbon fuels have been developed. For methane oxidation, mechanisms such as GRI-Mech 3.0 (Smith et al.) and Leeds Methane Mechanism (Hughes et al., 2001) have been developed and well validated against experiment data. For more complex hydrocarbons, detailed mechanisms have

been developed for C1-C4 alkanes (Marinov et al., 1998), n-pentane (Curran et al., 1998), n-heptane (Curran et al., 1998), iso-octane (Curran et al., 1998), primary reference fuels (PRF) (Curran et al., 2002), and C8-C16 n-alkanes (Westbrook et al., 2009), etc. These mechanisms have been applied as surrogate mechanisms for gasoline and diesel fuel combustion. The size of these detailed mechanisms ranges from hundreds to over a thousand species and several thousands of reactions.

At the meantime, with continuously increasing production each year, biodiesel has been the focus in many combustion studies. The efforts towards understanding the combustion kinetics and performance of biodiesel largely rely on the development of detailed biodiesel combustion mechanism. Biodiesel is usually derived from various bio-renewable feedstock, making it promising as an ideal sustainable source of energy. Biodiesel is a complex mixture of monoalkyl esters of long-chain fatty acids derived from a variety of bio-renewable sources like vegetable oils and animal fats (Um and Park, 2010b). The most commonly used biodiesel fuels, derived from soybean or rapeseed oil, are mainly composed of five methyl esters including methyl palmitate ( $C_{17}H_{34}O_2$ ), methyl stearate ( $C_{19}H_{38}O_2$ ), methyl oleate ( $C_{19}H_{36}O_2$ ), methyl linoleate ( $C_{19}H_{34}O_2$ ), and methyl linolenate ( $C_{19}H_{32}O_2$ ) (Herbinet et al., 2010). These components have similar structures of a methyl ester group attached to a long saturate or unsaturated hydrocarbon chain. The oxygen content in biodiesel could change the combustion features and also contribute to a smaller heating value compared to conventional diesel. Also, different physical properties (such as viscosity and volatility) of biodiesel also lead to different fuel spray and mixing process. (Pitz and Mueller, 2011; Zhu et al., 2011) Therefore, biodiesel combustion has different characteristics compared with the combustion of conventional diesel fuels.

In the past few years, chemical kinetic models for various biodiesel surrogates have been developed (Lai et al., 2011; Tran et al., 2012) to facilitate computational study of biodiesel combustion. The first methyl ester kinetic model, proposed by Fisher et al. (2000) is methyl butanoate (MB,  $C_5H_{10}O_2$ ), which is relatively small in size compared to the realistic biodiesel components. Um and Park (2010a) have used this mechanism to study the combustion and emission characteristics in HCCI engine simulations. In recent years, detailed kinetic mechanisms for more complex biodiesel surrogates, such as methyl decanoate (MD,  $C_{11}H_{22}O_2$ ), methyl-5-decenoate (MD5D,  $C_{11}H_{20}O_2$ ), and methyl-9-decenoate (MD9D,  $C_{11}H_{20}O_2$ ) have been developed (Herbinet et al., 2008, 2010). These large mechanisms are considered to be better surrogate mechanisms for biodiesel combustion. Most recently, kinetic models for real biodiesel components such as methyl stearate and methyl oleate have also been reported (Naik C., 2010). These kinetic modeling efforts have made possible the detailed characterization of biodiesel combustion.

## 1.2 Incorporation of detailed chemistry in reactive flow simulations

Although the comprehensive kinetic mechanisms provide us as much as possible information needed to characterize the details of fuel combustion process, the incorporation of these detailed mechanisms in the reactive flow simulations is usually prohibitive due to the large number of species and reactions in the mechanism. For instance, the detailed mechanism for biodiesel surrogate methyl decanoate ( $C_{11}H_{22}O_2$ ) mentioned above consists of 2,878 species and 8,555 reactions (Herbinet et al., 2008), and the detailed mechanism for fuel blends of methyl decanoate, methyl decenoate, and

n-heptane has 3,299 species and 10,806 reactions (Herbinet et al., 2010). Incorporating these large detailed mechanisms in the reactive flow simulations, especially complex computational fluid dynamics (CFD) calculations, is usually infeasible in practice due to extremely long CPU time needed to solve the large number of chemical kinetic ODEs. In addition, loops over large number of computational mesh points or cells in the multidimensional CFD calculation render the computation even more expensive.

To alleviate the computational intensity in the combustion simulations, various kinetic mechanism reduction approaches have been developed during the past few decades (Lu and Law, 2009). The first category of mechanism reduction approaches is global reduction aiming to develop skeletal mechanisms that will be used throughout the entire simulation tasks. Sensitivity analysis (Rabitz et al., 1983; Turanyi T., 1990), lumping methods (Wei and Kuo, 1969), optimization based methods (Androulakis, 2000; Bhattacharjee et al., 2003; Perini et al., 2012), time-integrated flux analysis (Androulakis et al., 2004), and path flux analysis (PFA) method (Sun et al., 2010) belong to this category. In recent years, the directed relation graph (DRG) method (Lu and Law, 2005) is developed based on the rate of production analysis and species dependence. And a series of methods based on DRG are then proposed to improve or extend the applicability of DRG approach, such as DRG with error propagation (DRGEP) (Pepiot-Desjardins and Pitsch, 2008), DRG-aided sensitivity analysis (DRGASA) (Zheng et al., 2007), and DRGEP with sensitivity analysis (DRGEP-SA) (I. Zsély, 2009; Niemeyer et al., 2010). These DRG-based approaches are able to generate skeletal kinetic models with high efficiency and satisfactory performance. However, the skeletal mechanism is only valid for the range of conditions under which it is developed, thus may not always be

appropriate (could be either inadequate or redundant) for the different reaction conditions that the simulations are undergoing. In addition, the simulation error minimization (SEM) approach (Nagy and Turányi, 2009; Zsély et al., 2011) is developed based on the SEM connectivity method (SEM-CM), but it requires a simulation with detailed mechanism. Another category is adaptive approaches, such as *in situ* adaptive tabulations (ISAT) (Pope, 1997), mathematical programming approaches (Banerjee and Ierapetritou, 2006), and flux-graph-based adaptive reduction (He et al., 2008). Unlike the global approaches, the adaptive approaches develop a library of reduced mechanisms by taking into account different ranges of conditions, and choose from the library an appropriate reduced mechanism according to the specific local condition at particular time point during the simulation. However, the adaptive approaches require prior analysis and calculations of the system to generate the library of reduced mechanisms, and need certain searching algorithms to select reduced mechanisms from the library. To overcome these issues, some dynamic reduction strategies are developed based on various criteria. The dynamic adaptive chemistry (DAC) method (Liang et al., 2009a; Liang et al., 2009b) derives a dynamically reduced mechanism for the specific local and instantaneous conditions using DRGEP-based criteria. The transport-flux-based DRG method (Tosatto et al., 2011) is developed by using transport flux to replace original DRG criteria and by operating the algorithm on a cell-by-cell basis. The DAC reduction is also coupled with ISAT to develop the tabulation of dynamic adaptive chemistry (TDAC) method (Contino et al., 2011) to further reduce the computational cost. Most recently, a new error controlled dynamic adaptive chemistry (EC-DAC) method (Gou et al., 2013) is developed to generate reduced mechanisms dynamically with a specified error bound using the path

flux analysis (PFA) method. These dynamic methods identify different reduced mechanisms according to the specific conditions at different time steps and different geometric locations within the computational domain.

The mechanism reduction approaches provide tools for simplify the kinetic mechanism and reduce computational costs when incorporating detailed kinetic models in the reactive flow simulations.

### 1.3 Element flux analysis and on-the-fly reduction

In our previous work, an on-the-fly reduction approach based on the element flux analysis was developed. The concept of element flux was first proposed by Revel et al. (Revel J., 1994). According to the definition in their study, the instantaneous element flux of atom  $A$  from species  $j$  to species  $k$  through reaction  $i$  is defined as  $\dot{A}_{ijk}$  by Eq. (1). The total instantaneous flux from species  $j$  to species  $k$  through all the reactions involving these species is given by Eq. (2).

$$\dot{A}_{ijk}(t) = q_i(t) \frac{n_{A,j} n_{A,k}}{N_{A,i}} \quad (1)$$

$$\bar{A}_{jk}(t) = \sum_{i=1}^{N_R} \dot{A}_{ijk}(t) \quad (2)$$

where  $q_i(t)$  is the instantaneous rate of reaction  $i$  (mol/s),  $n_{A,j}$  and  $n_{A,k}$  are the number of atoms  $A$  in species  $j$  and  $k$ , respectively,  $N_{A,i}$  is the total number of atoms  $A$  in reaction  $i$ , and  $N_R$  is the number of reactions in which species  $j$  and  $k$  participate as reactant or products. The time-integrated element flux, as defined by Eq. (3), was then implemented

in the mechanism reduction and pathway analysis applications by Androulakis et al. (Androulakis et al., 2004).

$$\hat{A}_{jk} = \frac{\int_{t=0}^{\tau} \bar{A}_{jk}(t) dt}{\sum_{j'} \sum_{k'} \int_{t=0}^{\tau} \bar{A}_{j'k'}(t) dt} \quad (3)$$

The mechanism reduction is done by sorting the time-integrated flux for all the source-sink pairs and applying a user defined cutoff to identify active species and reactions. The time-integrated element flux analysis removes the time dependence of element flux and provides a “global” insight and macroscopic view of reaction pathways. It also provides a powerful method to develop a skeletal mechanism based on the chemical kinetic characteristics.

The idea of element flux analysis was later implemented to develop an on-the-fly reduction scheme (He et al., 2010b) for the dynamic identification of active species and reactions during reactive flow simulations. Instead of time-integrated element flux, the total instantaneous flux defined in Eq. (2) is evaluated at every time step of the simulation based on the particular conditions at that time point. As an improvement, the total instantaneous flux is modified as in Eq. (4) to include both forward and reverse reaction rates instead of the net reaction rates.

$$\dot{A}_{ijk}(t) = (|q_{ifwd}(t)| + |q_{irev}(t)|) \frac{n_{A,j} n_{A,k}}{N_{A,i}} \quad (4)$$

where  $q_{ifwd}(t)$  and  $q_{irev}(t)$  are the reaction rates of forward and reverse reactions, respectively. The reason of such modification is that the net reaction rates of partial-equilibrium reactions are much smaller compared with the forward and reverse reaction rates, so that the element flux computed by Eq. (2) is relatively small although fast

chemical transition is occurring between the species in both directions. The modified flux could avoid inappropriate representation of element transition involving quasi-steady-state species in partial-equilibrium reactions.

In the on-the-fly reduction scheme, at every simulation time step, the total instantaneous flux for all the possible source-sink pairs in the mechanism is computed and sorted in a descending order. And a user defined cutoff is applied to identify active species and reactions specifically for the current time point. Only the active species and reactions are integrated in the ODE solver while the inactive species concentrations are kept unchanged for the current step. As the system evolves into the next time step, the instantaneous flux analysis is repeated based on the new conditions and the set of active species and reactions is updated. The on-the-fly reduction approach requires no *a priori* analysis or calculation of the system. It derives locally accurate reduced mechanisms to minimize the redundancy in the mechanism at every time instance during the simulation, which greatly reduces the computational costs by limiting the number of differential equations to integrate at each time step. The proposed on-the-fly reduction scheme has been applied in both zero-dimensional reactor model and multidimensional computational fluid dynamics (CFD) calculations with high efficiency and fidelity (He et al., 2009a, 2010a; He et al., 2009b; He et al., 2012). The on-the-fly reduction framework in our previous study established important foundation of this work.

#### 1.4 Automated mechanism generation

Computational automation approaches for the construction of chemical kinetic models has been studied extensively in the literature (Broadbelt et al., 1994, 1995; Broadbelt et

al., 1996; De Witt et al., 2000; Di Maio and Lignola, 1992; Grenda et al., 2003; Prickett and Mavrovouniotis, 1997a, b, c; Susnow et al., 1997; Van Geem et al., 2006). Automated mechanism generation software usually starts the reaction network construction with some initial reactants and conditions, and then automatically generates the reaction mechanism based on some pre-defined reaction templates. The software should also be able to generate all the necessary thermodynamic data for species and kinetic parameters for reactions. And finally the generation process is terminated under some stopping rules. However, the computational cost of automated mechanism generation can be tremendous due to large and complex reactant structure, large number of possible reactions, and required accuracy of the estimation of thermodynamic properties and rate constants. Therefore, the ability to reduce the size and scale of the generated mechanisms is usually preferred in the computer construction of reaction mechanisms (Klinke and Broadbelt, 1997). To limit the size of generated mechanisms, the rate-based mechanism generation scheme (Susnow et al., 1997) was developed to evaluate reactions rates and identify the kinetically significant species and reactions when constructing the reaction network automatically. The reduction of generated mechanisms based on flux analysis was also explored previously by combining the element flux analysis with the automated mechanism generation process (Androulakis et al., 2004).

## 1.5 Motivation and outline of the dissertation

As we have mentioned above, one of the biggest challenges in computational combustion research is the considerable computational intensity when incorporating detailed mechanisms in reactive flow or CFD calculations due to large mechanism size as well as

large number of computational cells. On the other hand, although we are able to reduce the mechanism size for the chemistry calculation, all the species are still involved in the transport calculation. In some realistic reacting flow scenarios, transporting large number of species will usually lead to prohibitive computational intensity. Therefore, the primary objective of this work is to develop advanced mechanism reduction techniques to tackle the above challenges, and apply the developed computational tools for the characterization of complex fuel combustion process with satisfactory accuracy and efficiency.

In this dissertation, we first extend the previous developed on-the-fly reduction approach to address the combustion characteristics, pollutant emission, and engine performance for biodiesel compared to the conventional fossil fuels. The large detailed mechanisms for various biodiesel surrogates are incorporated in the multidimensional engine CFD simulations using the dynamic element flux analysis and on-the-fly reduction framework. The results and discussion are presented in Chapter 2.

In Chapter 3, an advance hybrid reduction scheme by coupling the on-the-fly reduction with the global quasi-steady-state approximation (QSSA) is proposed and demonstrated in both zero-dimensional reactor model and multidimensional CFD simulations. In Chapter 4, we further studied the applicability of hybrid reduction scheme with the quasi-steady-state (QSS) species selected based on a simple element flux criteria. The proposed hybrid reduction scheme is not only able to reduce the complexity of chemistry calculation using the on-the-fly reduction procedure, but also able to reduce the number of species involved in the transport calculations. The hybrid reduction scheme has the potential ability to address some transport-intensive computational problems.

In Chapter 5, we take a step further to explore new ideas of conducting reactive flow simulations. By integrating automated mechanism generation software with our on-the-fly mechanism reduction approach, we are able to execute a reactive flow simulation without a pre-developed detailed mechanism in hand. The simulation starts with only the initial reactants, which in the combustion case are fuel and air. And mechanism generation and reduction are performed recursively to identify a specific mechanism for a certain period of simulation. The mechanism is enlarged by the automated mechanism generation, and limited by the on-the-fly reduction during the integration of ODEs. Using this integrated computational framework, we are able to obtain identical simulation results as in a normal reactive flow simulation based on one single detailed mechanism. The beauty of the proposed framework is that no mechanism is needed beforehand to start the simulation.

Finally, a summary of the major conclusions of this dissertation as well as suggestions for the future directions is presented in Chapter 6.

## Chapter 2

### **Biodiesel combustion characterization using element flux analysis**

#### 2.1 Computational framework

To study biodiesel combustion, two detailed mechanisms for large biodiesel surrogates, namely methyl decanoate (MD, 2,878 species and 8,555 reactions) and methyl-9-decenoate (MD9D, 3,298 species and 10,753 reactions), are incorporated for the first time in the multi-dimensional CFD simulation of homogeneous charge compression ignition (HCCI) engine with on-the-fly reduction approach. Two smaller mechanisms, including a conventional hydrocarbon fuel surrogate n-heptane (Curran et al., 1998) and a small biodiesel surrogate methyl butanoate (MB), are also used for comparison between different types of fuels. The combustion characteristics, emission features, and the engine performance parameters are evaluated and compared among these fuels. In order to capture  $\text{NO}_x$  formations,  $\text{NO}_x$  chemistry is introduced and a multi-element flux analysis approach is employed in the on-the-fly reduction to identify fuel oxidation network and  $\text{NO}_x$  formation network separately. KIVA-3V (Amsden, 1997) code is used as the CFD platform and CHEMKIN (R.J. Kee, 1996) is used to handle the chemistry calculation. A two-dimensional axial symmetric mesh (Figure 2.1) with 1,052 computational cells at bottom dead center (BDC) is employed in KIVA-3V to simulate HCCI engine combustion. The on-the-fly reduction is integrated with KIVA-3V and CHEMKIN code to generate locally accurate reduced mechanism for each computational cell during each time step (He et al., 2009b), and DVODE is applied to numerically solve the resulting ODE system based on each reduced mechanism.

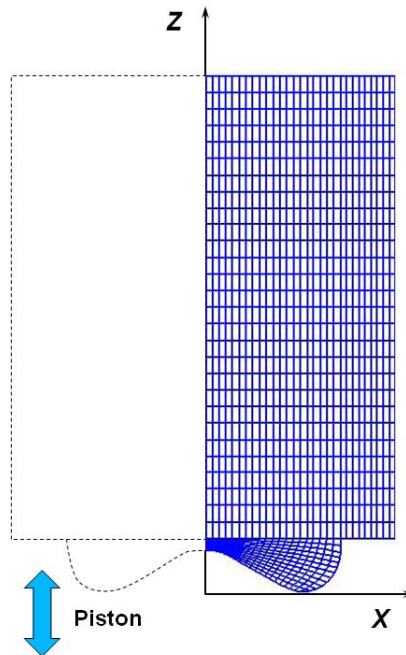


**Figure 2.1** Two-dimensional computational mesh used in KIVA engine simulations

To capture  $\text{NO}_x$  emission features of different fuels,  $\text{NO}_x$  chemistry is incorporated with the oxidation mechanism of each fuel and multi-element flux analysis is performed to include both C-element flux and N-element flux. However, as shown in our previous study (He et al., 2009a), N-element flux usually has much smaller value relative to C-element flux. Therefore, N-bearing species are always excluded from the reduced mechanism if both element fluxes are sorted together. In order to avoid this problem, fluxes based on different elements are calculated and sorted separately. The reduced fuel oxidation network based on C-element flux and the reduced  $\text{NO}_x$  formation network based on N-element flux are then combined to form the whole set of reduced mechanism.

In each computational cells and each time step in the CFD calculation, element fluxes are computed for all the source-sink pairs and sorted in descending order. A user-defined cutoff is then applied to identify active species as well as their involving reactions that will be included in the reduced mechanism, while species determined inactive are

considered dormant and maintain unchanged concentration within the current step. The reduced mechanism is then used in CHEMKIN and DVODE to update species composition, heat release and temperature profiles, which are passed to KIVA-3V code to formulate fluid mechanics and convection/diffusion process. The integration of on-the-fly reduction and KIVA-3V code is illustrated in Figure 2.2.

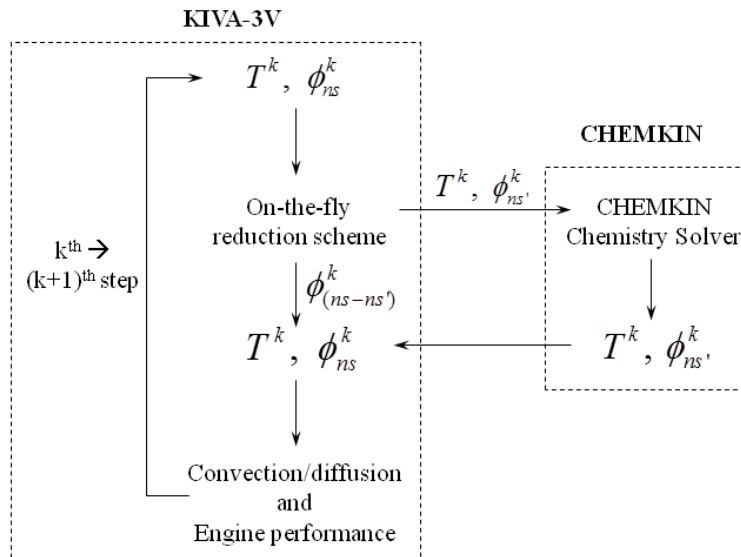


**Figure 2.2** Computational procedures integrating on-the-fly reduction in KIVA-3V

In addition, to compare the engine performance of different fuels, work done per cycle and engine power output are integrated in KIVA-3V code. Work done by the engine during one engine cycle is approximated by integrating pressure-volume curve according to Eq. (5). And power output is defined as the work done per unit time during the entire engine cycles in Eq. (6), where  $N$  is engine speed (rpm) and 2 in the denominator represents four-stroke engine cycle.(Heywood, 1988)

$$W = \int_{\text{cycle}} p dV \quad (5)$$

$$P = \frac{W \cdot N}{2} \quad (6)$$

**Table 2.1** Engine operation conditions and parameters

<b>Parameters</b>	<b>Value</b>
Engine speed /rpm	900, 1200, 1500, 1800
Initial temperature /K	1000
Initial pressure /MPa	10
Crank angle range /ATCD	-30° ~ 30°
Equivalence ratio	1.0
Compression ratio	16:1

The engine simulations run from crank angle (CA)  $-30.0^\circ$  after top dead center (ATDC) to  $30.0^\circ$  ATDC. For each fuel considered in this study, four different engine speeds are used to investigate the combustion and engine performance under different operation conditions. The engine parameters and operation conditions used in the simulations are summarized in Table 2.1. At lower or higher equivalence ratios, it is possible that the emission levels of CO or NO<sub>x</sub> are relatively small so that the difference between fuels is not obvious. Therefore, we choose to perform our study using equivalence ratio 1.0 at chemical stoichiometry so we can make better comparisons of the chemical characteristics between different fuels. The equivalence ratio mentioned here (and in the rest of this dissertation) is calculated just by the molar ratio of fuel and air without counting in the oxygen in the biodiesel surrogate molecules.

## 2.2 Validation of the computational framework

In order to validate the performance of on-the-fly reduction approach, we should compare the on-the-fly reduction results with the detailed mechanism simulation. However, for the two large biodiesel surrogates MD and MD9D, KIVA simulation with detailed

mechanisms without using on-the-fly reduction is not feasible due to extremely long CPU time. In this study, we first validate the on-the-fly reduction with the large mechanisms in Plug Flow Reactor (PFR) simulation. This allows us to select the appropriate cutoff to obtain the necessary accuracy. Then we use the smaller biodiesel surrogate mechanism MB with on-the-fly reduction in KIVA to verify the performance of the integration of on-the-fly reduction in KIVA engine simulations. Finally, we extend the validated KIVA/on-the-fly reduction scheme to the two large biodiesel surrogate mechanisms.

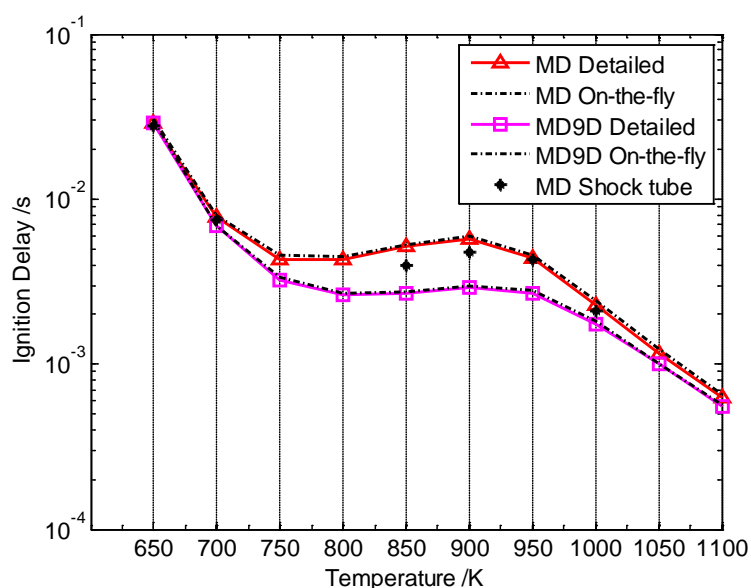


**Figure 2.3** Ignition delay time validation for methyl decanoate and methyl-9-decanoate in PFR simulations. Shock tube ignition data is obtained from Herbinet et al. (2008)

In the PFR simulation, the auto-ignition delay of MD and MD9D with different initial temperatures is characterized as shown in Figure 2.3. Stoichiometric fuel/air mixture is used for all the simulations in order to be consistent with engine simulations. The initial temperature ranges from 650K to 1100K to cover low-temperature, negative temperature coefficient (NTC), and high-temperature regions. The ignition delay time obtained using on-the-fly reduction is in good agreement with the ignition delay calculated with detailed

mechanism. A 99% cutoff used in the on-the-fly reduction is sufficient to produce accurate results. In addition, the predicted ignition delay time of MD is also consistent with shock tube ignition data simulated at the same pressure (12.0 atm) reported by Herbinet et al. (2008), which also provides a validation of the on-the-fly reduction for the two large mechanisms in the simulations. KIVA simulations with MB mechanism using on-the-fly reduction are compared with the simulations with detailed mechanism.

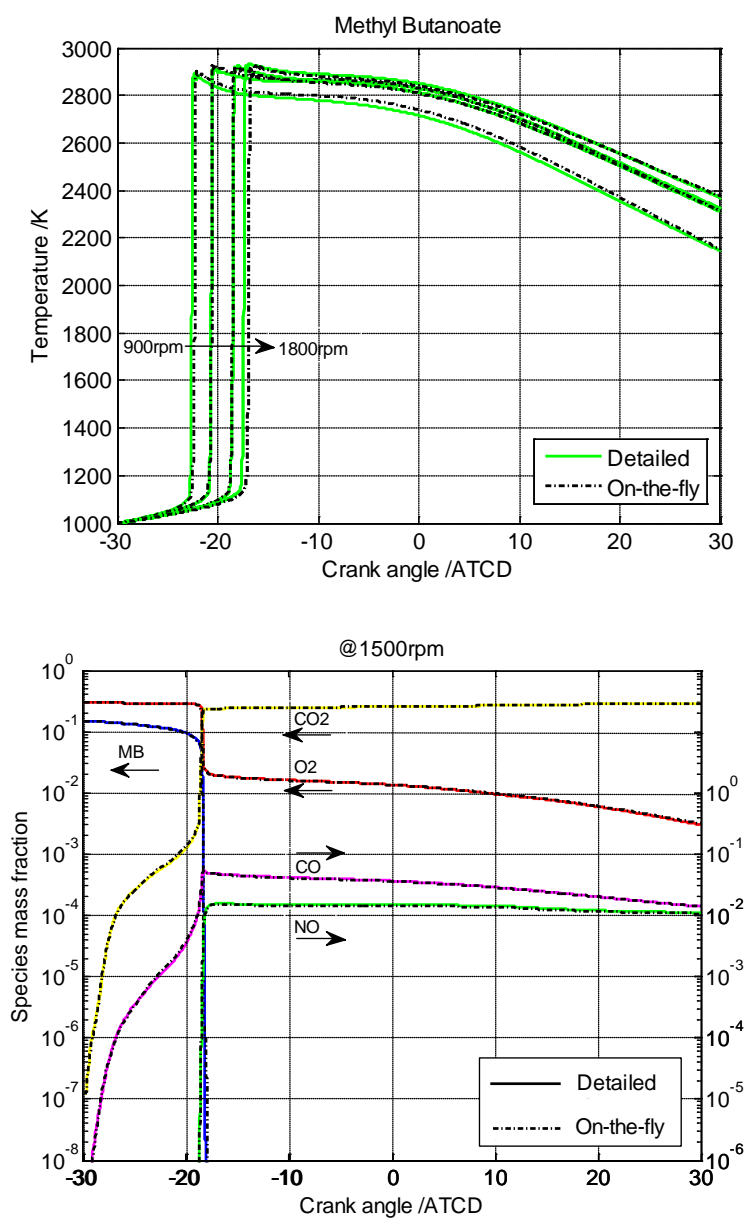


**Figure 2.4** Temperature and selected species profiles in KIVA simulations with methyl butanoate

In Figure 2.4, it is shown that the temperature profiles and selected important species profiles calculated using on-the-fly reduction and detailed mechanisms are identical for different engine operation conditions, indicating that the integration of on-the-fly reduction in KIVA can produce reliable simulation results. Based on the above validation, we then extend the same KIVA/on-the-fly reduction framework to the two large mechanisms, which finally enable us to conduct engine simulations in KIVA with complex biodiesel surrogate mechanisms while maintaining acceptable computational time and accuracy.

The CPU time of KIVA simulations with on-the-fly reduction is dramatically reduced in our study, especially for the two large mechanisms. As shown in Figure 2.5, the simulation time reduction for all the four mechanisms with on-the-fly is quite significant. Time needed for the two small mechanism simulations is reduced by more than 90% with on-the-fly reduction. For the two large mechanisms MD and MD9D, the computational time required using the on-the-fly reduction is reduced by several order of magnitudes (approximately 200-300 hr), compared with the estimated simulation time with detailed mechanisms which will be hundreds of days based on time it takes for the first several computational cycles. The size of reduced mechanisms throughout the simulation is also much smaller compared to the detailed mechanism. For example in the MD9D simulation (Figure 2.5), the largest reduced mechanism during the simulation is only over 400 species, about only 12% of the total number of species in the detailed mechanism. The simulation with MD mechanism also has similar ratio between reduced mechanisms and detailed mechanism. Therefore, on-the-fly reduction is a powerful and efficient

mechanism simplification tool that enables us to incorporate large chemistry networks in the engine CFD simulations.

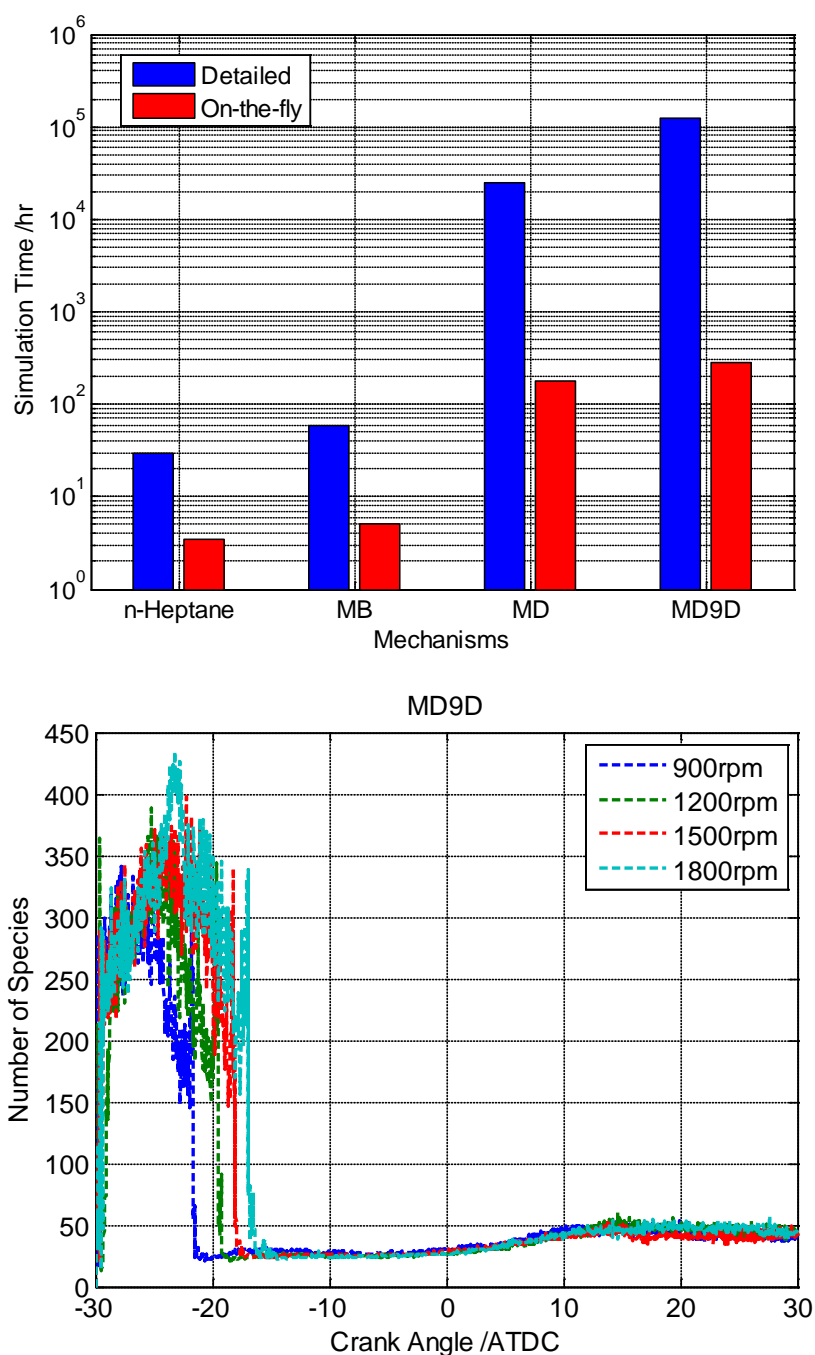


**Figure 2.5** Simulation time reduction for different fuels (upper figure) and mechanism reduction for methyl-9-decenoate (lower figure)

## 2.3 Combustion characteristics and fuel comparison in HCCI engine simulations

### 2.3.1 Combustion characteristics based on HCCI engine simulation

One of the most important combustion characteristics is the ignition timing. In Figure 2.6, we compare the ignition timing in terms of crank angle for the four considered fuels under HCCI engine condition obtained in KIVA simulations. As shown in the figure, the ignition timing of MB and MD9D is apparently earlier than that of the hydrocarbon fuel n-heptane by two to three crank angle degrees, while MD shows comparable ignition timing as n-heptane. These results appropriately reflect the reactivity of these fuels as reported in the literature. In general, biodiesel fuel is considered to have higher cetane number, i.e. earlier ignition timing. As reported in the study by Freedman et al. (Freedman and Bagby, 1990), cetane number of methyl esters increases as the carbon chain length becomes longer. The cetane number of MD reported in their study was 47.9, compared with cetane number 56 for n-heptane reported by Lü et al. (2007). Therefore, our simulation results demonstrate the relatively higher reactivity for biodiesel fuels, while the similar reactivity of MD and n-heptane is also consistent with their comparable cetane numbers.

It should also be observed from Figure 2.6 that as engine speed increases the ignition timing for all the tested fuel is delayed. As engine speed increases, the actual reaction rate in terms of absolute time does not necessarily change, but the piston is moving sufficiently faster relative to the rates of chemical reactions (Kelly-Zion and Dec, 2000). Therefore, at higher engine speed, the same reaction progress will occur at a later crank angle, which is observed as retarded ignition timing in terms of crank angle degrees.

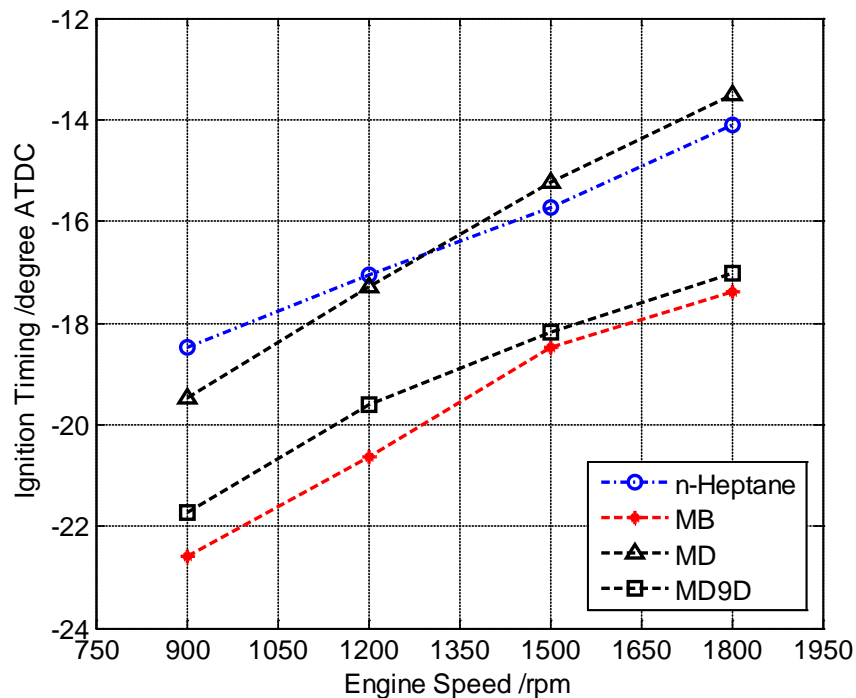


**Figure 2.6** Ignition timing for different fuels in HCCI engine simulations

In addition to the ignition timing study, we also successfully captured the early formation of CO and CO<sub>2</sub> in biodiesel combustion process. The early formation of CO and CO<sub>2</sub> is experimentally observed in the studies of rapeseed oil methyl ester oxidation (Dagaut et al., 2007). Herbinet et al. reports that CO and CO<sub>2</sub> formation is mainly due to the oxidation of the ester groups before the main ignition, in which one of the oxygen atoms in the produced CO<sub>2</sub> is contributed by the ester group via OCHO radical (Herbinet et al., 2008). In our simulation, the early formation of CO and CO<sub>2</sub> of oxygenated biodiesel surrogates is successfully captured as shown in Figure 2.7, compared with n-heptane which does not exhibit such phenomena due to its hydrocarbon molecular structure.

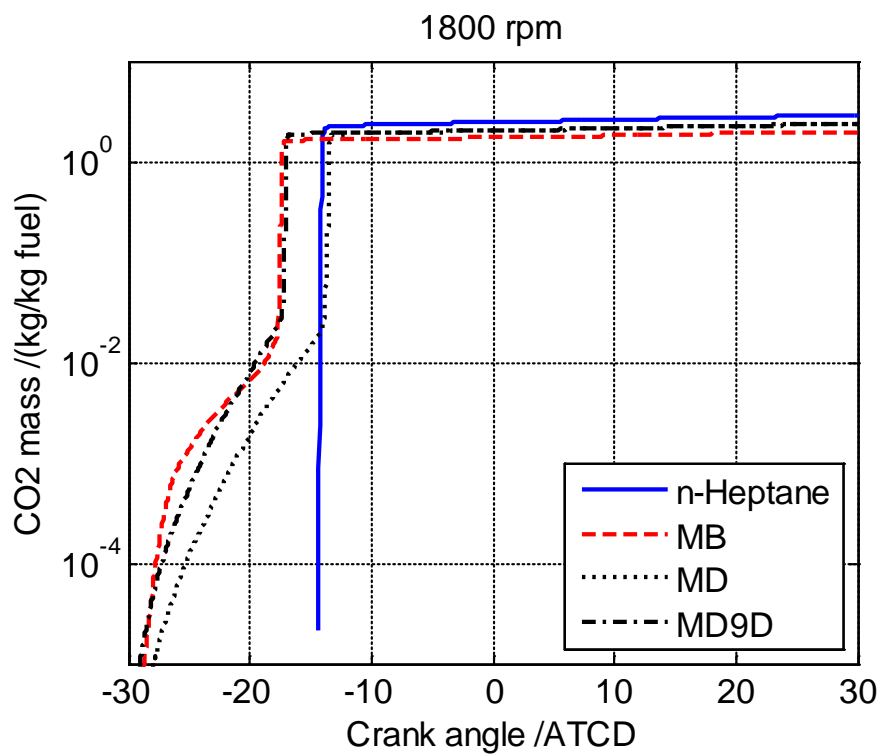
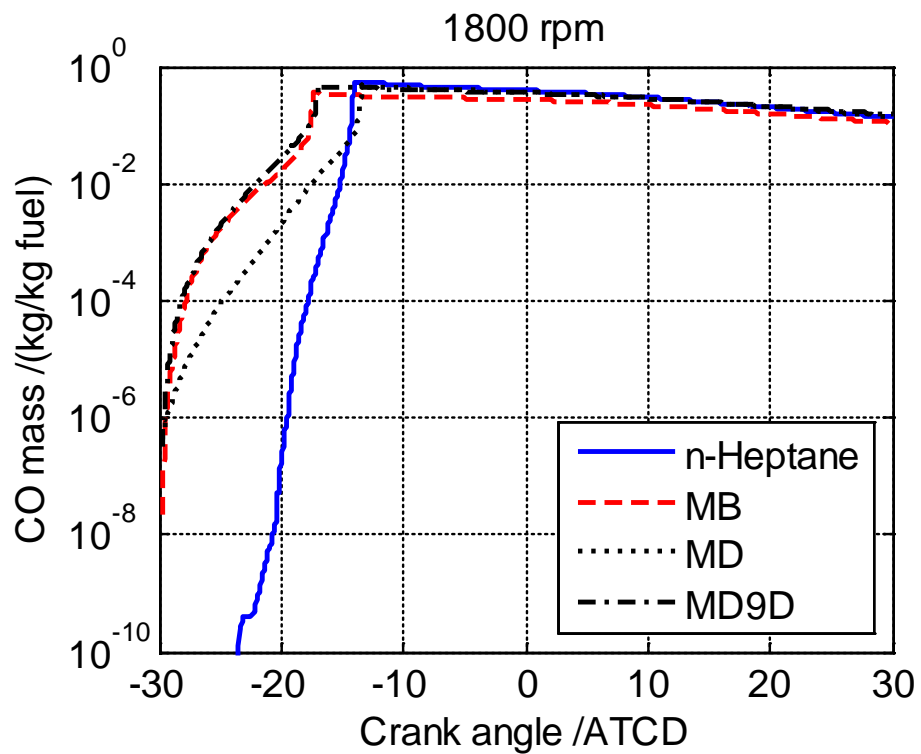
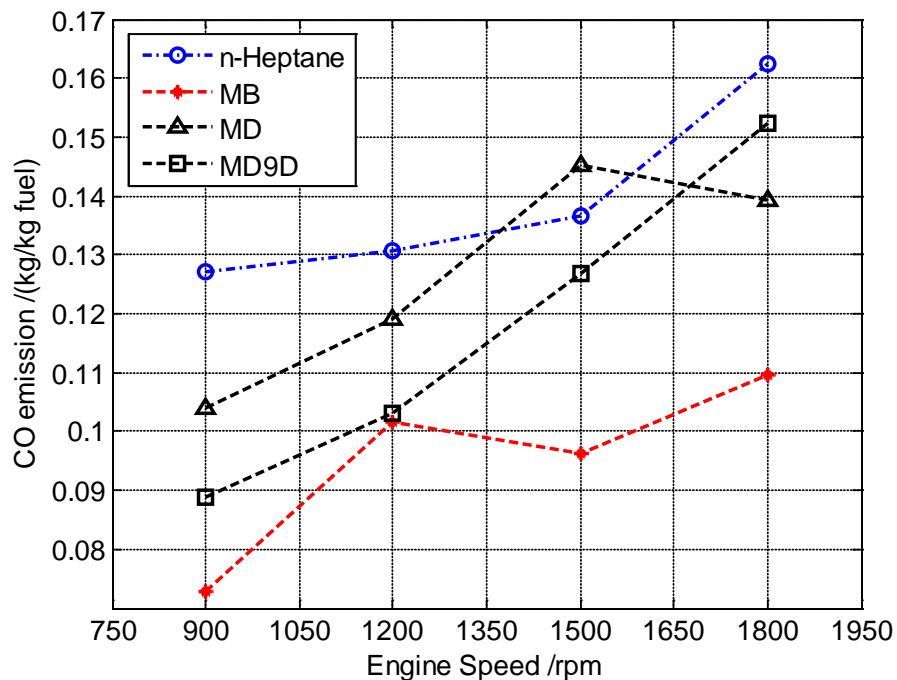


Figure 2.7 Early formation of CO and CO<sub>2</sub> for biodiesel fuels compared with n-heptane

### 2.3.2 CO and NO Emissions

In order to evaluate the emission features of different types of fuels, CO and NO emissions are calculated and compared at different engine speeds for each fuel, as shown in Figure 2.8 and Figure 2.9.

In the literature, CO emission of biodiesel fuels reported in most studies (Lapuerta et al., 2008) are reduced compared to that of conventional fuels. The oxygenated feature of biodiesel fuels is widely considered as the reason of lower CO emissions since the presence of extra oxygen in the molecule results in more complete combustion possible. This is also reflected in our HCCI engine simulation results shown in Figure 8. CO emission of MB at different engine speeds is apparently lower than the other fuels because it has the highest oxygen content in the molecule. For the two larger biodiesel mechanisms MD and MD9D, which have oxygen content lower than MB but higher than n-heptane, the CO emissions are correspondingly higher than MB and lower than n-heptane. N-heptane with no oxygen in the molecule has the highest CO emission among the tested fuels. The above results consistently show the trend that biodiesel has the potential to reduce CO emission due to its oxygenated chemical structure. On the other hand, we can observe from Figure 2.8 as well that different CO emissions for these fuels are also related with their different cetane numbers, i.e. different reactivity. The higher the cetane number is, the faster the reaction completion is, and thus the lower the probability to form fuel-rich regions that is usually related to CO emissions. For instance, although MD and MD9D have similar oxygen content, the faster ignition of MD9D leads to an overall lower CO emission compared to that of MD. Therefore, both oxygenation and advanced ignition contribute to the lower CO emissions.



**Figure 2.8** CO emissions for different fuels at different engine speeds

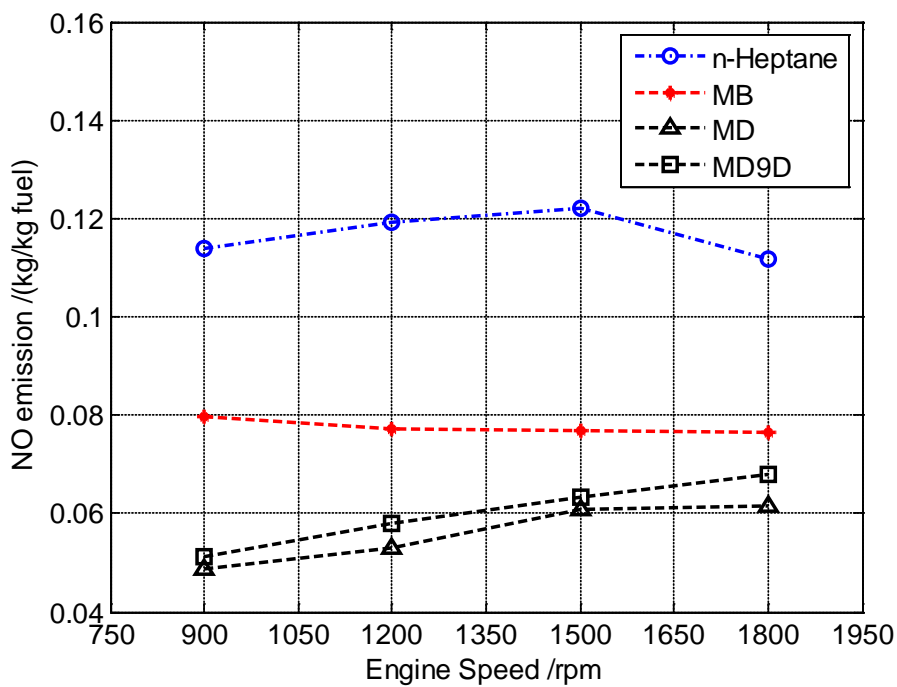


**Figure 2.9** NO emissions for different fuels at different engine speeds

Besides, we observed that CO emission increases for all the tested fuels as engine speed increases. This result can be due to the retarded ignition and slower kinetic processes relative to piston movement at higher engine speed, which leads to less actual time for chemical reactions to complete.

By using nitrogen flux analysis with NO<sub>x</sub> formation chemistry, we are also able to capture NO emissions of different types of fuels. NO emission is highly related with temperature (Brakora and Reitz, 2010; Um and Park, 2010b). The higher the temperature is, the more NO is formed. In the literature, different trends of biodiesel NO<sub>x</sub> emissions compared with conventional fuels have been reported. Most studies found higher NO emission under diesel engine conditions (Lapuerta et al., 2008) because faster ignition after fuel injection could result in higher peak temperature in the cylinder. However, this is not usually the case under HCCI engine conditions. In HCCI engine, ignition does not necessarily occur at around top dead center (TDC) as it is the case in compression and spark ignition engines. Therefore, we do not observe a distinct correlation between peak temperature and NO emission level in our results. Instead, NO emission is most likely to be related with the overall in-cylinder temperature as a result of the different fuel heating values.

In Figure 2.9, NO emissions for each fuel obtained in the HCCI engine simulations are compared. As described in the figure, NO emission predicted with the three biodiesel surrogates mechanisms is less than that predicted by n-heptane mechanism. The lower NO emission could be due to the lower heating value of biodiesel fuels, which is reflected by the total heat release data shown in Figure 2.10. Lower

heating value decreases the overall in-cylinder temperature that can possibly be reached and thus reduces NO formation.

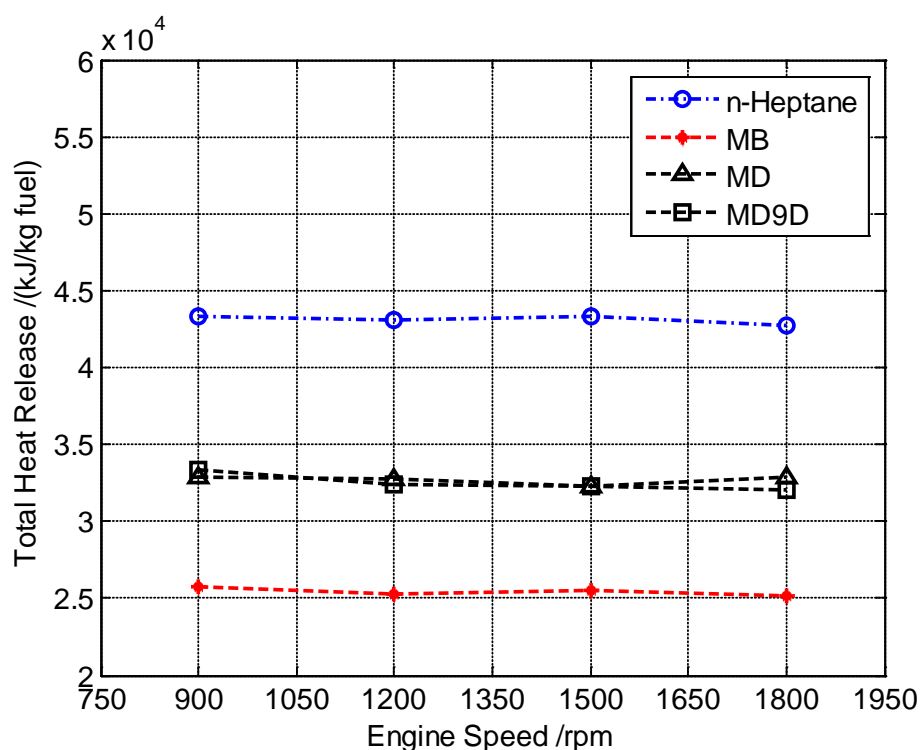


**Figure 2.10** Total heat release for different fuels at different engine speeds

Another feature we can observe from Figure 2.9 is that MB generates higher NO emission than the other two biodiesel surrogates. This phenomenon could be explained by the fact that NO emission is also connected with fuel-air ratio during the combustion process. As pointed out by Um and Park (2010b) in their numerical study of HCCI engine fueled with biodiesel, high NO emission is likely to occur under fuel lean conditions where fuel oxidation tends to be more complete. Since the small surrogate MB has about 31% oxygen content by molecular weight, which is much higher than about 17% for MD and MD9D, it can reach more complete fuel oxidation than the two large biodiesel surrogates, giving birth to more possible fuel lean regions in the cylinder and thus higher NO formation.

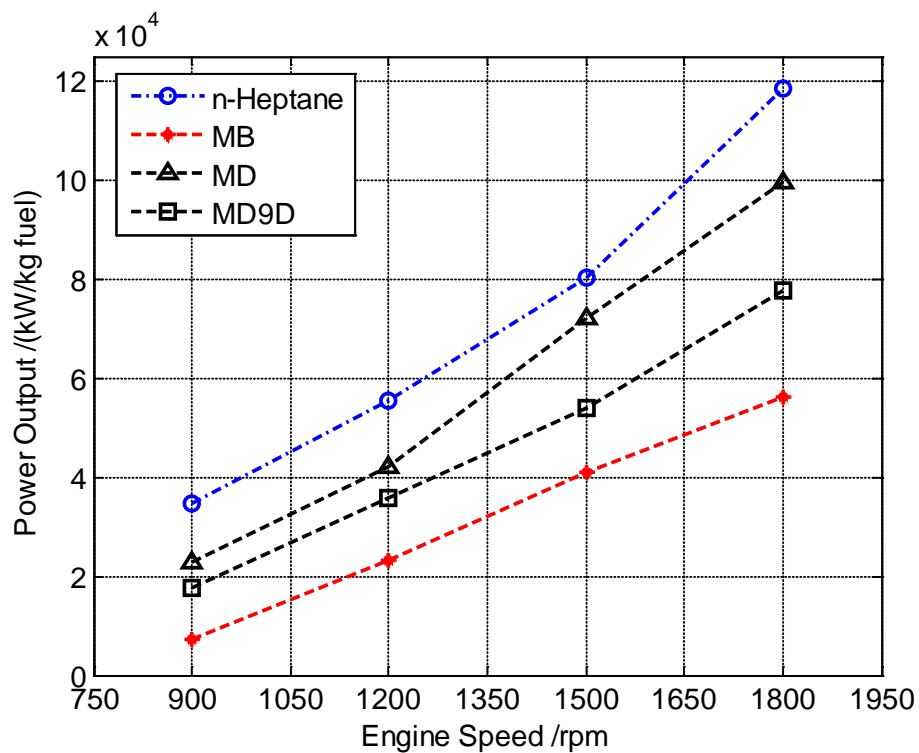
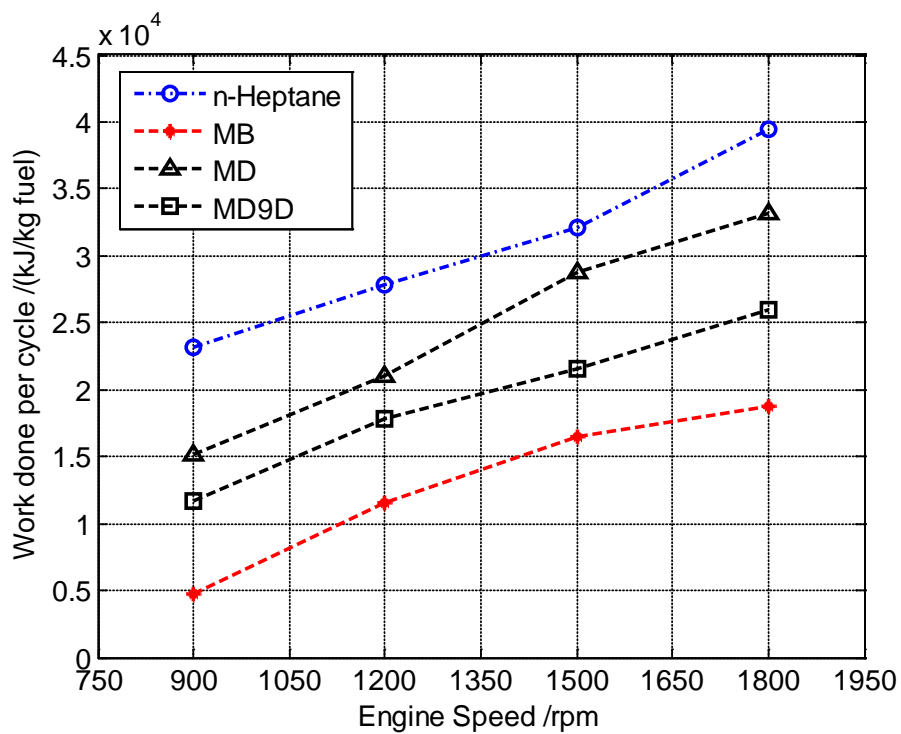


**Figure 2.11** Work done per cycle and power output for different fuels at different engine speeds

### 2.3.3 Engine performance

The calculated engine performance parameters are shown in Figure 2.11, including work done per cycle and the power output at different engine speeds for each fuel. It is found that the three biodiesel surrogates produce less work per engine cycle and correspondingly less engine power output compared to n-heptane. This energy production trend is also consistent with the observation illustrated in Figure 2.10 that biodiesel has lower total heat release, or heating value, than conventional diesel.

However, if we focus on the two large biodiesel surrogates MD and MD9D, we can see from Figure 2.10 and Figure 2.11 that although similar amount of total heat release is observed, they still produce different level of engine power output. To understand this, we also need to take into account the different ignition timing of the two fuels (see Figure 6). Because at all the considered engine speeds, MD9D exhibits advanced ignition compared to MD, the in-cylinder pressure in MD9D combustion increases earlier than that in the MD combustion. According to Eq. (5), work done by the engine is reflected by the integration area under p-V curve. Since the volume change is negative during the compression stroke, the engine has to perform more negative work in MD9D combustion, which lowers the overall work done during the entire engine cycle and accordingly leads to less engine power output. Although MD9D has similar total heat release during the engine cycle, more portion of the released energy is used to overcome the compression resistance, and thus less energy is left to output engine power.

For the same reason, we can also observe from Figure 2.11 that for each fuel, as engine speed increases, the overall power output is also increasing because the delayed ignition timing at higher engine speeds reduces the negative work done in the

compression stroke, although the total heat release maintains almost the same level at different engine speeds.

The above discussion reveals that the power output in HCCI engine is related with both the heating value and the ignition timing of the fuel. For biodiesel, with advanced ignition timing and lower heating value, the power output under HCCI engine conditions is less than that of the conventional diesel fuels.

## 2.4 Summary

In this chapter, two detailed mechanisms for large biodiesel surrogates are incorporated in the multi-dimensional CFD for the first time with on-the-fly reduction technique. The engine simulation with these large mechanisms is enabled by reducing the computational time to an acceptable range. The size of mechanism used in the chemistry calculation in our study is also significantly reduced while still maintain reliable accuracy. Important combustion characteristics, emission features, and engine performance of biodiesel are successfully captured and compared with conventional diesel fuels under HCCI engine conditions. The fuel comparison suggests that biodiesel has advanced ignition timing than conventional diesel fuels under various conditions. It is also observed that biodiesel generates lower CO and NO emission due to its oxygenation and lower heating value feature. The work done and engine power output for biodiesel fuels are also found to be lower due to lower heating value and advanced ignition timing. These engine simulations can provide important insight to study the chemical characteristics of biodiesel and its impact on the engine design and operation.

It is also realized from our study that the on-the-fly reduction is a powerful tool to simplify detailed chemistry in realistic reactive flow simulations. With the capacity of reducing computational intensity and mechanism complexity, we can have the confidence to employ our integrated KIVA/on-the-fly reduction framework to more realistic flow models and more complicated biodiesel kinetic mechanisms.

Although on-the-fly reduction greatly reduces the computational costs, KIVA simulations with large biodiesel mechanisms still take relatively long time at approximately 200 to 300 hours with our Dell T7500 workstation. Also, despite the mechanism reduction for chemistry calculation, the full species set are still involved to handle transport. In practical or industrial applications, transport of thousands of species is extremely unaffordable. Therefore, we still need to focus on the integration of both global and dynamic reduction approaches to further facilitate the accommodation of larger detailed chemical kinetic mechanisms in reactive flow simulations.

## Chapter 3

### Development of the hybrid reduction scheme

#### 3.1 Quasi-steady-state approximation

Although the engine CFD simulations with large detailed mechanisms is enabled, the multidimensional CFD calculation still takes substantially long time due to the too large size of the starting mechanism and the full species set involved in the transport calculation. Therefore, we are interested in developing a hybrid scheme combining both global reduction and dynamic reduction approaches to further improve the applicability of the on-the-fly reduction.

In this work, we focus on the global reduction methods based on the quasi-steady-state approximation (QSSA) (Turanyi et al., 1993). In the application of QSSA, the quasi-steady state (QSS) species with short timescales will quickly reach the chemical equilibrium so that their production rates can be approximated by zero, and thus the ODEs for the QSS species production rates can be replaced by a set of algebraic equations by assigning the right-hand side to zero. The QSSA approach has been used in various mechanism reduction algorithms, such as augmented reduced mechanism (ARM) method (Sung et al., 2001), reaction lumping approach (Hughes et al., 2009). The DRG based method (Lu and Law, 2005, 2008b) and DRGEP algorithm (Pepiot-Desjardins and Pitsch, 2008) also use QSSA as an additional step to further reduce the mechanism size. A key issue in the application of QSSA is the selection of QSS species. Several methods have been developed to identify QSS species based on the computational singular perturbation (CSP) (Lam and Goussis, 1994; Lu et al., 2001; Lu and Law, 2008a) and

optimization based method (Montgomery et al., 2006). Moreover, in order to obtain efficient solution of the resulting system of differential-algebraic equations, methods such as linearized QSSA and QSSA graph (LQSSA-QSSG) (Lu and Law, 2006), and combination of fixed-point iteration (FPI) and matrix inversion algorithm (Chen and Tham, 2008), are also developed.

### 3.2 Hybrid scheme based on on-the-fly reduction and global QSSA

#### 3.2.1 Implementation of quasi-steady-state approximation

The chemical kinetics of a reaction system is described by the following system of ODEs for the production rates of each species in Eq. (7).

$$\begin{aligned}\frac{d\mathbf{z}}{dt} &= \mathbf{f}(\mathbf{z}) \\ \mathbf{z} &= (\mathbf{z}^{(1)}, \mathbf{z}^{(2)})^T \\ \mathbf{f} &= (\mathbf{f}^{(1)}, \mathbf{f}^{(2)})^T\end{aligned}\tag{7}$$

where  $\mathbf{z}$  is the species concentration consisting of the concentration of non-QSS species  $\mathbf{z}^{(1)}$  and the concentration of the selected QSS species  $\mathbf{z}^{(2)}$ ; and  $\mathbf{f}$  is the set of rate equations for all the species consisting of the equations  $\mathbf{f}^{(1)}$  for non-QSS species and  $\mathbf{f}^{(2)}$  for the selected QSS species, respectively. By applying QSSA to the selected QSS species, the original ODE system (Eq. (7)) is transformed to the following system of differential-algebraic equations.

$$\begin{aligned}\frac{d\mathbf{z}^{(1)}}{dt} &= \mathbf{f}^{(1)}(\mathbf{z}) \\ \mathbf{0} &= \mathbf{f}^{(2)}(\mathbf{z}) \\ \mathbf{z} &= (\mathbf{z}^{(1)}, \mathbf{z}^{(2)})^T\end{aligned}\tag{8}$$

If the selection of QSS species is appropriate, the solutions obtained from the original system of ODEs Eq. (7) should be well approximated by the solutions from Eq. (8). The detailed definition, QSS species selection criteria, and error analysis of the application of QSSA were discussed in detail by Turanyi et al (Turanyi et al., 1993).

In the application of QSSA in our hybrid reduction scheme, we employ a two-step method to solve the above system of equations in Eq. (8). During each integration time step, we have two intermediate steps. The first step solves the system of ODEs in Eq. (8) with respect to the non-QSS species concentrations  $\mathbf{z}^{(1)}$ , while temporarily keeping the concentrations of QSS species  $\mathbf{z}^{(2)}$  as constants. And then in the second step, we take the “inner iteration” to solve the set of nonlinear algebraic equations in Eq. (8) with respect to the QSS species concentrations  $\mathbf{z}^{(2)}$ , while using the new values of  $\mathbf{z}^{(1)}$  obtained in the first step as constants. By doing this two-step calculation, the concentrations of all the species are updated for the new time point at each integration time step, and the concentrations of QSS species  $\mathbf{z}^{(2)}$  are always completely determined by all the non-QSS species concentrations  $\mathbf{z}^{(1)}$  via the set of algebraic equations. A nonlinear algebraic equation solver C05NBF in the Numerical Algorithms Group (NAG) Fortran Library (<http://www.nag.co.uk/numeric/fl/FLdescription.asp>) is used to solve the set of nonlinear algebraic equations.

By applying QSSA, it is assumed that the concentrations of the QSS species are always chemistry-controlled and will always reach the quasi-steady state that is determined by the other non-QSS species concentrations. Therefore, it is not necessary to involve the QSS species in the transport calculation, and the concentrations of the QSS species are completely dependent on the non-QSS species. In order to implement the

QSSA calculation, we introduce the dual-mechanism implementation in which two CHEMKIN-format mechanisms are incorporated. In the transport calculation, since only the non-QSS species are involved, a “reduced” mechanism containing only non-QSS species and their involving reactions is used to perform necessary initialization and transport calculations that require CHEMKIN; whereas in the chemistry solver, the original detailed mechanism consisting of all the species and reactions is used to formulate all the kinetic rate equations (both ODEs and algebraic equations). A store-and-retrieve scheme is established in the QSSA implementation so that we can easily choose which mechanism to use in the simulation. During the initialization stage of the program, the two mechanisms are both initialized in CHEMKIN and stored in common block variables, and later either of the mechanisms can be retrieved to CHEMKIN and can be easily switched as needed. The validation results of the above implementation techniques are presented in the demonstration of the methodology in section 3.3.1.

### 3.2.2 Hybrid mechanism reduction framework

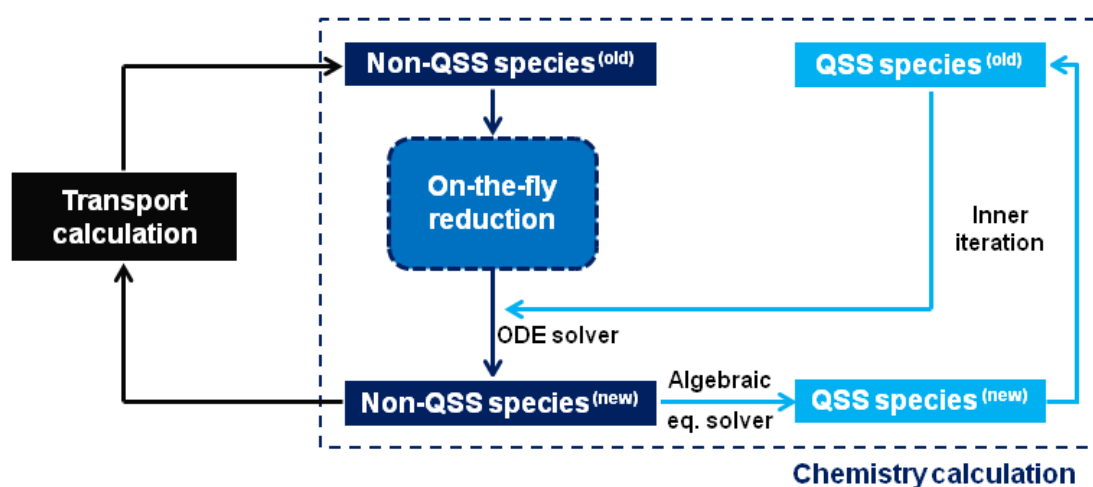


**Figure 3.1** Schematic illustration for the integration of on-the-fly reduction with QSSA

The next step is to apply the on-the-fly reduction to identify the active non-QSS species and integrate the on-the-fly reduction with QSSA in the reactive flow simulations. The details of the on-the-fly reduction framework can be found in our previous work (He et al., 2010b). A schematic illustration for the integration of on-the-fly reduction and global QSSA is shown in Figure 3.1.

Having certain selections of global QSS species, at each integration step, we first perform the on-the-fly element flux analysis to the non-QSS species to generate the reduced mechanism only consisting of active non-QSS species. During the flux analysis, the instantaneous element fluxes are computed between each pair of species using the full mechanism, but only the fluxes between non-QSS species pairs are gathered and sorted in a descending order. Subsequently, a user-specified cutoff is applied to the ranked fluxes, and only the species pairs with flux above the cutoff threshold are considered active and retained in the reduced mechanism for the non-QSS species. Since the flux analysis is only to eliminate the inactive non-QSS species, the active reactions in the reduced mechanism are determined as the reactions involving only the active non-QSS species or the reactions involving only QSS species and active non-QSS species, so that the QSS species information is fed back to the reduced system of ODEs through the reactions connecting QSS species and the active non-QSS species. Then the concentrations of these active non-QSS species are updated by solving their describing kinetic ODEs in which QSS species concentrations are temporarily assumed constant, while the concentrations of the inactive non-QSS species identified through the flux analysis are kept unchanged for the current integration step. The updated active non-QSS species concentrations along with the unchanged inactive non-QSS species concentrations are then used as the new

values of  $\mathbf{z}^{(1)}$  in Eq. (8) to solve for the updated value of the QSS species concentrations through the algebraic equations via the inner iteration sub-step. Here, the algebraic equations are formulated by the full mechanism since the global QSS species is selected using the full mechanism and the resulting algebraic equations are only valid when all the species and reactions in the full mechanism present. At last, only the updated values of non-QSS species concentrations  $\mathbf{z}^{(1)}$  are passed from the chemistry solver to the main program that handles mixing or transport calculations. As the system advances to the next time step, the hybrid reduction procedure is repeated. A summary of the steps in the hybrid mechanism reduction algorithm is provided in Figure 3.2.

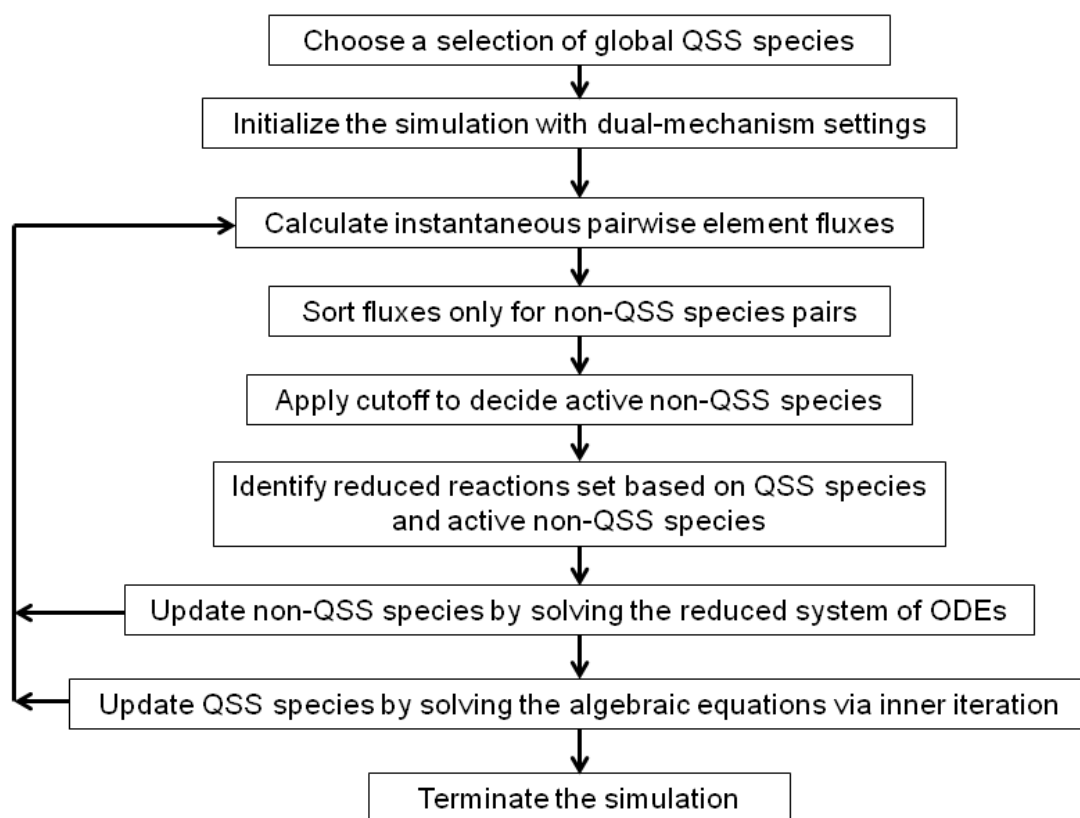


**Figure 3.2** Summary of the steps in the hybrid reduction algorithm

### 3.3 Demonstration of the proposed hybrid scheme

To validate feasibility and accuracy of the proposed hybrid mechanism reduction scheme, the computational framework is demonstrated using a detailed mechanism GRI-Mech 3.0 (Smith et al.) for methane oxidation with 53 species and 325 reactions. Different flow models, including PFR model and internal combustion engine CFD model, are used for the demonstration. The PFR model used is a zero-dimensional reactor model in which all the species can be tracked, and it is simple for quick model validation. The engine CFD calculation is handled by KIVA-3V code, which employs the same two-dimensional computational mesh (as shown in Figure 2.1) with 1052 cells at the bottom dead center (BDC). The multidimensional CFD environment provides a severe scenario with wide range of reaction conditions and various timescales to test the robustness of the hybrid reduction scheme. Both models can be solved with the detailed mechanism to provide temperature and species concentration profiles for the evaluation of the results obtained by the hybrid reduction scheme.

The selection of QSS species is a very important issue for the hybrid reduction scheme. However, since the main focus of this paper is to demonstrate the idea of hybrid reduction scheme, we do not place much emphasis on the QSS species selection in this paper although we are currently working on studying the methods and criteria of the selection in detail. The QSS species selections reported by Montgomery et al. (2006) are used in the present work. In their work, a genetic algorithm was applied to select different number of QSS species from the GRI-Mech 3.0 detailed mechanism for methane. In their optimization process, three different options for selecting independent reactions were discussed. We choose to employ the selections obtained with the option that not

eliminating the independent reactions, so that the selected QSS species is suitable for the application of QSSA in our hybrid reduction framework. A list of the different QSS species selections used in the current work is shown in Table 3.1.

**Table 3.1** List of the QSS species selections obtained by Montgomery et al. (2006) for methane mechanism GRI-Mech 3.0

Number of non-QSS species	Number of QSS species	Selected QSS species
53	0	None (Detailed mechanism)
52	1	C <sub>2</sub> H <sub>3</sub>
46	7	CH CH <sub>2</sub> NH NO <sub>2</sub> HNO HNCO NCO
41	12	HCO N NH NO <sub>2</sub> HNO HCNN HOCN HNCO NCO C <sub>3</sub> H <sub>7</sub> CH <sub>2</sub> CHO CH <sub>3</sub> CHO
36	17	CH CH <sub>2</sub> (s) HCO C <sub>2</sub> H <sub>3</sub> C <sub>2</sub> H <sub>5</sub> HCCOH N NH NH <sub>2</sub> NO <sub>2</sub> HNO HCNN HNCO NCO C <sub>3</sub> H <sub>7</sub> CH <sub>2</sub> CHO CH <sub>3</sub> CHO
31	22	C CH <sub>2</sub> (s) HCO C <sub>2</sub> H C <sub>2</sub> H <sub>3</sub> C <sub>2</sub> H <sub>5</sub> HCCOH N NH NH <sub>2</sub> NNH NO <sub>2</sub> HNO CN H <sub>2</sub> CN HCNN HOCN HNCO NCO C <sub>3</sub> H <sub>7</sub> CH <sub>2</sub> CHO CH <sub>3</sub> CHO
26	27	C CH CH <sub>2</sub> CH <sub>2</sub> (s) HCO CH <sub>2</sub> OH C <sub>2</sub> H C <sub>2</sub> H <sub>3</sub> C <sub>2</sub> H <sub>5</sub> HCCO HCCOH N NH NH <sub>2</sub> NNH NO <sub>2</sub> HNO CN H <sub>2</sub> CN HCNN HCNO HOCN HNCO NCO C <sub>3</sub> H <sub>7</sub> CH <sub>2</sub> CHO CH <sub>3</sub> CHO
21	32	C CH CH <sub>2</sub> CH <sub>2</sub> (s) HCO CH <sub>2</sub> OH CH <sub>3</sub> O CH <sub>3</sub> OH C <sub>2</sub> H C <sub>2</sub> H <sub>3</sub> C <sub>2</sub> H <sub>5</sub> HCCO CH <sub>2</sub> CO HCCOH N NH NH <sub>2</sub> NNH NO <sub>2</sub> N <sub>2</sub> O HNO CN H <sub>2</sub> CN HCNN HCNO HOCN HNCO NCO C <sub>3</sub> H <sub>7</sub> C <sub>3</sub> H <sub>8</sub> CH <sub>2</sub> CHO CH <sub>3</sub> CHO
16	37	O OH H <sub>2</sub> O <sub>2</sub> C CH CH <sub>2</sub> CH <sub>2</sub> (s) HCO CH <sub>2</sub> OH CH <sub>3</sub> O CH <sub>3</sub> OH C <sub>2</sub> H C <sub>2</sub> H <sub>3</sub> C <sub>2</sub> H <sub>5</sub> HCCO CH <sub>2</sub> CO HCCOH N NH NH <sub>2</sub> NH <sub>3</sub> NNH NO <sub>2</sub> N <sub>2</sub> O HNO CN HCN H <sub>2</sub> CN HCNN HCNO HOCN HNCO NCO C <sub>3</sub> H <sub>7</sub> C <sub>3</sub> H <sub>8</sub> CH <sub>2</sub> CHO CH <sub>3</sub> CHO

### 3.3.1 Validation of the QSS selection and the QSSA implementation

Before we conduct any demonstration of the algorithm, the QSS species selections and the dual-mechanism QSSA implementation are first validated using the PFR model. The isothermal PFR simulation results shown in Montgomery et al. (2006) with different number of QSS species are reproduced using exactly the same conditions at a constant temperature of 1650 K and equivalence ratio 1.0 (stoichiometric methane/air mixture). Selections of 27, 32, and 37 QSS species are used to compare with the detailed mechanism calculation. As shown in Figure 3.3, the reproduced species mole fraction profiles for CH<sub>4</sub>, O<sub>2</sub>, CO, and NO using our dual-mechanism implementation are identical with that in ref. (Montgomery et al., 2006) where these QSS species are optimally selected.

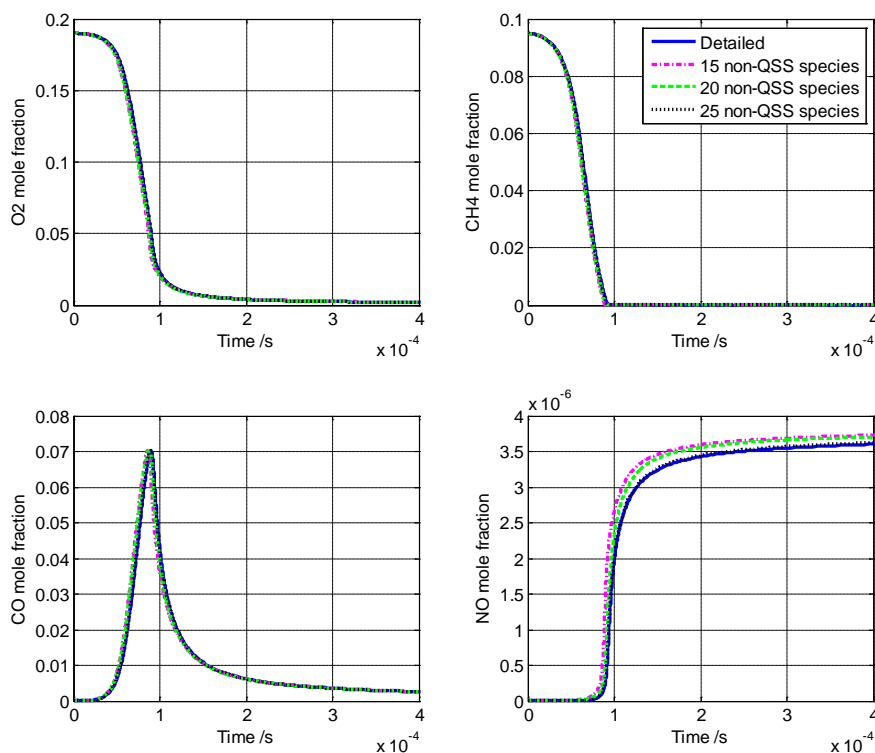


**Figure 3.3** Reproduced species mole fractions for different QSS species selections in PRF isothermal runs. Temperature at 1650 K and equivalence ratio 1.0.

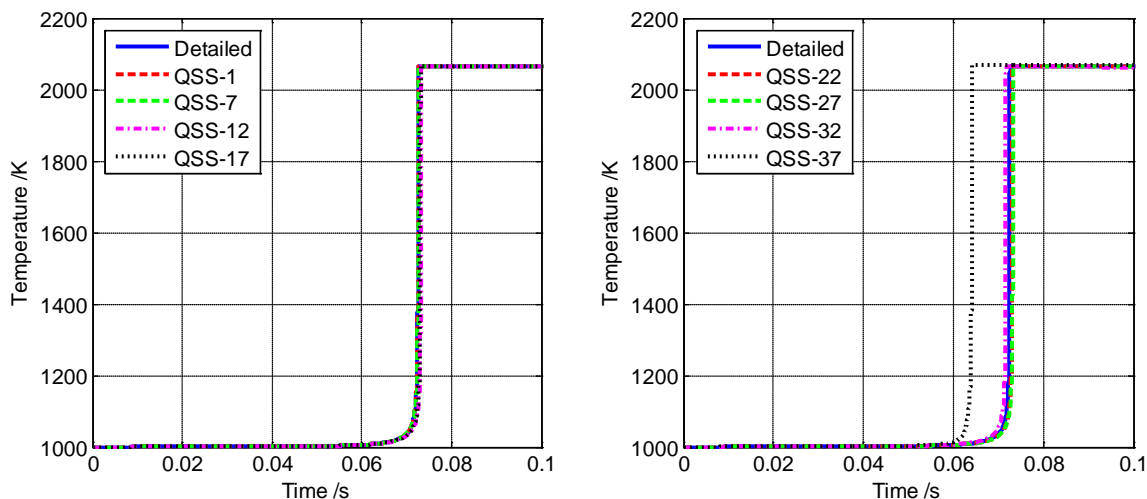


**Figure 3.4** Temperature profiles obtained by applying QSSA with different QSS species selections.

Initial temperature at 1000 K and pressure at 9.6 atm, equivalence ratio is 0.5

Furthermore, the adiabatic PFR simulations using dual-mechanism QSSA implementation with different QSS species selections are performed. Combustion for fuel lean methane/air mixture with equivalence ratio 0.5 is calculated with initial temperature at 1000 K and constant pressure 9.6 atm. Eight groups of selected QSS species as listed in Table 3.1 are all tested. A typical flux cutoff value of 99% in the on-the-fly reduction is used. The temperature profiles as well as species concentration profiles are illustrated in Figure 3.4 and Figure 3.5, with left-hand side columns showing results with 1, 7, 12, and 17 QSS species, and right-hand side columns showing results with 22, 27, 32, and 37 QSS species, respectively. Except for the case with 37 QSS species, it is observed that the results obtained using the dual-mechanism QSSA implementation exhibit satisfactory agreement compared to the profiles obtained using the detailed mechanism without the application of QSSA. However, for the case with 37 QSS species, there is an obvious departure of the predicted ignition timing as well as species concentrations from the detailed mechanism predictions. Also, this 37-species selection does not correctly capture

the species profiles in the isothermal PFR case both in ref. (Montgomery et al., 2006) and in our tests. This is because too many QSS species are assumed in the calculation while some of them are actually not good candidates to be approximated by the quasi-steady state. We can see from Table 3.1 that the 37 QSS species, already about two thirds of the total species, even include O, OH, and H<sub>2</sub>O<sub>2</sub> which are actually quite actively reacting species in the reaction network and should have production rates much greater than zero during the calculation. Therefore, assuming these species as quasi-steady state will result in amplified errors due to the inappropriate approximations.

By conducting the above validation work, the effectiveness of the QSS species selections we obtained in the literature is tested, and the dual-mechanism technique we proposed to implement the QSSA in our mechanism reduction framework is validated. Having verified the QSS species selection as well as the QSSA implementation, we are then able to integrate the flux-based on-the-fly reduction with the QSSA implementation to build the complete hybrid reduction algorithm, which are demonstrated in the following subsections. Since using too many QSS species will deteriorate the simulation results, we will limit the number of QSS species in the demonstrations.

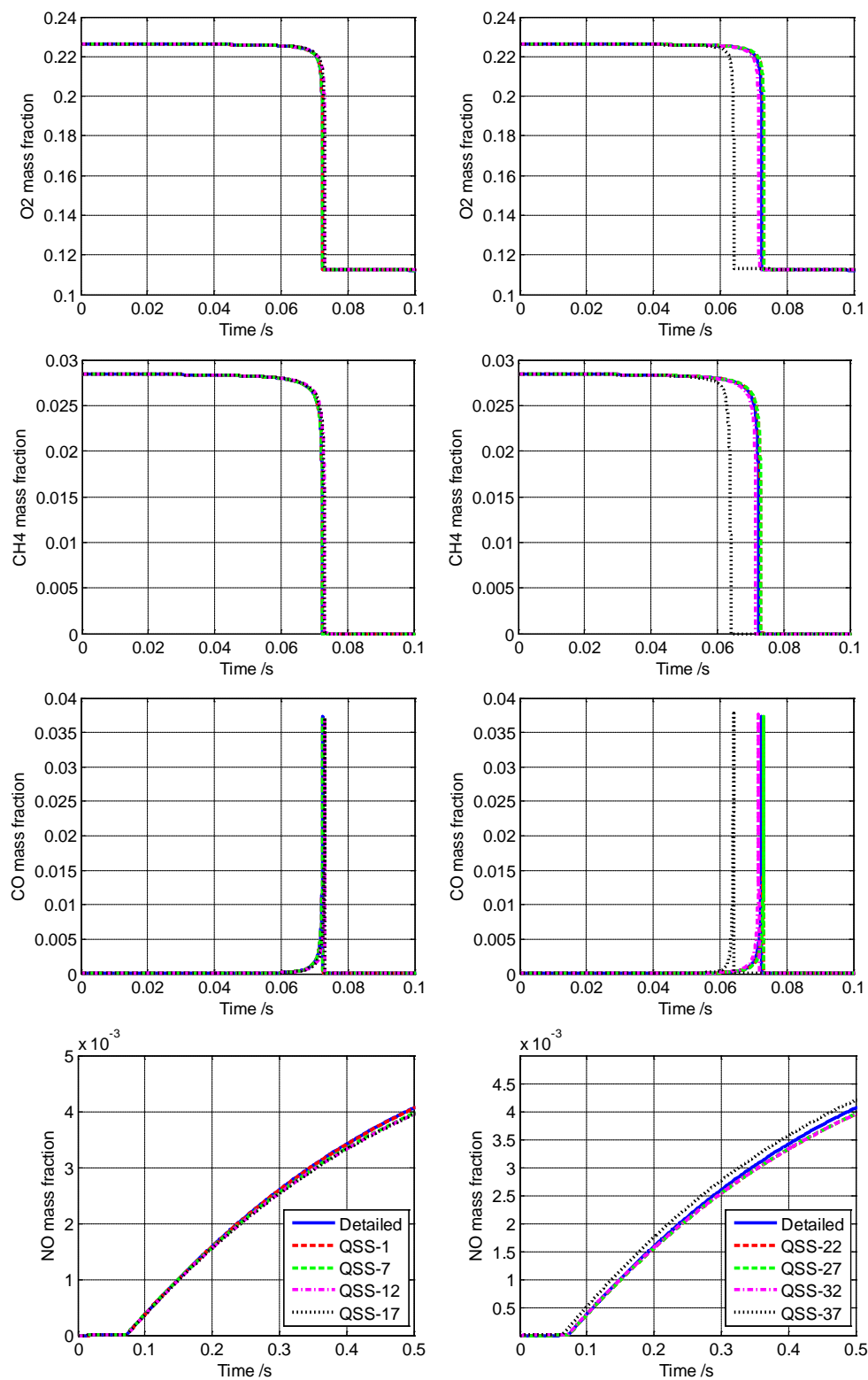


**Figure 3.5** Species mass fractions profiles obtained in the PFR simulations with different QSS species selections. Initial temperature at 1000 K and pressure at 9.6 atm, equivalence ratio is 0.5.

### 3.3.2 Demonstration in PFR model

On the basis of the verified QSSA implementation, the hybrid mechanism reduction scheme is established by integrating the on-the-fly reduction for the non-QSS species with QSSA application. Element flux analysis is performed to determine the active non-QSS species at each time step. The integration and the resulting hybrid reduction algorithm are first demonstrated in an adiabatic PFR model with various reaction conditions. PFR simulations are relatively easy and low cost in terms of computation, which allow us to quickly test the applicability of the QSSA with different selections of QSS species and to study the feasibility of hybrid reduction for a wide range of conditions.

PFR model calculation is first performed using the same condition as in the validation for QSSA implementation, i.e. initial temperature 1000 K, constant pressure 9.6 atm, and lean methane-air mixture with equivalence ratio 0.5. The flux cutoff value used for these simulations is still the typical value 99%, which has been suggested in our previous work about the on-the-fly reduction (He et al., 2010b). The time step size is automatically determined by the ODE solver DVODE, and the absolute and relative error tolerance of the ODE solver are set to 1.0E-12 and 1.0E-4, respectively. Four QSS species selections with 1, 7, 12, and 17 QSS species are employed in the hybrid mechanism reduction scheme. As mentioned before, we choose to use selections with relatively smaller number of QSS species because too many species assumed at quasi-steady state will deteriorate the results due to excessive inappropriate QSSA assumptions imposed to the reaction system, thus make less sense for the evaluations of the mechanism reduction algorithm. On the other hand, 17 QSS species, which is about one

third of the species in the detailed mechanism, already reduce the mechanism size considerably solely by applying global QSSA and are adequate for the demonstration of the hybrid reduction scheme. The temperature profiles for these simulations are shown in Figure 3.6 and compared to the result from simulation using the detailed mechanism. Satisfactory agreement in the temperature predictions is achieved for all the QSS species selections.

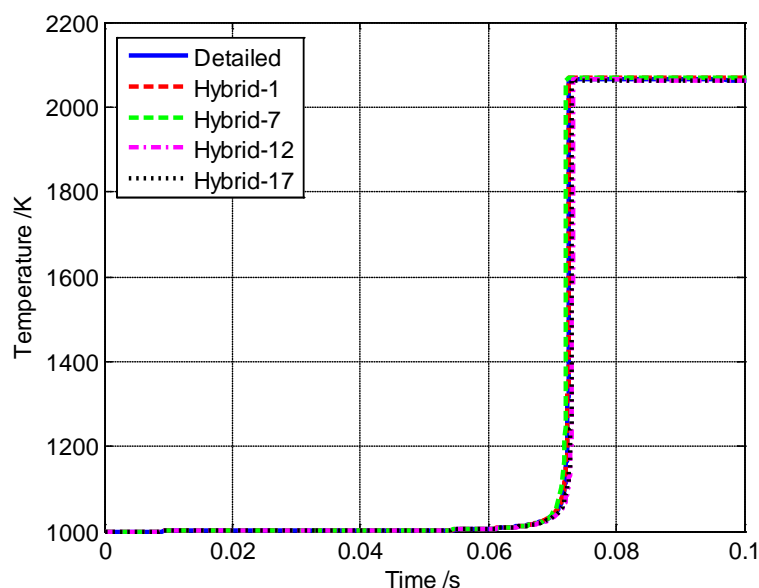


**Figure 3.6** Temperature profiles obtained in adiabatic PFR model with different QSS species selections. Initial temperature at 1000 K and pressure at 9.6 atm, equivalence ratio is 0.5

In addition, to test the proposed hybrid reduction scheme for various conditions, the ignition delay time predicted with different initial temperature and pressure is calculated in the PFR model for each QSS species selection. The tested temperature ranges from 950 K to 1350 K, which covers the typical medium and high temperature regions that the GRI-Mech 3.0 mechanism is suitable for. And the tests are repeated at constant pressure of 9.6 atm and 30.0 atm, respectively. The ignition delay data calculated in these tests are plotted in Figure 3.7. It is shown that for both pressure conditions, the ignition delay time

curve predicted using hybrid reduction scheme with each QSS species selection are almost identical and excellently matches the detailed mechanism simulation results. The results imply that the global QSSA applied on the selected QSS species is a good approximation for a wide range of conditions. It is also illustrated that given an appropriately selected QSS species set, the hybrid mechanism reduction scheme is able to accurately capture the essential characteristics of combustion process under various reaction conditions. The demonstration in PFR model provides us the faith of applying the hybrid reduction approach in more complex reactive flow models.

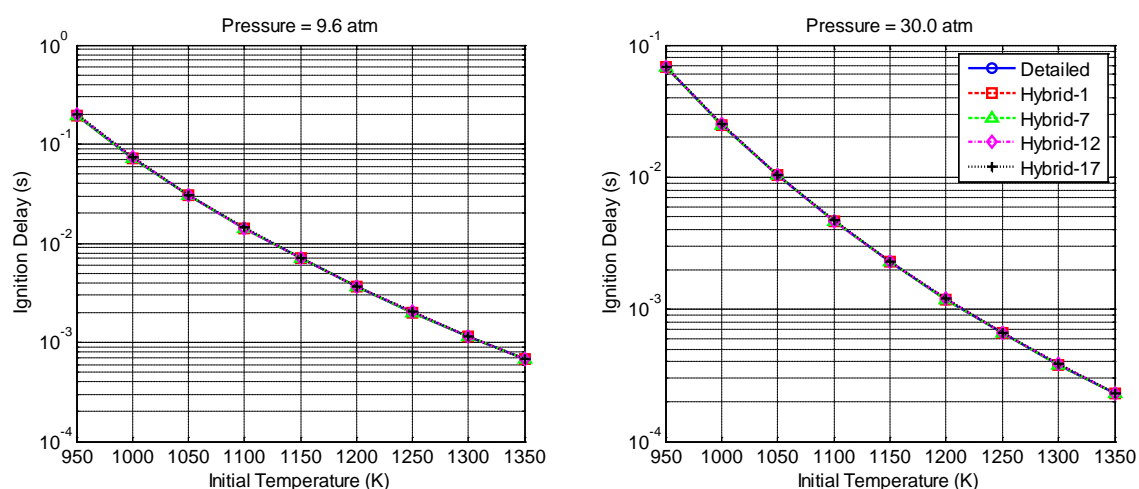


**Figure 3.7** Ignition delay timing predicted in PFR with different QSS species selections. Initial temperature from 950 K to 1350 K, pressure at 9.6 atm (left) and 30.0 atm (right)

### 3.3.3 Demonstration in HCCI engine CFD model

The hybrid reduction scheme is then demonstrated in a homogeneous charge compression ignition (HCCI) engine CFD model using KIVA-3V. The homogeneous charge in this model eliminates the effect of fuel physical properties on the fuel-air mixing. Therefore, the engine combustion process is primarily dominated by the chemistry, and the kinetic characteristics are directly reflected in the simulation results. The engine simulations run

from crank angle (CA)  $-30.0^\circ$  after top dead center (ATDC) to  $30.0^\circ$  ATDC. Again, fuel lean methane-air mixture with equivalence ratio 0.5 is used. Similar to the settings for PFR model, a 99% flux cutoff is applied for the on-the-fly reduction, and the timestep size is automatically determined by the ODE solver DVODE. The absolute error tolerance  $1.0\text{E-}12$  and relative error tolerance  $1.0\text{E-}4$  are used for the integration. The same four QSS species selections with 1, 7, 12, and 17 species used in the PFR model demonstration are employed again in the CFD simulations in KIVA-3V. The engine specifications and operation parameters are summarized in Table 3.2. The engine CFD model will help us test the hybrid reduction algorithm in a more rigorous reactive flow environment.

**Table 3.2** Engine specifications and operation parameters used in KIVA

<b>Parameter</b>	<b>Value</b>
Bore diameter /cm	13.716
Stroke /cm	16.51
Compression ratio	16:1
Engine speed /rpm	900
Initial temperature /K	1000
Initial pressure /MPa	10
Equivalence ratio	0.5
Crank angle range /ATCD	$-30^\circ \sim 30^\circ$

The temperature and pressure profiles captured by the hybrid scheme for each QSS species selection are presented in Figure 3.8, and are compared with the results obtained using detailed mechanism as well as only applying QSSA. The departure between results

from detailed mechanism simulations (solid lines) and from simulations only applying QSSA (dash lines) reflects the error introduced by the application of QSSA, or, more precisely, by the assumption of the QSS species. Whereas the departure between the results of simulations only applying QSSA (dash lines) and results from hybrid reduction scheme (dotted lines) reflects the additional error actually introduced by the hybrid reduction scheme given a set of selected QSS species. In Figure 3.8, if we compare the results from detailed mechanism and from only applying QSSA, it is shown that the temperature and pressure curves for 1 and 7 QSS species cases are perfectly predicted compared to the detailed mechanism results, while for the 12 and 17 QSS species cases, the profiles depart from the detailed mechanism results a little but still reflect reasonable in-cylinder temperature and pressure variations. Also, if we compare the results from hybrid scheme and from only applying global QSSA without the flux-based reduction, we can find that the profiles (dotted lines and corresponding dash lines) are identical for all the cases. Therefore, the departure from the detailed mechanism in the results is mainly attributed to the assumption of global QSS species other than the hybrid reduction algorithm. In other words, if we can improve the selection of the QSS species, the hybrid scheme will produce better results with excellent accuracy. Moreover, the ignition timing, which is an important engine design and operation parameter especially for HCCI engines, is accurately predicted by the hybrid scheme in all cases. These results suggest that the hybrid reduction scheme works well in predicting important HCCI engine operation and fuel combustion characteristics.

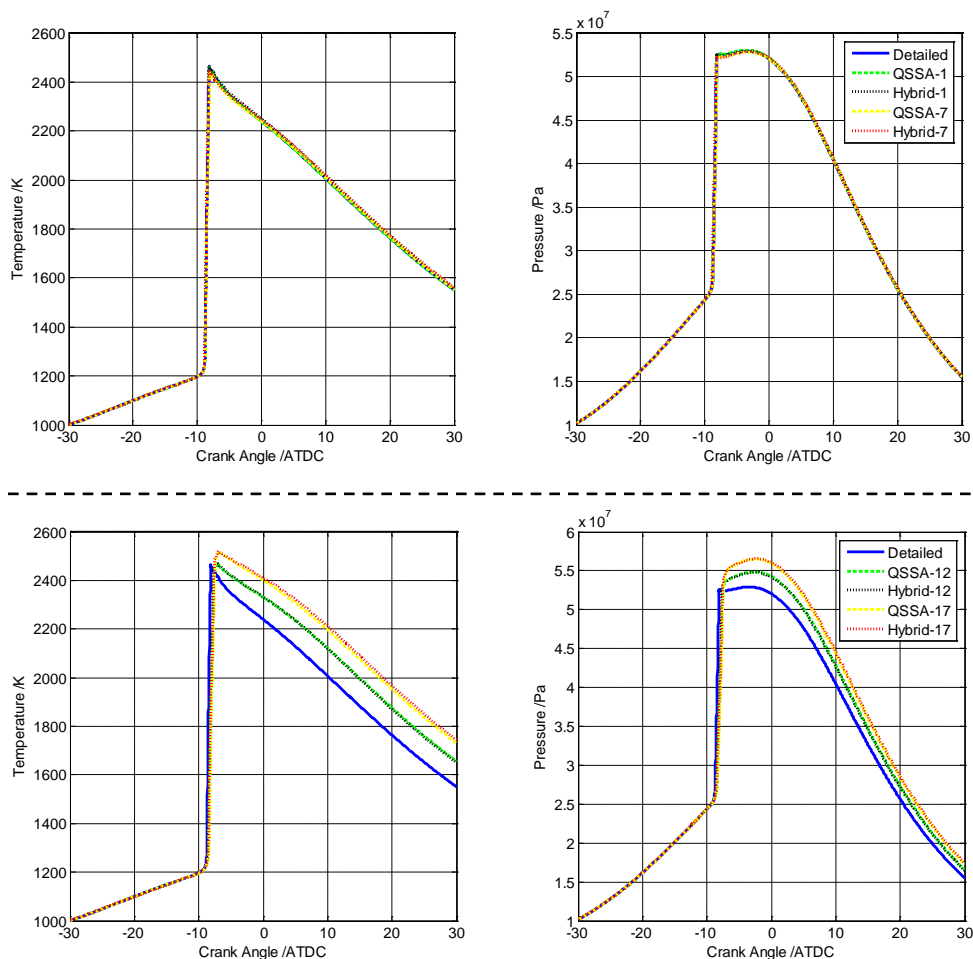


**Figure 3.8** Temperature and pressure profiles obtained in KIVA engine simulations with 1, 7, 12, and 17 QSS species

In addition, selected important species profiles obtained in each case above are shown in Figure 3.9. For the major species methane,  $O_2$ ,  $CO$ , and  $CO_2$ , the concentration profiles are well captured by the hybrid scheme. There is some deviation for the  $CO$  and  $CO_2$  profiles, but similar situation for the error control can be observed that the deviation of the results compared to the detailed mechanism simulations are mainly related to the assumption of selected QSS species in all the four cases since the dotted lines (hybrid reduction) and corresponding dash lines (only applying QSSA) are very identical.

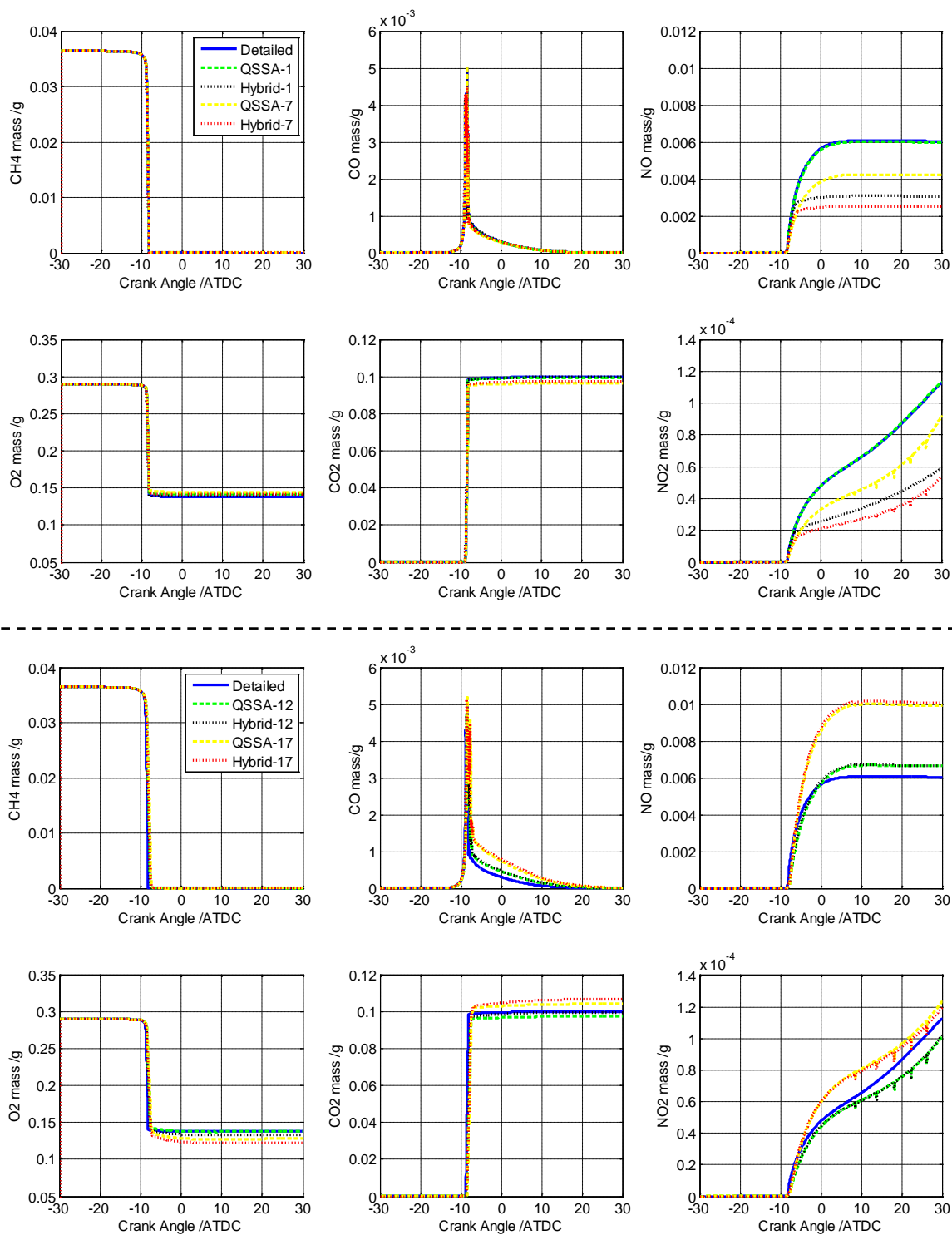


**Figure 3.9** Selected species composition profiles obtained in KIVA engine simulations with 1, 7, 12, and 17 QSS species

For the two nitrogen species NO and NO<sub>2</sub>, it is observed that the deviation of the profiles compared to the detailed mechanism results is related to both QSS species selection and the element flux analysis procedure in the hybrid reduction scheme. In Figure 3.9, we observe better agreement between results from hybrid reduction (dotted lines) and only applying QSSA (dash lines) in the 12 and 17 QSS species cases; while in the cases with 1 and 7 QSS species, some differences in the profiles obtained from the hybrid reduction and only applying QSSA are observed. Such results are actually related to the multi-element flux analysis (He et al., 2009a; Zhang et al., 2012) procedure we performed when applying on-the-fly reduction. Due to different magnitudes of flux values for different elements, the carbon flux analysis and nitrogen flux analysis have to be performed separately so that the active C-bearing and N-bearing species can both be identified. However, since the nitrogen reaction network in GRI-Mech 3.0 is relatively small (18 species with nitrogen element), the active N-bearing non-QSS species set identified by applying flux cutoff will be very small. As shown in Figure 3.10, it can be seen that in the case with only 1 QSS species, we have only 5 N-bearing non-QSS species involved in the calculation, while there is no N-bearing QSS species since the only QSS species in this case is C<sub>2</sub>H<sub>3</sub>. Therefore, in this case we are using at most 5 species out of the total 18 N-bearing species to predict the nitrogen network. In the case with 12 QSS species, although there are only 3 active N-bearing non-QSS species identified, but there are still another 8 N-bearing QSS species involved, so we have totally 9 to 11 N-bearing species involved in the nitrogen network calculations. Since more species information is included in the simulations, we obtain better results in the 12 QSS species case compared to the 1 QSS species case.

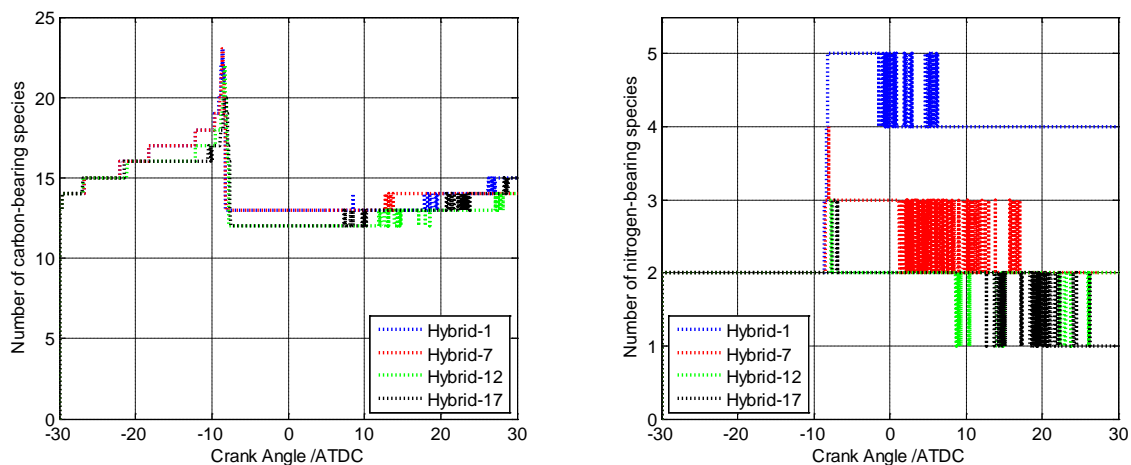


**Figure 3.10** Number of active C-bearing and N-bearing non-QSS species identified during KIVA-3V engine simulations

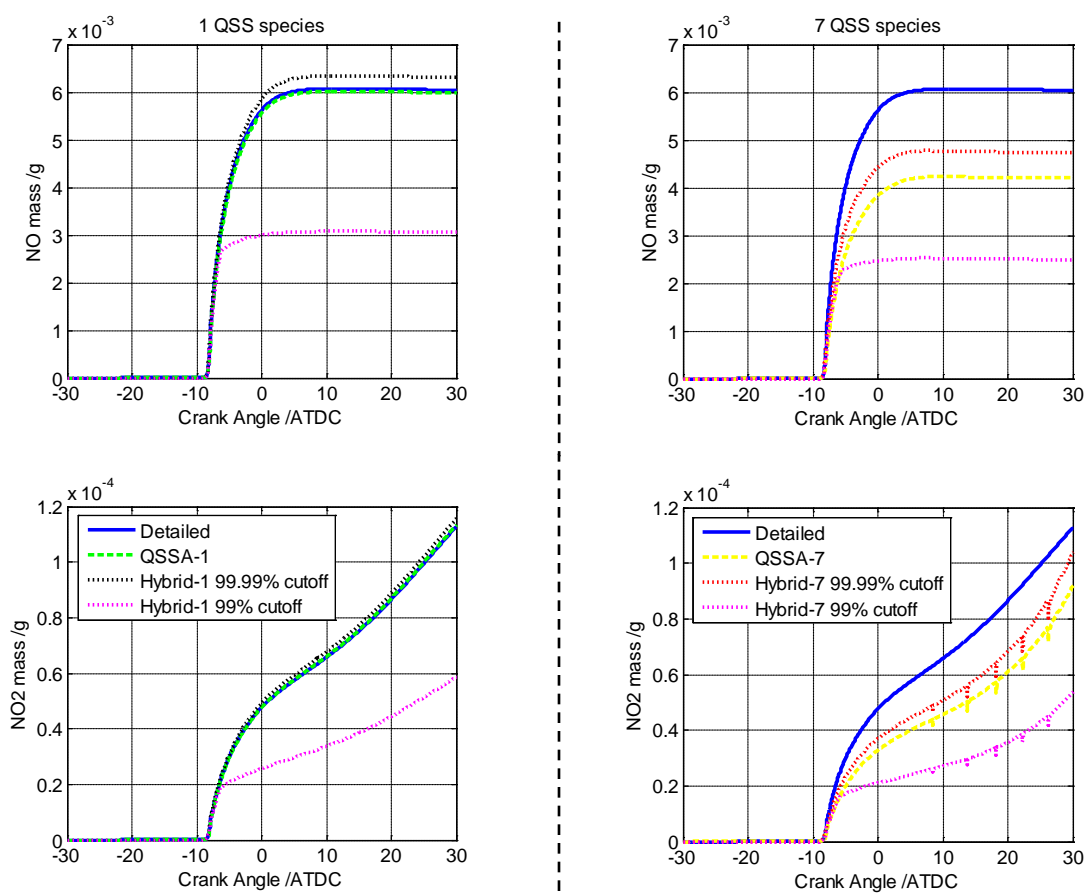


**Figure 3.11** Improvement of NO and NO<sub>2</sub> species concentration profiles by increasing cutoff value from 99% to 99.99%

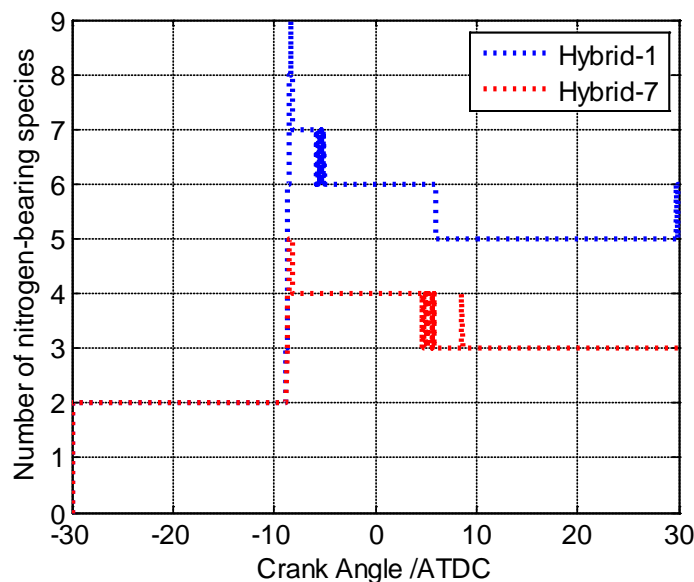


**Figure 3.12** Number of nitrogen-bearing species during the simulations with higher nitrogen flux cutoff 99.99%

On the other hand, the nitrogen flux cutoff also affects the agreement between results from hybrid reduction and from only applying QSSA. If a higher cutoff value is applied in the nitrogen flux analysis, better results can be obtained for species NO and NO<sub>2</sub>. As an example, Figure 3.11 shows the NO and NO<sub>2</sub> concentration profiles obtained by using nitrogen flux cutoff 99.99% versus 99% for cases with 1 and 7 QSS species. As shown in the figure, for both of the two cases, the deviation between the profiles obtained from only applying QSSA and from the hybrid reduction scheme, which is introduced by the application of on-the-fly reduction, is smaller with the higher flux cutoff value 99.99%. Correspondingly, it is observed in Figure 3.12 that more active N-bearing non-QSS species are retained during the simulations for both cases, indicating that the higher cutoff value does lead to more active species in the reduced mechanism and thus better accuracy in the simulation results. For nitrogen species network in GRI-Mech 3.0 mechanism with only 18 species, the retention of even only one or two more species in the reduced

mechanism will have obvious impact on the model simulation. Therefore, choosing an appropriate flux cutoff value in the element flux analysis is important for the hybrid reduction scheme, especially when the reaction network is small. In our previous work (He et al., 2010b), we have suggested that the flux cutoff value should be chosen by experience or preliminary studies, and a 99% cutoff is usually adequate to produce effective mechanism reduction with satisfactory accuracy. For the smaller nitrogen network in GRI-Mech 3.0 mechanism, however, it is reasonable to use a slightly higher cutoff value since the computation would not be increased too much with several more species but the accuracy is significantly improved with the higher cutoff value.

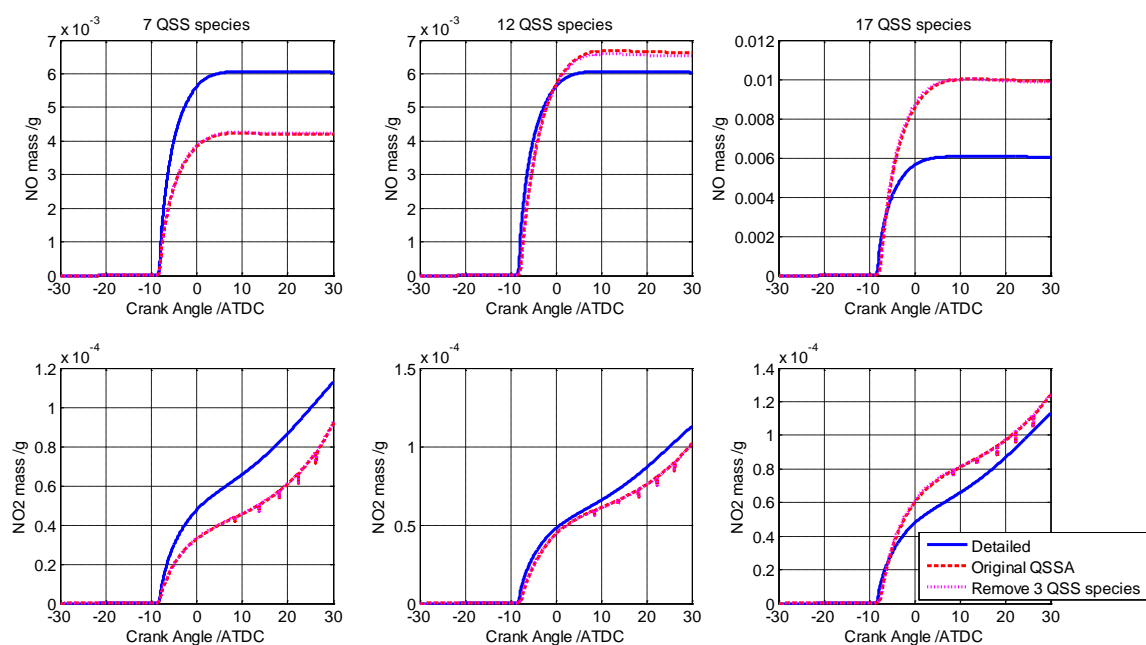


**Figure 3.13** Comparison of the QSSA assumption of species in nitrogen reaction network

We also examined the QSS species assumption of the nitrogen reaction network. As seen in Table 3.1, the assumed QSS species in cases with 7 or more QSS species include some slow-reacting species, such as HNO, HNCO, and NCO, which may have great impact on the prediction of prompt NO under HCCI engine conditions. In order to check

the QSS species assumption with for these species, we performed simulations only applying QSSA and excluding HNO, HNCO, and NCO from the QSS species lists. The results of NO and NO<sub>2</sub> predictions for the 7, 12, and 17 QSS species cases are shown in Figure 3.13 (purple dotted lines) and compared to the original results only applying QSSA (red dash lines). It is shown that the two profiles are almost identical and the assumption of QSS species is not significantly improved if HNO, HNCO, and NCO are excluded under the current conditions. Even though, the ability of the algorithm to avoid eliminating certain important species is still necessary. In the hybrid scheme, we do have such ability in the flux-based on-the-fly reduction procedure to specify particular species that should not be eliminated during the simulation. Also, we should also take into account such ability in the development of QSS species selection approaches to detect and avoid inappropriate assumption of QSS species.

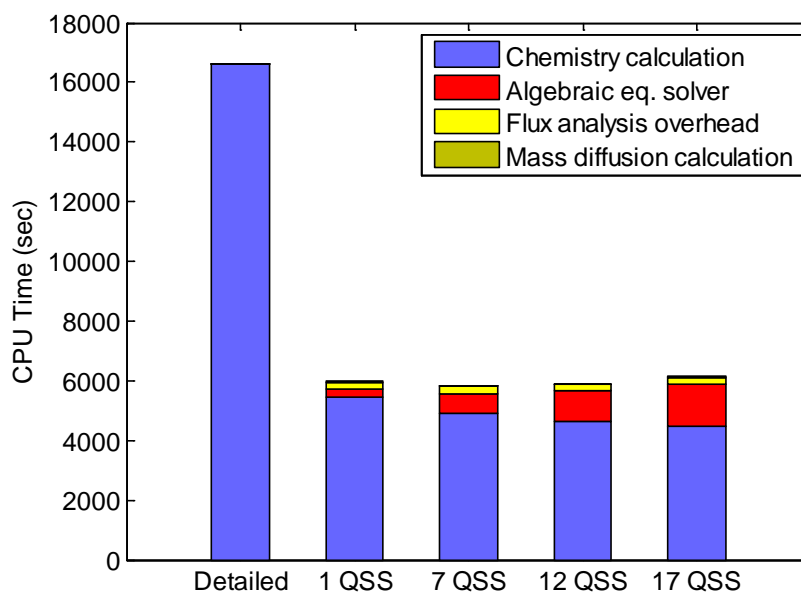


**Figure 3.14** CPU time of the hybrid reduction simulations in KIVA-3V

In addition, the CPU time for the hybrid reduction simulations with different number of selected QSS species is tracked and shown in Figure 3.14. We find that the total CPU

time of all the simulations using hybrid reduction scheme is significantly reduced compared to the detailed mechanism simulation. We also observe that the CPU time spent on chemistry calculations is further reduced as more QSS species are assumed, which is expected under our algorithm design since we have less non-QSS species considered in the flux based on-the-fly reduction when we assume more QSS species. The CPU time results suggest that the hybrid reduction scheme is able to effectively reduce the computational cost. At the same time, we also notice two problems that worth further study and improvement. First, we may notice that the CPU time for mass diffusion/transport calculation is hardly visible in the figure due to very small values, although the transport calculation does cost less CPU time when more QSS species are assumed. This is because the transport calculation we used in the HCCI model is quite easy and takes much shorter time compared with chemistry calculations. Therefore, we are now working on a case study with much more complicated transport calculation in order to further explore the benefit of hybrid reduction scheme on the transport reduction. Another observation is that as more QSS species are assumed, the computation needed for solving the algebraic equations also increases. In order to control the algebraic equation solver overhead, speedy solution algorithm of nonlinear algebraic equations is needed, which is also the future direction of this work. Overall, the computational intensity is significantly reduced using the hybrid reduction scheme, and the proposed framework can be further applied to address transport-intensive computations.

### 3.4 Summary

In this chapter, a hybrid mechanism reduction scheme based on the on-the-fly reduction and global quasi-steady-state approximation is proposed. The methodology is demonstrated in both PFR model and multidimensional HCCI engine CFD calculations with detailed GRI-Mech 3.0 methane mechanism and optimally selected QSS species sets. The demonstration results present satisfactory performance of the proposed hybrid reduction scheme. The temperature, pressure, and species concentrations profiles under various reaction conditions are well captured with reasonable agreement compared to the detailed mechanism simulations. With up to one third of the total species assumed as quasi-steady state and excluded in the transport calculation, the hybrid reduction framework is also able to capture important combustion characteristics such as ignition delay time with excellent accuracy. Moreover, by applying global QSSA, the number of species involved in transport calculation is significantly reduced, and highly efficient chemistry calculation is still maintained by coupling the element flux based on-the-fly reduction with the global QSSA. The proposed computational framework combines the advantages of both global QSSA method and dynamic on-the-fly reduction approach, and can be applied with faith to address reactive flow problems with complex chemical kinetic models and wide range of reaction conditions.

## Chapter 4

### Hybrid reduction scheme with flux-based QSS species selection

#### 4.1 Selection of quasi-state-state species based on element flux

In this chapter, we will further discuss the applicability of the hybrid reduction scheme in reactive flow simulations with more complex fuel oxidation chemistry. In the application of QSSA, a critical issue is the identification of QSS species. Although there are already several approaches for the selection of QSS species (see section 3.1), the selection procedure requires complex time scale analysis or iterative optimization algorithm, which is not a trivial task. In this work, in order to demonstrate the hybrid reduction scheme with more complex chemistry in a simple way, we are first trying to establish a relatively simple procedure for the quick selection of global QSS species to be assumed in the hybrid reduction scheme.

Recall that in section 1.3 we have introduced the total instantaneous flux for species computed by Eq. (1) and Eq. (2). Since the instantaneous flux reflects the dynamic activity of species in the system, we are thinking to take advantage of the element flux to identify global QSS species. The underlying assumption of qualified global QSS species is that the net production rate can always be approximated by zero during the entire simulation. To evaluate the production and consumption of each species based on element flux, we propose the concept of influx and outflux of each species at a transient time point. As shown in Eq. (9), the influx of a species  $j$ , denoted as  $\bar{A}_j^m$ , is defined as the summation of the total instantaneous flux from all other species to species  $j$ .

Similarly in Eq. (10), the outflux of a species  $j$ , denoted as  $\bar{A}_j^{out}$ , is defined as the summation of the total instantaneous flux from species  $j$  to all other species.

$$\bar{A}_j^{in}(t) = \sum_{k \neq j} \bar{A}_{kj}(t) \quad (9)$$

$$\bar{A}_j^{out}(t) = \sum_{k \neq j} \bar{A}_{jk}(t) \quad (10)$$

If the total instantaneous fluxes between all the possible species pairs are stored in a  $n \times n$  matrix  $\mathbf{A}_{n \times n}$  (where  $n$  is the total number of species), in which the entry in the  $j^{\text{th}}$  row and  $k^{\text{th}}$  column is the flux from species  $j$  to  $k$ , i.e.  $\bar{A}_{jk}(t)$  in Eq. (2). The influx of species  $j$  defined above is then the summation of all the entries except for the diagonal entry in the  $j^{\text{th}}$  column of matrix  $\mathbf{A}_{n \times n}$ , while the outflux of species  $j$  is the summation of all the entries except for the diagonal entry in the  $j^{\text{th}}$  row of matrix  $\mathbf{A}_{n \times n}$ . The influx and the outflux reflect the total production and consumption of the species, respectively, and thus can be used to represent the transient activities of species. We further define the net flux  $\bar{A}_j^{net}(t)$  for a species, which is given by Eq. (11) as the absolute difference of the values of influx and outflux.

$$\bar{A}_j^{net}(t) = abs\left(\left|\bar{A}_j^{in}(t)\right| - \left|\bar{A}_j^{out}(t)\right|\right) \quad (11)$$

Based on the above definition, if the value of a species net flux  $\bar{A}_j^{net}(t)$  is close to zero, it indicates that the production and consumption activities of the species is roughly in a equilibrium, suggesting the species is potentially in a quasi-steady state. Based on the above assumption, we establish a simple procedure to quickly identify potential QSS species. In the element flux analysis calculation, we compute the net flux for each species

at each time point. The maximum value of the net flux of each species over all the time points is then obtained. If the maximum net flux for a species is a very small value, then the net flux of the species is always smaller than that value throughout the entire simulation. We then claim that those species with relatively smaller maximum net flux values are more likely to be appropriate candidates of global QSS species.

The purpose of introducing the flux-based QSS species selection is to quickly identify some appropriate QSS species for the evaluation of hybrid reduction scheme. Although the flux-based QSS species selection may not be strictly validated from mathematical point of view, we just employ the flux-based selection as a simple substitute of the existing strict QSS species selection procedure. Once we have selected the QSS species, similar computational framework of hybrid reduction scheme as described in Chapter 3 is employed to demonstrate the performance of the selected QSS species as well as the hybrid reduction algorithm.

#### 4.2 Demonstration of hybrid scheme with flux-based QSS species selection

To demonstrate the procedure of the proposed QSS species selection method, two detailed mechanisms are used, namely the methane mechanism GRI-Mech 3.0 with 53 species and 325 reaction and the *n*-heptane mechanism with 161 species and 1540 reactions. A zero-dimensional plug-flow reactor (PFR) model and a two-dimensional homogeneous charge compression ignition (HCCI) engine CFD model are employed to evaluate the performance of the selected QSS species. KIVA-3V code is used to handle the CFD calculations with a two-dimensional computational mesh of about one thousand cells at the bottom dead center (as shown in Figure 2.1).

### 4.2.1 Demonstration with methane mechanism GRI-Mech 3.0

The hybrid reduction scheme with flux-based QSS species selection is first demonstrated on a detailed methane mechanism GRI-Mech 3.0. The PFR model is used for the element flux analysis during the selection process. For demonstration, a constant-pressure simulation with initial temperature 1000K is conducted, and stoichiometric methane/air mixture is used. The detailed mechanism is used in this simulation without any reduction, and element flux analysis is performed to compute the influx and outflux for each species at every time point. As mentioned in section 4.1, the net flux of each species is computed and tracked during the simulation. Based on our assumption, species with smaller maximum net flux values are considered closer to the quasi-steady state than those species with larger net flux values.

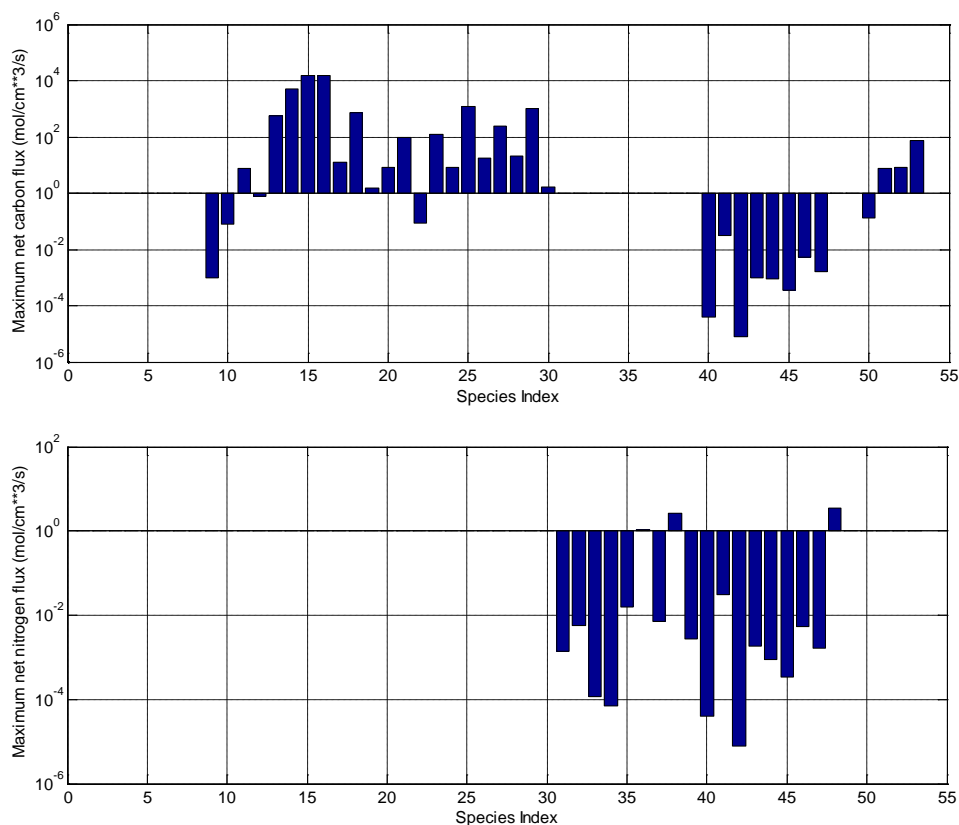


**Figure 4.1** Maximum net flux for species

To compare the maximum net flux for all the species in the detailed mechanism, the maximum values of the net carbon flux and net nitrogen flux during the simulation for each species are plotted in Figure 4.1. We treat carbon-bearing species and nitrogen-bearing species separately since the values of nitrogen flux are much smaller than the carbon flux due to the smaller nitrogen species reaction rates. Therefore, it is not reasonable to compare the maximum net flux for carbon element and nitrogen element together. From Figure 4.1, the species with small value of maximum net carbon flux and maximum net nitrogen flux can be easily identified respectively. These species are considered potential candidates of global QSS species based on our assumption. As an example, four different selections with 2, 7, 12, and 15 QSS species are selected according the value of maximum net flux, which are in the combination of both carbon-bearing and nitrogen-bearing species as listed in Table 4.1.

**Table 4.1** QSS species selections for GRI-Mech 3.0 mechanism

QSS species	C-species	N-species
2	C(9)	H <sub>2</sub> CN(42)
7	C(9), CH(10), C <sub>2</sub> H(22), C <sub>3</sub> H <sub>7</sub> (50)	H <sub>2</sub> CN(42), CN(40), NH <sub>3</sub> (34)
12	C(9), CH(10), C <sub>2</sub> H(22), C <sub>3</sub> H <sub>7</sub> (50), CH <sub>2</sub> (S)(12), CH <sub>2</sub> OH(19), HCCOH(30)	H <sub>2</sub> CN(42), CN(40), NH <sub>3</sub> (34), NH <sub>2</sub> (33), HOCN(45)
15	C(9), CH(10), C <sub>2</sub> H(22), C <sub>3</sub> H <sub>7</sub> (50), CH <sub>2</sub> (S)(12), CH <sub>2</sub> OH(19), HCCOH(30), CH <sub>2</sub> (11), C <sub>2</sub> H <sub>3</sub> (24)	H <sub>2</sub> CN(42), CN(40), NH <sub>3</sub> (34), NH <sub>2</sub> (33), HOCN(45), HCNO(44)

Before testing the selected QSS species in reactive flow simulations, we first compare our selections with some existing selections in the literature. For example, Lu and Law (Lu and Law, 2008a) identified several QSS species for GRI-Mech 3.0 mechanism using CSP method (only carbon species are considered in their work), which are C(9), CH(10),

$\text{CH}_2(11)$ ,  $\text{CH}_2(\text{S})(12)$ ,  $\text{HCO}(17)$ ,  $\text{CH}_2\text{OH}(19)$ ,  $\text{CH}_3\text{O}(20)$ ,  $\text{C}_2\text{H}_3(24)$ ,  $\text{C}_2\text{H}_5(26)$ ,  $\text{HCCO}(28)$ ,  $\text{CH}_2\text{CHO}(52)$ . We can see that there is some overlap species, as marked bold in Table 4.1, between their selection and our selection. If we select more QSS species based on Figure 4.1 results, addition species such as  $\text{CH}_3\text{O}(20)$ ,  $\text{CH}_2\text{CHO}(52)$ ,  $\text{HCO}(17)$ ,  $\text{C}_2\text{H}_5(26)$ ,  $\text{HCCO}(28)$  will be selected, which suggests that the flux-based QSS selection is able to roughly identify similar QSS species as in existing literature in a relatively simpler way.

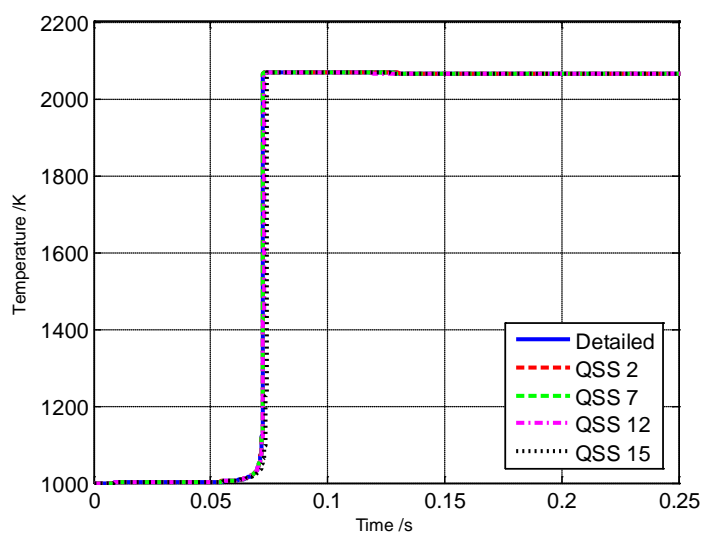


**Figure 4.2** PFR simulation with application of QSSA

To test the validity of the above selected QSS species, simulations with only the application of QSSA are first conducted in PFR and engine CFD model. Same initial temperature 1000 K and stoichiometric fuel/air composition are used in the simulations. All the non-QSS species concentrations are solved by the system of ODEs, while all the QSS species concentrations are obtained via a set of algebraic equations by replacing the right-hand side of their original ODEs with zero. The results of the PFR simulations using the four different QSS species selections are shown in Figure 4.2. The temperature profiles with the application of global QSSA for all the four selections are in good

agreement with the profile produced by the detailed mechanism. The net production rates for the selected 15 QSS species are calculated in a PFR simulation with detailed mechanism to further verify the goodness of the QSS species assumptions. If the selected species are good QSS species candidates, the net production rates should be close to zero so that it is appropriate to approximate the rates by zero under QSSA. Figure 4.3 shows the calculated net production rates for selected QSS species plotted versus temperature, compared to some major non-QSS species. The first row shows net production rate for three QSS species that are in common with Lu and Law's selection. The second row shows three different QSS species that we selected. And the third row shows the rates for major non-QSS species to compare the magnitude of the rate values. It is seen that the net production rate for the selected QSS species are much smaller and very close to zero, indicating that the general assumption for species in quasi-steady state is satisfied.

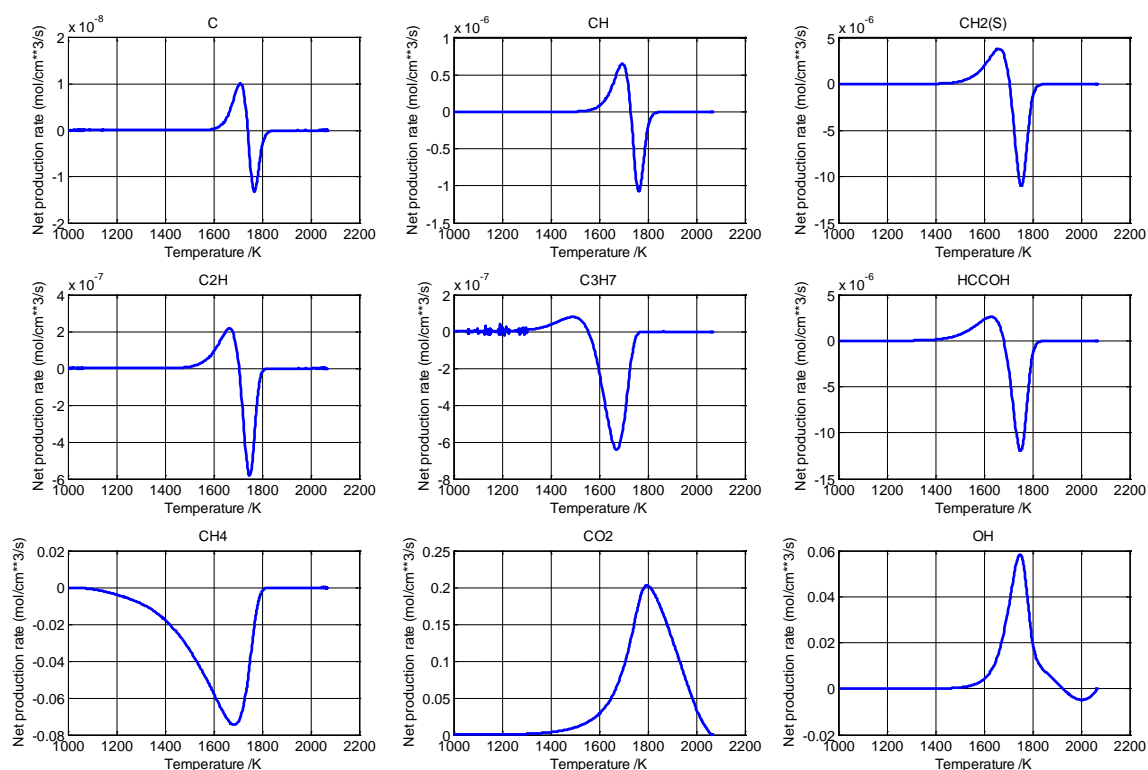


**Figure 4.3** Net production rate with detailed mechanism for selected QSS species

In addition, the engine CFD simulations with only the application of global QSSA are performed in KIVA-3V with crank angle from  $-30^\circ$  to  $30^\circ$  after top dead center (ATDC). Similar conditions as in Table 3.2 are used. The in-cylinder temperature and pressure profiles obtained in KIVA-3V with the four QSS species selections are shown in Figure 4.4, compared with the result from detailed mechanism. Satisfactory agreement between the results can be observed. The above results suggest that the selected QSS species can be considered appropriate to be applied global QSSA under the tested conditions.

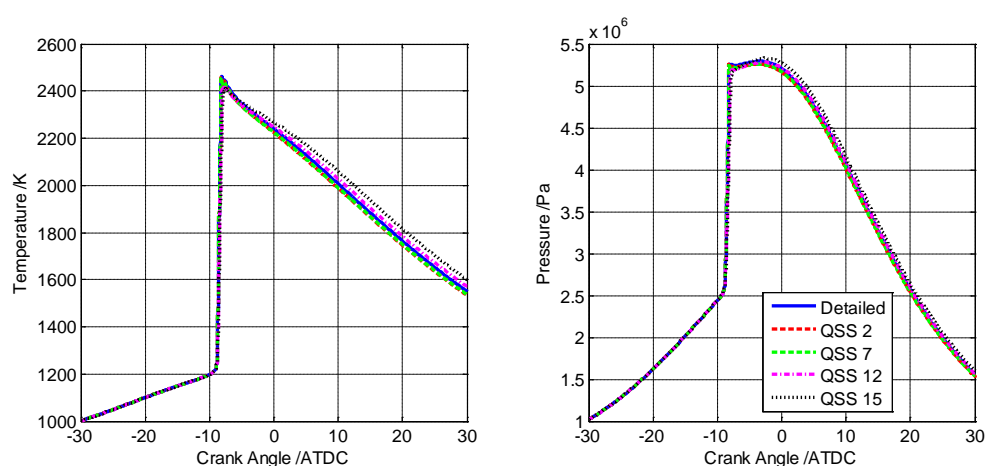


**Figure 4.4** Temperature and pressure profiles obtained in KIVA with application of QSSA

To further examine the performance of the QSS species selections, engine CFD simulations with hybrid reduction scheme are conducted using the selected QSS species. The on-the-fly reduction is integrated with the application of QSSA for the chemistry calculations, and a 99% flux cutoff is used in the on-the-fly element flux analysis. The engine simulation results for the four different selections of QSS species are compared with the results from detailed mechanism. As illustrated in Figure 4.5, the in-cylinder temperature and pressure profiles show very good accuracy compared to the detailed mechanism simulation and the on-the-fly reduction simulation.

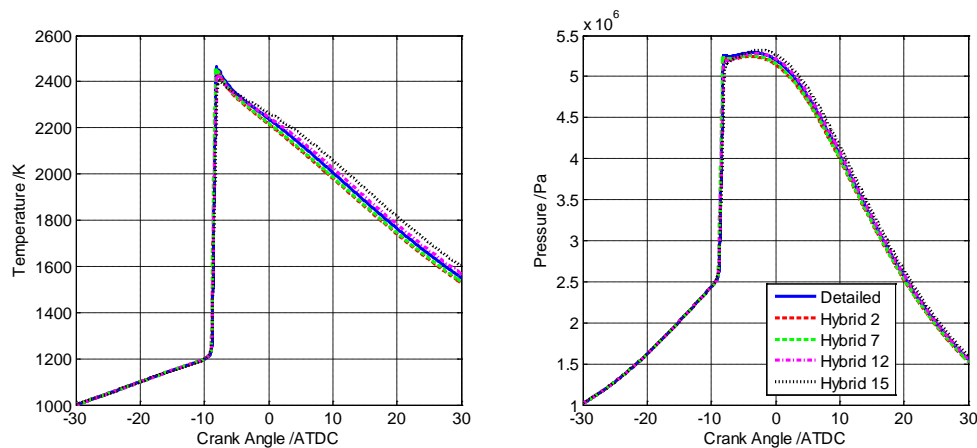


**Figure 4.5** Temperature and pressure profiles obtained in KIVA with hybrid reduction

The above results suggest that with up to 15 QSS species, which is about one third of the total number of species in the detailed mechanism, highly accurate simulation results can still be achieved by using the hybrid reduction scheme. In addition, the number of species involved in the transport calculations is significantly reduced, which is very important for some realistic multidimensional CFD simulations with very rigid limits on the number of transported species due to computational capacity. In those transport-intensive applications, the hybrid reduction scheme along with the QSS species selection procedure is a promising tool for enabling the CFD computation with the detailed reaction mechanism.

#### 4.2.2 Demonstration with *n*-heptane mechanism

The proposed hybrid reduction scheme with flux-based QSS species selection is then extended to a larger detailed mechanism with 161 species and 1540 reactions for *n*-heptane oxidation to further verify the applicability of the method. This time only the net carbon flux for each species in the mechanism is calculated in the PFR simulation using the detailed *n*-heptane mechanism since the nitrogen reaction network is not included in the mechanism. And the value of maximum net flux during the entire simulation for each

species is obtained using similar procedure. The net flux calculations are carried out for two different initial temperatures, 1000K and 800K, to cover the high temperature and low-medium temperature regions respectively. The calculated maximum net carbon flux for each species at the two initial temperatures is presented in Figure 4.6.

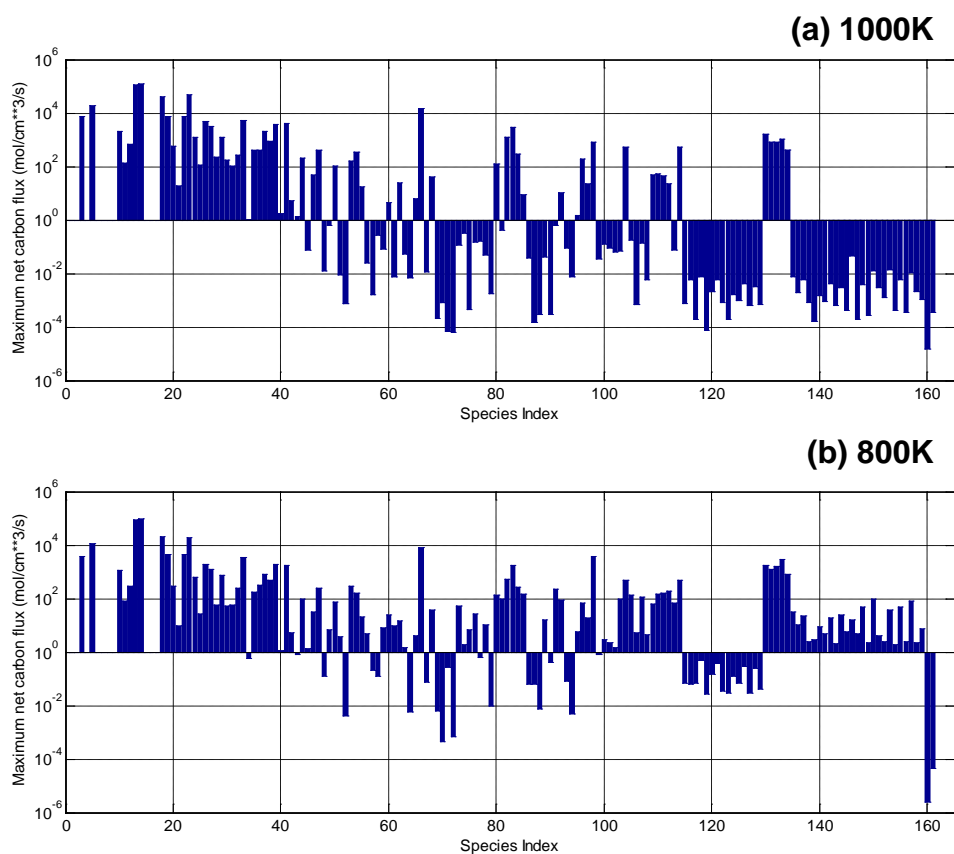


**Figure 4.6** Maximum net carbon flux for species at two different initial temperatures

To determine the appropriate QSS species, we need to find the group of species with the smallest maximum net flux values. Since this *n*-heptane mechanism does not include the species and reaction in nitrogen oxidation chemistry, we can simply use the calculated carbon flux of all the species to select potential QSS species candidates. As shown in Table 4.2, the maximum net flux for all the species are ranked in ascending order and those species with the smallest non-zero values are considered possible QSS species. The first 5, 10, 15, and 20 species as listed in Table 4.2 are selected as four different groups of

global QSS species for each temperature. From the table, we can also find that the values of maximum net flux for the selected QSS species at 1000K are generally closer to zero than those at 800K, which may imply that the assumption of the selected QSS species at 800K may not be as strong as that at 1000K. To further evaluate the performance of selected QSS species, hybrid reduction scheme using the selected QSS species is then demonstrated in the engine CFD simulations in KIVA-3V.

**Table 4.2** Selected QSS species for n-heptane mechanism at two different temperatures

Number of QSS species			1000 K		800K	
			Species	Max net flux*	Species	Max net flux*
20	10	5	c4h7o1-4	1.50E-05	c4h7o1-4	2.38E-06
			ic3h7o	6.09E-05	c5h9o1-4	4.34E-05
			nc3h7o	6.93E-05	c3h6ooh2-1	4.54E-04
			c7h14ooh1-4	7.42E-05	ic3h7o	6.80E-04
			c3h6cho-2	1.52E-04	c2h5co	4.14E-03
	15		c7h14ooh3-1o2	1.55E-04	hoch2o	4.87E-03
			c7h14ooh3-1	1.87E-04	c2h4o2h	5.86E-03
			c7h14ooh1-2	1.87E-04	c3h6ooh1-2	6.49E-03
			nc7ket23	1.94E-04	ch2ch2coch3	7.72E-03
			c3h6ooh1-2	2.03E-04	c4h8ooh1-2	9.94E-03
			nc7ket25	2.58E-04	c7h14ooh1-4	2.57E-02
			ch2ch2coch3	2.88E-04	c7h14ooh3-6	2.85E-02
			c2h5coc2h4p	3.00E-04	c7h14ooh3-1	2.86E-02
			nc7ket43	3.33E-04	c7h14ooh2-5	3.52E-02
			c5h9o1-4	3.47E-04	c7h14ooh4-3	4.18E-02
		nc7ket36	4.12E-04	c3h6cho-2	6.26E-02	
		c7h14ooh4-3o2	4.13E-04	c7h15o-3	6.41E-02	
		c4h7o	4.49E-04	nc3h7co	6.49E-02	
		c7h14ooh3-6o2	6.15E-04	c7h14ooh3-4	6.54E-02	
		c7h14ooh3-6	6.50E-04	c7h14ooh1-2	6.84E-02	

\* Flux unit: mol/(cm<sup>3</sup>\*s)

The selected QSS species are first tested in the simulations with only the application of global QSSA to examine the validity of the QSS species assumptions. The engine CFD

simulations are carried out from  $-30^\circ$  to  $30^\circ$  ATDC using the two initial temperatures respectively. The equivalence ratio of the fuel/air mixture is 1.0. The results for the engine simulations at the two initial temperatures are shown in Figure 4.7.

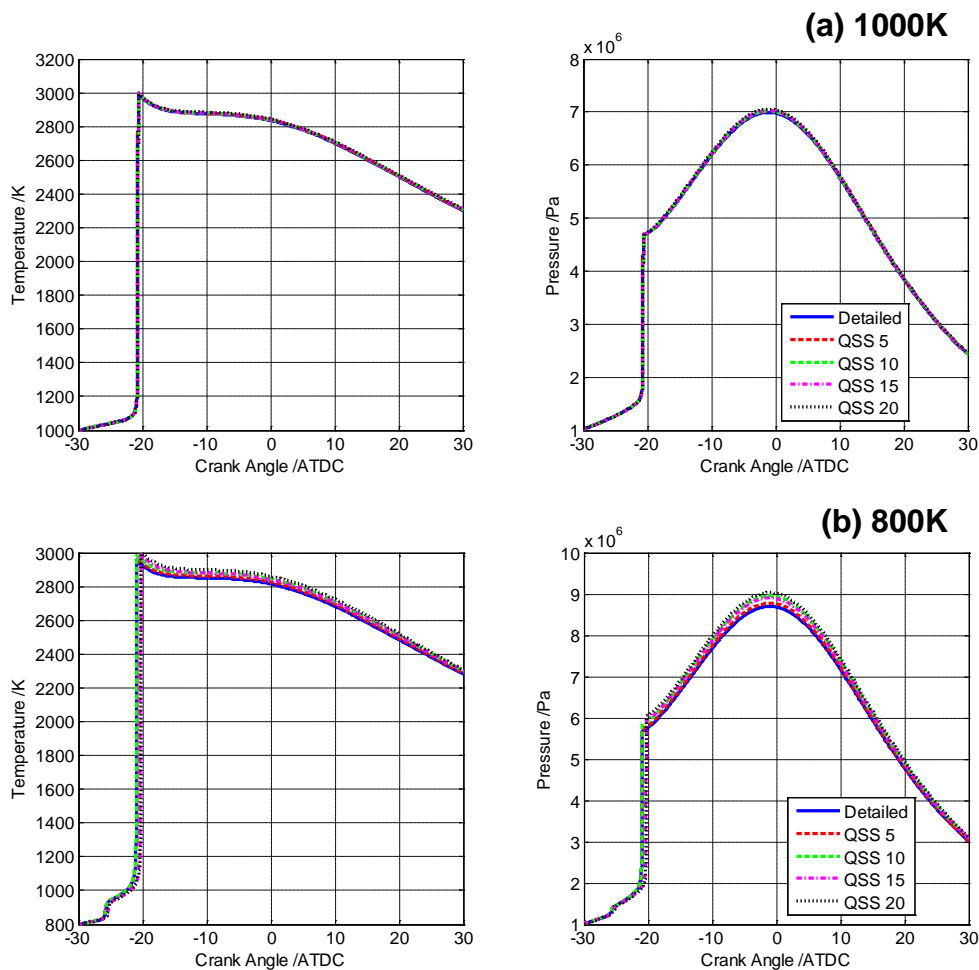


**Figure 4.7** Simulation results in KIVA with application of QSSA at two initial temperatures

For the 1000K case, excellent agreement between results for all the QSS species selections and the detailed mechanism simulation is obtained, indicating that the selected species are appropriate QSS species under the corresponding conditions. For the 800K case, the in-cylinder temperature and pressure profiles with the QSS species are still in a good agreement with the detailed mechanism simulation, but the deviation from the detailed mechanism simulation results is slightly larger compared to that in the 1000K

case. Such deviation may be explained by the slightly larger maximum net flux value for the QSS species selected at 800K. The validity of the QSS species at 800K may not be as strong as the 1000K case, but is still acceptable in capturing the major in-cylinder combustion profiles.

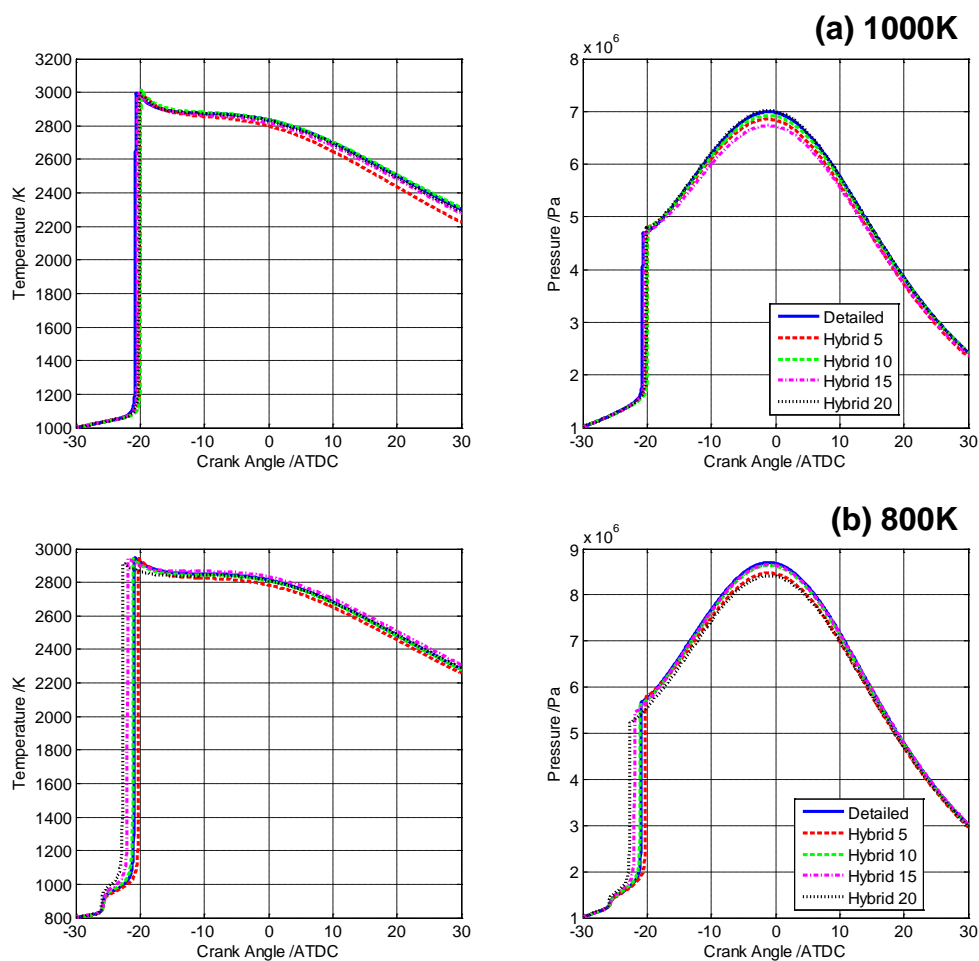


**Figure 4.8** Simulation results in KIVA with hybrid reduction at two initial temperatures

The selected QSS species are then used to further demonstrate the hybrid reduction scheme (as described in Figure 3.1) in engine CFD simulations. A 99.9% flux cutoff is used in the hybrid reduction scheme for all the four QSS species selections. The predicted in-cylinder temperature and pressure profiles are presented in Figure 4.8, in comparison with the prediction with the detailed mechanism.

### 4.3 Computational cost evaluation of hybrid reduction scheme

In order to evaluate the effects of hybrid reduction scheme on the computational costs in a more realistic scenario, the hybrid reduction scheme is embedded into commercial CFD software CRUNCH CFD<sup>®</sup> developed by Combustion Research and Flow Technology, Inc. (CRAFT Tech), with considerable efforts and dedication from Dr. Andrea Zambon.

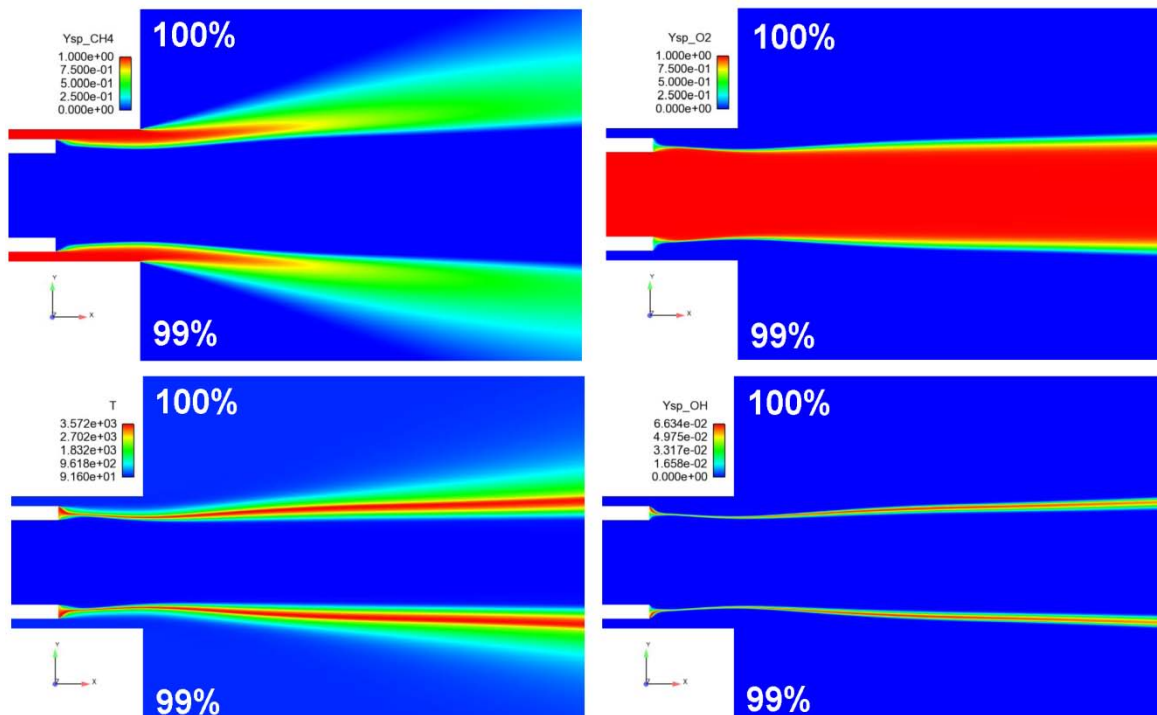


**Figure 4.9** Simulation results of the generic CH<sub>4</sub>/LOX injector simulated in CRUNCH CFD with hybrid reduction scheme

Initially, a generic axisymmetric CH<sub>4</sub>/LOX (gas-phase CH<sub>4</sub> – liquid O<sub>2</sub>) injector at supercritical conditions is simulated within RANS framework using the coupled CFD/hybrid reduction code with GRI-Mech 3.0 mechanism and 7 QSS species assumed. A 99% flux cutoff is applied in the hybrid reduction scheme, and simulation is compared to the full chemistry calculation with only application of global QSSA. Figure 4.9 shows the calculated temperature (bottom left) and major species (CH<sub>4</sub>, O<sub>2</sub>, and OH radical)

mole fraction results of hybrid reduction (on the 99% side) compared to the QSSA only simulation (on the 100% side). Although the simulation takes considerable time to fully converge, the results obtained in Figure 4.9 do suggest satisfactory fidelity of hybrid reduction scheme in predicting the important combustion characteristics. However, for the computational cost in this case, the CPU time reduction using hybrid scheme is not so clear since the speed-up might be deteriorated by the possible stiffness induced by the high pressure conditions.

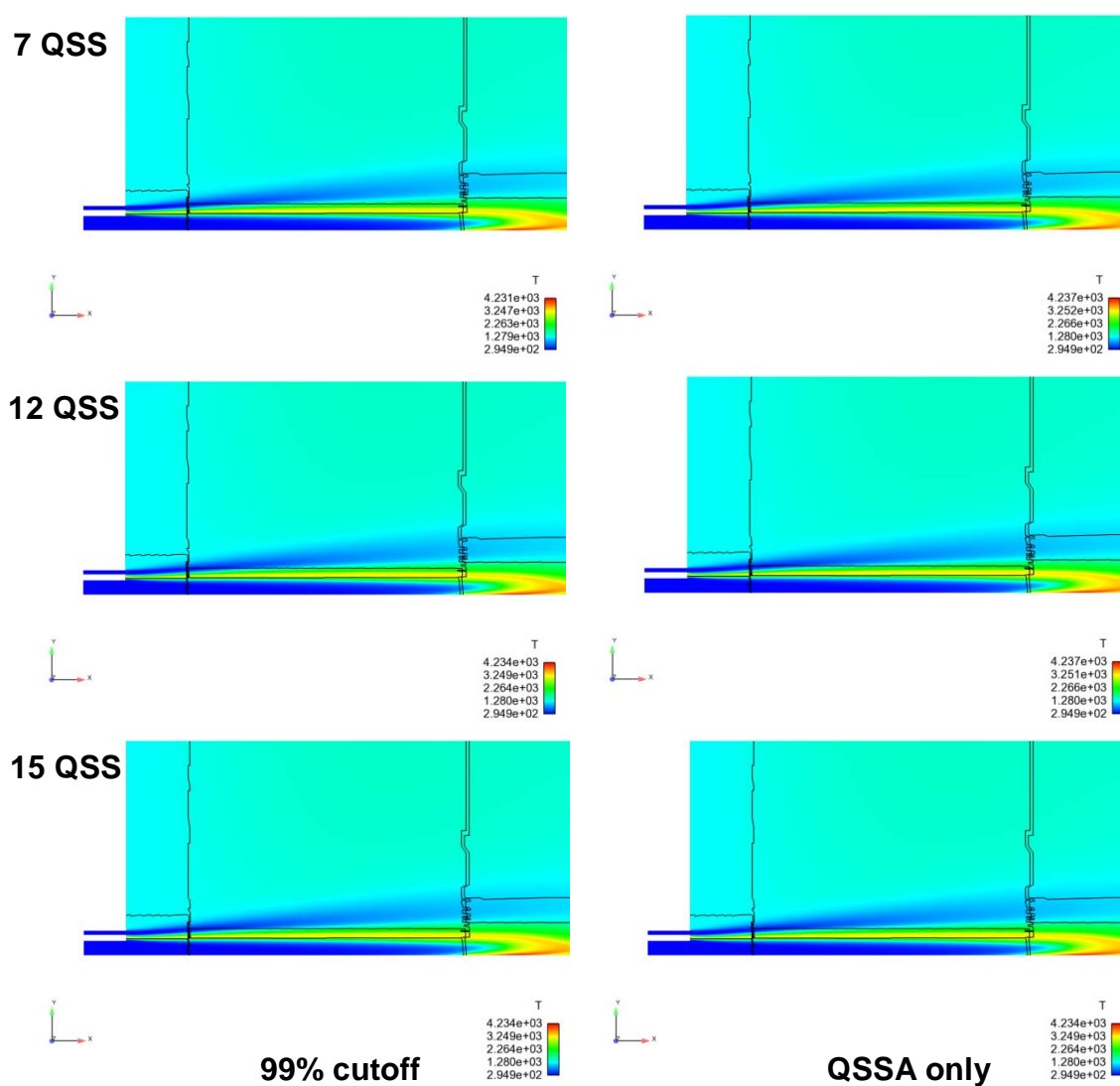


**Figure 4.10** Temperature at the last iteration step for different QSS species cases

To better illustrate the effects on the computational cost using hybrid scheme, a gas-gas  $\text{CH}_4/\text{O}_2$  combustor case is considered. Since the main purpose is to estimate the computational costs, fully converged simulation is not essentially necessary. Therefore, in this case study, each case is simulated with 50 iterations and CPU time evaluations are based on the 50-iteration simulation. Due to the computational limitation, the 2 QSS species case, with total 51 transported non-QSS species, cannot run successfully in CRUNCH CFD. Therefore, only the other three QSS species selections (7, 12, and 15 QSS species) for GRI-Mech 3.0 mechanism listed in Table 4.1 are used for evaluation. Also, since it is not possible to run a detailed mechanism simulation (all 53 transported species) in CRUNCH CFD, the simulations with 99% flux cutoff in hybrid reduction scheme are compared against the simulations with only the application of global QSSA. In Figure 4.10, the temperature contours in the combustor geometry using hybrid scheme are compared with the QSSA only simulation for each of the three QSS species selections. Good results accuracy using hybrid scheme are still maintained in the CRUNCH CFD simulations.

In addition, the non-reacting cases (without calling the hybrid reduction chemistry solver) with the three QSS species selections are also performed to estimate the CPU time needed for transport in each case. And the chemistry CPU time in the hybrid reduction cases as well as QSSA only cases above is estimated by subtracting the corresponding transport time from the total CPU time in each case. The CPU time in these cases are summarized in Table 4.3. First, we can find that the transport CPU time decreases as more QSS species are assumed. This is expected since with more species assumed as quasi-steady state, the number of species involved in the transport calculation is reduced,

which leads to reduced transport CPU time. On the other hand, if we examine the chemistry CPU time, we can see the savings of chemistry CPU time in the hybrid reduction with 99% flux cutoff is around 25% - 35% compared to the QSSA only cases. However, we do observe that the chemistry CPU time in hybrid reduction increase slightly as more QSS species are assumed. The increased chemistry CPU could be contributed to by the additional computational cost needed to solve more algebraic equations when a few more QSS species are assumed. There may also be stiffness issues that are worth further investigation in the future.

**Table 4.3** Summary of CPU time for 50 iterations in CRUNCH CFD simulations

QSS species	Transport CPU	QSSA only		Hybrid, 99% cutoff		Chemistry savings
		Total CPU	Chemistry	Total CPU	Chemistry	
7	1117	3898	2781	2964	1847	34%
12	847	3701	2854	2885	2038	29%
15	810	3614	2804	2962	2152	23%

**Table 4.4** Summary of CPU time in KIVA CFD simulations for n-heptane oxidation

QSS species	QSSA only			Hybrid, 99% cutoff			Chemistry savings
	Total	Tran	Chem	Total	Tran	Chem	
05	87247	515	86732	35028	512	34516	60%
10	85082	510	84572	35403	508	34895	59%
15	84090	505	83585	37833	505	37328	55%
20	81943	502	81441	33438	500	32938	59%

In addition, we can also examine the computational cost in the n-heptane oxidation simulations performed in KIVA. In the n-heptane case, since the detailed mechanism is

larger, the effect of reduction by applying hybrid reduction might be more obvious. Table 4.4 summarizes the CPU time in engine CFD simulation in KIVA. We could observe about 60% chemistry CPU time savings for the hybrid reduction in these simulations. Since the transport calculation cost is much smaller in the HCCI engine simulations, we can find that the overall savings in CPU time is also around 60% in this case. Besides, the cost of chemistry calculation basically decreases as more QSS species are assumed in these simulations. In this case, the additional cost to solve more algebraic equations with more QSS species may be covered by the savings in solving less number of ODEs of non-QSS species. Therefore, the overall cost reduction can be seen. However, an exception is found for the 15 QSS species case with hybrid reduction. The chemistry cost is more than the other cases, which again may be resulted in by the possibly increased stiffness.

#### 4.4 Summary

In this chapter, a method for quick selection of QSS species is proposed based on the maximum net flux of species during a PFR simulation with detailed mechanism. Although the method may not strictly reflect the definition of QSS species, the ability to quickly find satisfactory global QSS species candidates allow us to further evaluate the performance of hybrid reduction scheme. Using the flux-based selection procedure, QSS species are selected for the GRI-Mech 3.0 mechanism as well as the 161-species n-heptane mechanism. The hybrid reduction scheme is then demonstrated using these selected QSS species in both PFR and multidimensional engine CFD simulations. Excellent simulation results with high fidelity are obtained using the hybrid scheme with

flux-based QSS species selection. In addition, in order to further evaluate the computational effects of hybrid reduction framework on the transport and chemistry calculations, the hybrid reduction scheme is embedded in a commercial CFD software CRUNCH CFD<sup>®</sup> developed by Combustion Research and Flow Technology, Inc. to simulate a more realistic combustion scenario. The CFD simulation results in good prediction accuracy compared to the cases in which only global QSSA are applied. The CPU time for transport calculation is reduced as more QSS species is assumed. We can also observe CPU time savings on the chemistry calculations as well as the overall computational cost for the entire simulation. The results suggest that the hybrid scheme has the ability to accurately capture combustion characteristics and to reduce the computational cost in the simulation. At the same time, further study is still necessary to investigate the limiting factors for further computational speed-up.

## Chapter 5

### Integration of mechanism generation and reduction

#### 5.1 Integration of mechanism reduction during mechanism generation

The traditional reactive flow simulations rely on the information from a detailed mechanism before the simulation can be performed. The simulation is usually done by using a skeletal mechanism derived from the comprehensive detailed mechanism, or by applying some mechanism reduction techniques on the detailed mechanism to reduce the number of species and reactions during the simulation. However, the challenges of incorporating detailed mechanism, such as expensive computation and large number of species in transport, promotes us to consider alternative ways for conducting reactive flow simulation. With automated mechanism generation tools, one idea that we can think of is that instead of having a mechanism beforehand, we start the simulation just with the initial reactants and without having an actual mechanism. During the simulation, we use the mechanism generation and reduction tools to generate only necessary species and reactions for the simulation instantaneously. Based on this idea, in this chapter, we propose to integrate the automated mechanism generation tools with our on-the-fly reduction approach to perform reactive flow simulation without using a mechanism.

In our previous work (Androulakis et al., 2004), we have explored the coupling of element flux analysis in the mechanism generation to prevent the generated mechanism from growing too large. In the coupled framework, the mechanism generation is performed for a certain steps, and then time-integrated element flux analysis is applied to remove redundant species and reactions from the currently generated mechanism. The

next generation step then continues to grow the reaction network until the next reduction is applied. In this chapter, we adopt similar iterative procedure to generate the mechanism in a series of specific reaction periods while performing on-the-fly reduction and simulation.

## 5.2 Stepwise integration of mechanism generation and reduction

In the integration of automated mechanism generation with on-the-fly reduction, we have some requirements for the mechanism generation package in addition to the basic features of automated reaction network construction and thermodynamic/kinetic data generation. Since our on-the-fly reduction implementation relies on CHEMKIN applications, the mechanism generation package should be able to write the generated mechanism, along with all the thermodynamic data and kinetic parameters, in CHEMKIN mechanism format. Also, since our mechanism reduction tools are written in FORTRAN, the mechanism generation package should be able to have the compatibility to work with or be compiled with FORTRAN code. With these considerations, we determined that the NetGen package developed by Broadbelt et al. (Broadbelt et al., 1994; Susnow et al., 1997) and RMG (Reaction Mechanism Generator) developed by Green et al. (Green et al.) are two appropriate packages for the integration with on-the-fly reduction.

In this chapter, we will mainly use RMG as the automated mechanism generation package for our computational framework. In RMG, the inputs for mechanism generation include initial temperature and pressure, initial reactants with structures and concentrations, designated thermo/transport/kinetic libraries, as well as termination rules and error control parameters. The unavailable thermodynamic data will be estimated by

Benson group additivity method, and the termination options are available to stop the generation at certain reaction time or reactant conversion. RMG will generate the mechanism automatically using rate-based network enlargement and output the generated mechanism with thermodynamic data and kinetic parameters in CHEMKIN format mechanism files.

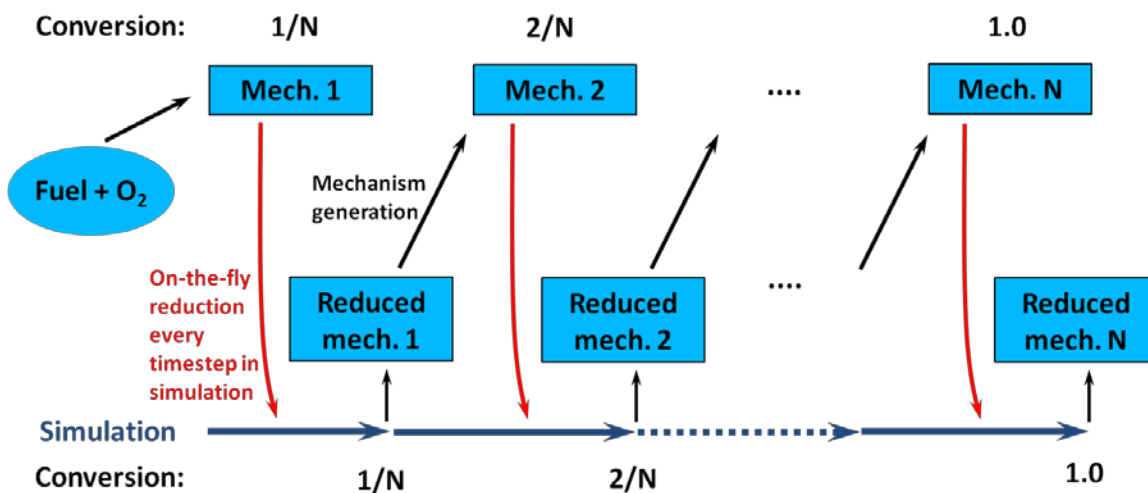


**Figure 5.1** A schematic illustration of the stepwise implementation of the integration of mechanism generation and reduction

To demonstrate the idea of coupling mechanism generation and reduction, we proposed a stepwise implementation of the integration using RMG and our on-the-fly reduction code. A schematic illustration of the implementation is shown in Figure 5.1. In this stepwise procedure, we increment the entire reaction process into several steps by fuel conversions. The procedure starts from just fuel and  $O_2$ , and generates a mechanism in the generation phase using RMG terminating at the first increment of fuel conversion ( $1/N$  if total  $N$  steps). This generated mechanism is not a full mechanism, but can be used to describe the reaction process up to the current fuel conversion. Then in the reduction and simulation phase, on-the-fly reduction is applied on the generated mechanism to

perform simulation from the initial condition until the fuel conversion also reaches the first increment in the simulation. Subsequently, we take the conditions and the reduced species at the end of the first step simulation as the inputs for the mechanism generation in the second step. The second mechanism is then generated terminating at the second fuel conversion increment  $2/N$ , and on-the-fly reduction is applied again on the second generated mechanism to perform simulation until the fuel conversion also reaches the second increment. The reduced mechanism and conditions at the end of the second step simulation is taken as the starting point for the next step mechanism generation. The procedure is repeated until reaction is completed, and the entire simulation results can be obtained.

From the above description, we can see that the automated mechanism generation and on-the-fly reduction are combined together to perform simulation using the stepwise implementation. There is no mechanism before we start the simulation. All we need as input is the initial temperature, pressure, fuel and  $O_2$  concentrations as well as structure representations. The integration of mechanism generation and reduction using stepwise implementation provides an alternative way of running simulations without having a mechanism beforehand.

### 5.3 Case studies of the stepwise implementation

In this section, a few case studies using the stepwise implementation are presented to demonstrate the idea of integration of automated mechanism generation and on-the-fly reduction. For simplicity, PFR simulations of methane oxidation are performed in these demonstrations.

### 5.3.1 Two-step integration with isothermal PFR simulation

Since the RMG mechanism generation is carried out at constant temperature and pressure, we demonstrate the integration also at constant temperature and pressure using isothermal PFR simulations. As an initial attempt, two-step integration for methane oxidation is implemented as shown in Figure 5.2. In the first step, a mechanism is generated start from stoichiometric methane/air mixture at constant temperature 1000K and pressure 10 atm, terminating at methane conversion 0.5. And then simulation with on-the-fly reduction is performed also up to 0.5 methane conversion. The second step generation and simulation is then performed until the end of reaction.

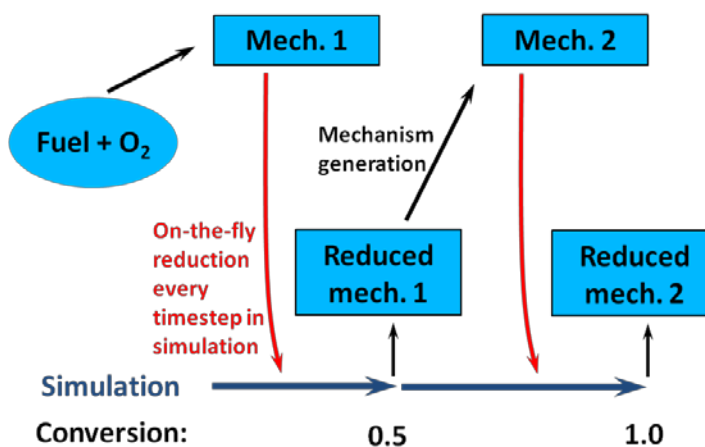


**Figure 5.2** Schematic illustration of two-step integration

The species concentration profiles obtained in the two-step integration are presented in Figure 5.3. For comparison, a single mechanism is also generated using the same initial conditions with termination at methane conversion 1.0 directly. The single mechanism is used to perform the same simulation in the traditional way using detailed mechanism as well as on-the-fly reduction, respectively. It can be seen that the simulation results of the two-step integration shown in Figure 5.3 are in good agreement with the single mechanism simulation results.

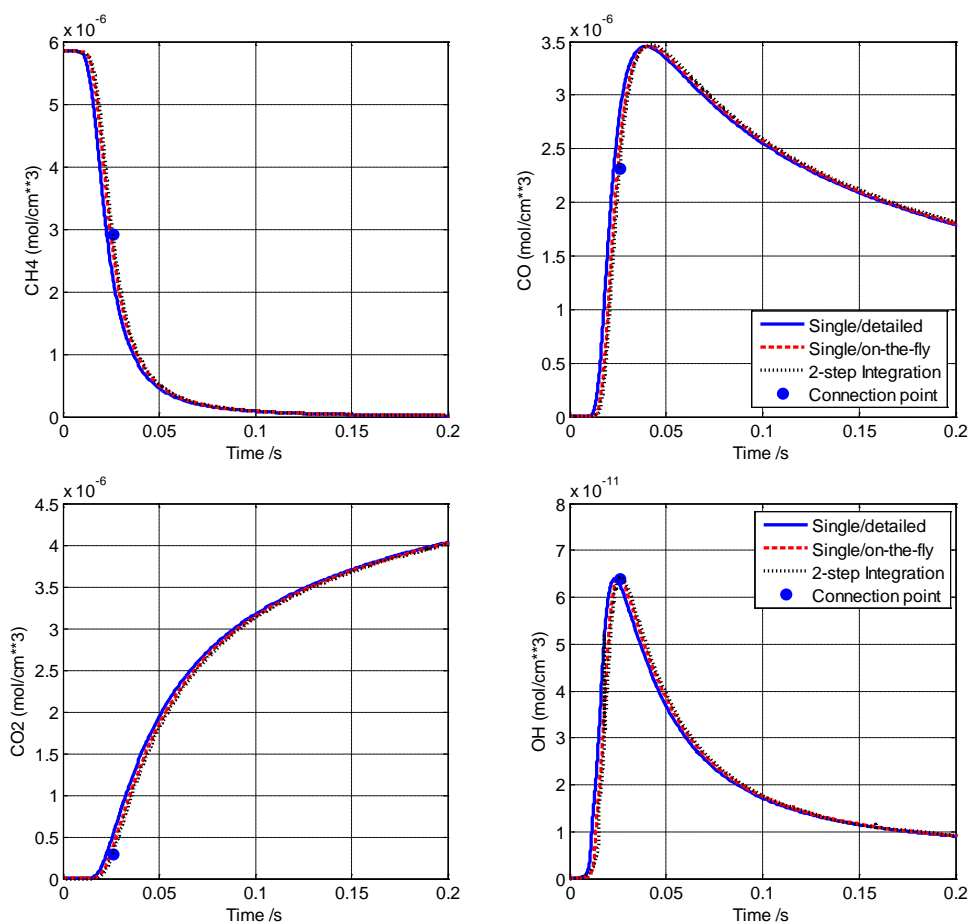


**Figure 5.3** Species concentration profiles obtained in the two-step integration

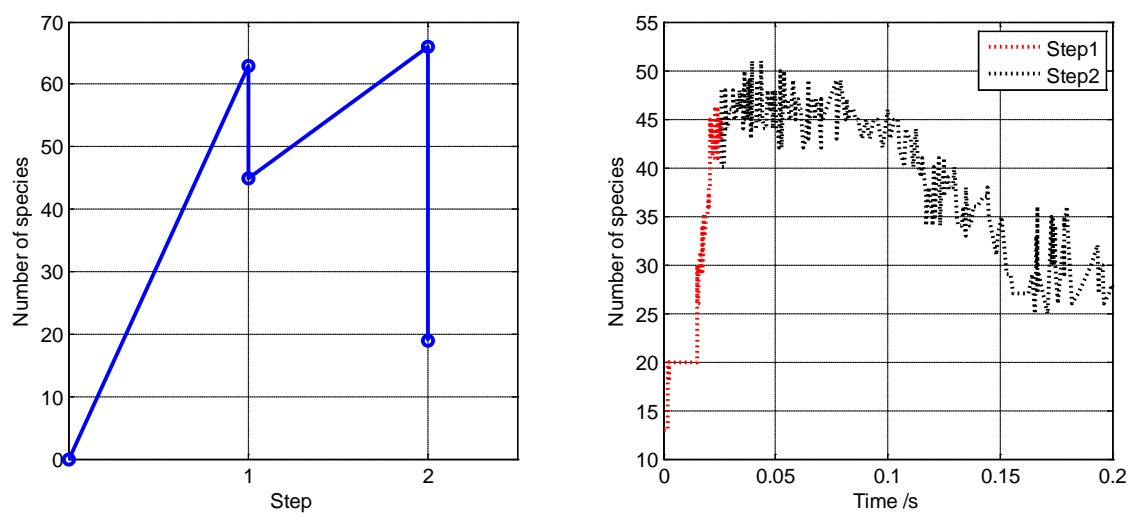


**Figure 5.4** Mechanism size and reduced number of species in the two-step integration

Figure 5.4 shows the evolution of mechanism size in the integration as well as number of species in the reduced mechanism by applying on-the-fly reduction during the simulation. It clearly shows how the mechanism size increase and decrease during the generation-reduction process. And with on-the-fly reduction, we can prevent the generated mechanism from growing too large.

### 5.3.2 Multi-step integration with isothermal PFR simulation

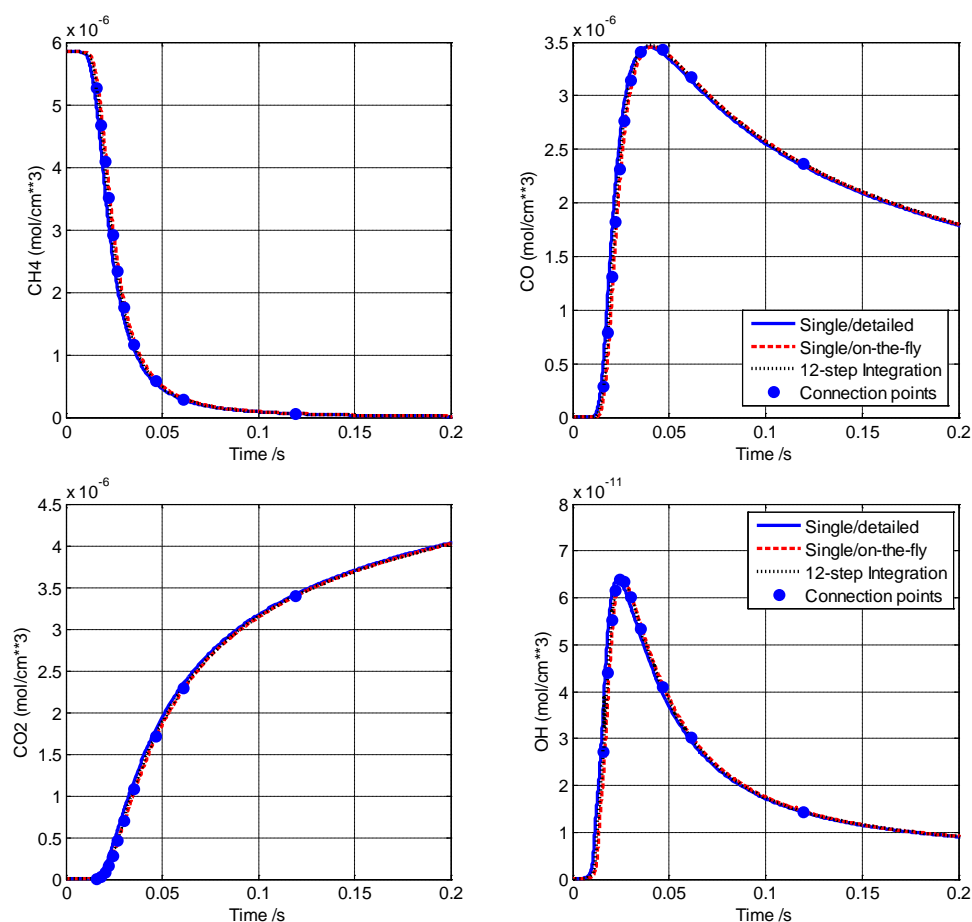


**Figure 5.5** Species concentration profiles obtained in the 12-step integration

In the second case study, a multi-step integration with isothermal PFR simulation is implemented. In this case, we use every 0.1 methane conversion as the increments for the steps, with two additional increments at methane conversion 0.95 and 0.99 to better

illustrate the reaction process after the ignition, making it total 12 steps. The same initial conditions and mechanism generation settings are used.

Figure 5.5 shows select species concentration profiles obtained in the multi-step integration, also compared with the same single mechanism simulation results. The blue dot shows the connection between steps. Excellent agreement in the results is achieved, which suggests that accurate simulation results can be obtained by using the stepwise integration of mechanism generation and on-the-fly reduction.

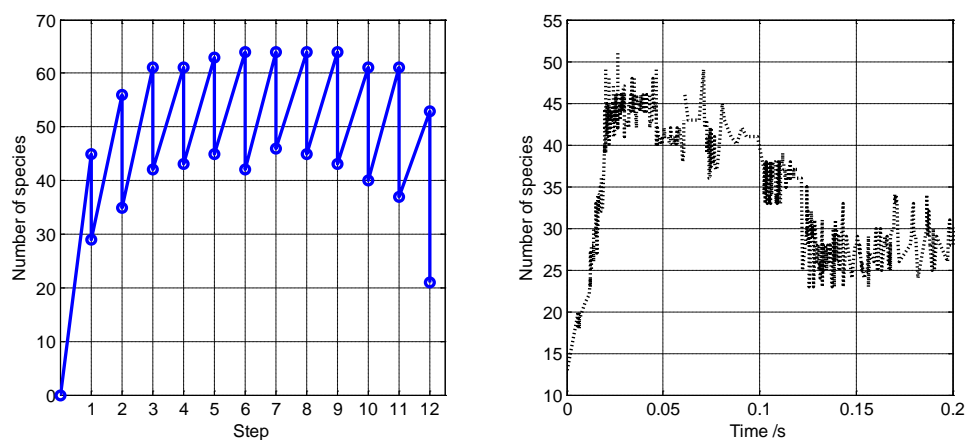


**Figure 5.6** Mechanism size and reduced number of species in the 12-step integration

The size of mechanism and number of species in the reduced mechanism during the stepwise integration is shown in Figure 5.6. We can see that the size of the generated mechanism increases during the ignition since more species are involved in the reaction, and decrease after the ignition. By integrating on-the-fly reduction with the automated mechanism generation, the proposed computational framework is able to reduce the size of generated mechanism when less species are necessary in the system. Otherwise, if no reduction is introduced, the size of the generated mechanism can only increase. If less species and reactions are necessary to describe the chemistry of the system in a specific

period of the reaction, the integrated framework has the ability to reduce the size of generated mechanism.

### 5.3.3 Multi-step integration with adiabatic PFR simulation

In addition to the isothermal PFR simulation, in this case study, we extend the stepwise integration to the normal adiabatic PFR model. Again, methane conversion 0.1 is used as the step increment with additional increments at methane conversion 0.99, 0.9999, and 0.9999999, making it 13-step integration.

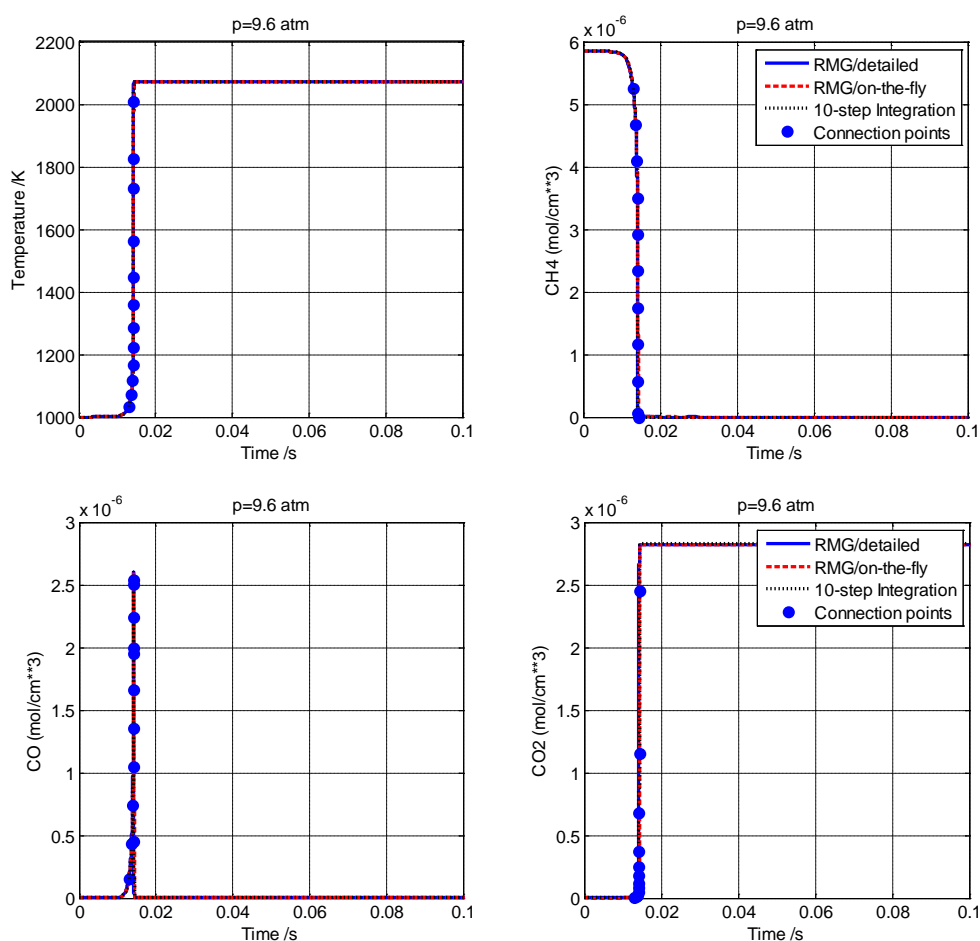


**Figure 5.7** Temperature and species concentration profiles obtained in the 13-step integration with adiabatic PFR simulation

The temperature and species concentration profiles obtained in the integration are shown in Figure 5.7, which are also compared to a single mechanism simulation results. Since in each step of the integration the temperature at which the mechanism is generated is no longer constant, it makes no sense to compare the 13-step results with a single mechanism generated at one constant temperature. However, RMG package currently is only able to model constant temperature and pressure conditions. Therefore, when generating an appropriate single mechanism for comparison, we assign multiple temperatures, namely 1000K, 1300K, and 1600K, which roughly cover the temperature range of the entire reaction for RMG. RMG will then generate the mechanism (still using isothermal, isobaric model) at each of all the assigned temperatures. Here, the generated single mechanism consists of 103 species and 1783 reactions. The results in Figure 5.7 show excellent agreement between with the single mechanism simulation results.

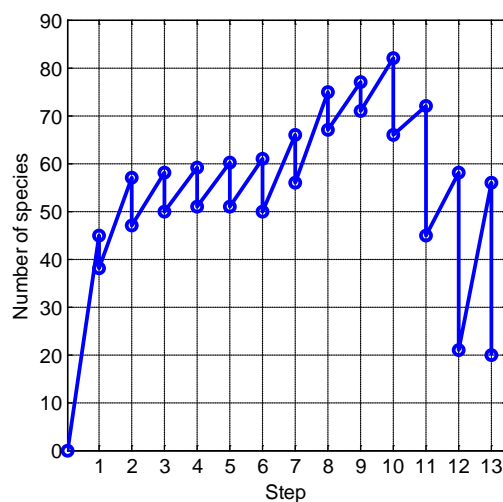


**Figure 5.8** Mechanism size evolution in the 13-step integration

The evolution of mechanism size during the 13-step integration is shown in Figure 5.8. The size of generated mechanism is changing during the reaction as needed to include only necessary species as possible. Also, the largest generated mechanism in the stepwise

integration is around 80 species, much smaller than the 103 species single mechanism. Therefore, by using the stepwise integration, we are able to perform simulation with a series of smaller mechanism containing only necessary species for the specific reaction stage instead of a large single mechanism consisting of all the species. From this perspective, with the integration of mechanism generation and reduction, we are not only able to run reactive flow simulation without having a mechanism beforehand, but also able to limit the size of mechanism used in the simulation so that the computational cost can be potentially reduced.

#### 5.4 Summary

In this chapter, we propose the idea of integrating automated mechanism generation with on-the-fly reduction to establish a novel framework for performing reactive flow simulations. A stepwise implementation is employed for the integration. The stepwise integration is first demonstrated in the isothermal PFR case study with 2 step and 12 steps, respectively. The implementation is further tested in adiabatic PFR model case study. The simulation results obtained from the stepwise integration are in very good agreement with traditional single mechanism simulation results.

The proposed methodology provides a novel way to run reactive flow simulation. The procedure starts with only fuel and air as initial reactants, and no mechanism is needed beforehand to perform the simulation. The proposed framework is also promising in reducing the computational cost of reactive flow simulations.

## Chapter 6

### Conclusions and future perspectives

#### 6.1 Conclusions

In this dissertation, we established several tools for the accurate and efficient characterization of fuel combustion and chemical kinetics. These tools are tested and demonstrated in different reactive flow simulation case studies. This work provides important insight for incorporation of detailed kinetic models in computational combustion studies, and generates innovative idea for conducting reactive flow simulations with high fidelity and efficiency.

In this dissertation, we first extend the previously developed on-the-fly reduction to the characterization of complex biodiesel combustion. With on-the-fly reduction, detailed biodiesel surrogate mechanisms are incorporated and the multidimensional HCCI engine CFD simulations are enabled with acceptable computational intensity. The important combustion characteristic for biodiesel fuels, such as ignition timing, pollutant emission, as well as engine performance parameters, are evaluated in the engine simulation and compared with those for the conventional hydrocarbon fuels. The fuel comparison and performance analysis provide important information for the chemical characteristics of biodiesel as well as appropriate utilization of biodiesel fuels under engine conditions.

In this dissertation, we developed a novel hybrid reduction scheme by coupling the global QSSA and the on-the-fly reduction approach. The hybrid reduction scheme is demonstrated with methane oxidation and n-heptane oxidation simulations with both zero-dimensional PFR model and multidimensional engine CFD simulations. To aid the

application of hybrid scheme, a QSS species selection procedure based on the maximum net flux of species is introduced for the quick selection of appropriate QSS species candidate under certain conditions. The combined tools of QSS species selection and hybrid reduction provide a platform for efficient reactive flow simulation, especially for some transport intensive applications. The computational cost of hybrid reduction scheme is evaluated in a realistic CFD simulation of gas phase injector. The results suggest that the hybrid scheme has the ability to reduce the transport calculation by reducing the number of transported species while still maintaining an efficient chemistry calculation with the application of on-the-fly reduction.

In this dissertation, we also proposed a new way to perform reactive flow simulation without having a mechanism beforehand. The proposed computational framework is based on the integration of automated mechanism generation and on-the-fly reduction. A stepwise implementation of the integrated framework is developed and tested in several methane oxidation case studies. The results of the case study show that the stepwise integration of automated mechanism generation and on-the-fly reduction produces accurate simulation results while no mechanism is needed to start the simulation. With on-the-fly reduction, the integrated framework is able to limit the growth of the generated mechanism during the simulation, and also reduce the generated mechanism when less species and reaction is actually needed. Hence the approach has the potential reduce computational cost of reactive flow simulation. The proposed framework provides a novel methodology to perform reactive flow simulation compared to the tradition simulation based on a pre-developed reaction mechanism.

## 6.2 Suggestions for future work

This work has created a few future directions that are of great interest to investigate. The hybrid reduction scheme proposed in this work provides an advanced platform to incorporate detailed kinetic mechanism in the realistic flow simulations with satisfactory efficiency and accuracy. However, there are still several aspects in which the hybrid reduction scheme can be further improved. From the computational perspective, further study is needed to explore the factors that affect the CPU time speed-up in the application of hybrid reduction scheme, to evaluate the stiffness of the chemical kinetics system during the reactive flow simulation, and to optimize the hybrid reduction algorithm for computational performance enhancement. Since the hybrid reduction scheme introduces additional overhead to solve the system of algebraic equations, it is also of interest to develop more efficient numerical solution procedure of nonlinear algebraic equations.

Another possible future direction is to explore the approach for identification of appropriate QSS species. Although in this work, we use a flux-based procedure to select QSS species for the demonstration of hybrid reduction scheme, the method is still preliminary and requires further studies based on the mathematical description and definition of quasi-steady-state approximation. It is crucial to develop effective, easy-to-implement QSS species selection approach for the generalization of hybrid reduction scheme to more complex chemical kinetic networks such as biodiesel combustion.

Moreover, for the integration of automated mechanism generation and on-the-fly reduction, further work is still needed. The current implementation is based on a stepwise integration using RMG and on-the-fly reduction using manual connection between steps since RMG is written in Java and cannot be directly compiled with FORTRAN code. In

the future, we can further explore the possibility to use NetGen, which is written in C/C++, instead of RMG to compile with our FORTRAN code so that the integration can be implemented automatically. Currently, the major issue with NetGen is to generate a CHEMKIN format mechanism file as input for the on-the-fly reduction. Another important issue that requires further study is to determine the steps and when the generated mechanism should be updated in the integrated generation-reduction framework. Such information would be helpful to modify and improve the integration procedure.

## Bibliography

Amsden, A.A., 1997. KIVA-3V: A Block-Structured KIVA Program for Engines with Vertical or Canted Valves. Los Alamos National Laboratory, Los Alamos, NM.

Androulakis, I.P., 2000. Kinetic mechanism reduction based on an integer programming approach. *AIChE Journal* 46, 361-371.

Androulakis, I.P., Grenda, J.M., Bozzelli, J.W., 2004. Time-integrated pointers for enabling the analysis of detailed reaction mechanisms. *AIChE Journal* 50, 2956-2970.

Banerjee, I., Ierapetritou, M.G., 2006. An adaptive reduction scheme to model reactive flow. *Combustion and Flame* 144, 619-633.

Bhattacharjee, B., Schwer, D.A., Barton, P.I., Green, W.H., 2003. Optimally-reduced kinetic models: reaction elimination in large-scale kinetic mechanisms. *Combustion and Flame* 135, 191-208.

Brakora, J.L., Reitz, R.D., 2010. Investigation of NO<sub>x</sub> Predictions from Biodiesel-fueled HCCI Engine Simulations Using a Reduced Kinetic Mechanism. SAE Technical Paper Series No. 2010-01-0577.

Broadbelt, L.J., Stark, S.M., Klein, M.T., 1994. Computer Generated Pyrolysis Modeling: On-the-Fly Generation of Species, Reactions, and Rates. *Industrial & Engineering Chemistry Research* 33, 790-799.

Broadbelt, L.J., Stark, S.M., Klein, M.T., 1995. Termination of Computer-Generated Reaction Mechanisms: Species Rank-Based Convergence Criterion. *Industrial & Engineering Chemistry Research* 34, 2566-2573.

Broadbelt, L.J., Stark, S.M., Klein, M.T., 1996. Computer generated reaction modelling: Decomposition and encoding algorithms for determining species uniqueness. *Computers & Chemical Engineering* 20, 113-129.

Chen, J.Y., Tham, Y.F., 2008. Speedy solution of quasi-steady-state species by combination of fixed-point iteration and matrix inversion. *Combustion and Flame* 153, 634-646.

Contino, F., Jeanmart, H., Lucchini, T., D'Errico, G., 2011. Coupling of in situ adaptive tabulation and dynamic adaptive chemistry: An effective method for solving combustion in engine simulations. *Proceedings of the Combustion Institute* 33, 3057-3064.

Curran, H.J., Gaffuri, P., Pitz, W.J., Westbrook, C.K., 1998. A Comprehensive Modeling Study of n-Heptane Oxidation. *Combustion and Flame* 114, 149-177.

Curran, H.J., Gaffuri, P., Pitz, W.J., Westbrook, C.K., 2002. A comprehensive modeling study of iso-octane oxidation. *Combustion and Flame* 129, 253-280.

Dagaut, P., Gai, S., Sahasrabudhe, M., 2007. Rapeseed oil methyl ester oxidation over extended ranges of pressure, temperature, and equivalence ratio: Experimental and modeling kinetic study. *Proceedings of the Combustion Institute* 31, 2955-2961.

De Witt, M.J., Dooling, D.J., Broadbelt, L.J., 2000. Computer Generation of Reaction Mechanisms Using Quantitative Rate Information: Application to Long-Chain Hydrocarbon Pyrolysis. *Industrial & Engineering Chemistry Research* 39, 2228-2237.

Di Maio, F.P., Lignola, P.G., 1992. KING, a KInetic Network Generator. *Chemical Engineering Science* 47, 2713-2718.

Fisher, E.M., Pitz, W.J., Curran, H.J., Westbrook, C.K., 2000. Detailed chemical kinetic mechanisms for combustion of oxygenated fuels. *Proceedings of the Combustion Institute* 28, 1579-1586.

Freedman, B., Bagby, M., 1990. Predicting cetane numbers of n-alcohols and methyl esters from their physical properties. *Journal of the American Oil Chemists' Society* 67, 565-571.

Gou, X., Chen, Z., Sun, W., Ju, Y., 2013. A dynamic adaptive chemistry scheme with error control for combustion modeling with a large detailed mechanism. *Combustion and Flame* 160, 225-231.

Green, W.H., Allen, J.W., Beat A. Buesser, Robert W. Ashcraft, Gregory J. Beran, Caleb A. Class, Connie Gao, C. Franklin Goldsmith, Michael R. Harper, Amrit Jalan, Murat Keceli, Gregory R. Magoon, David M. Matheu, Shamel S. Merchant, Jeffrey D. Mo, Sarah Petway, Sumathy Raman, Sandeep Sharma, Jing Song, Yury Suleymanov, Kevin M. Van Geem, John Wen, Richard H. West, Andrew Wong, Hsi-Wu Wong, Paul E. Yelvington, Nathan Yee, Yu, J., "RMG - Reaction Mechanism Generator v4.0.1", 2013 <http://rmg.sourceforge.net/>.

Grenda, J.M., Androulakis, I.P., Dean, A.M., Green, W.H., 2003. Application of Computational Kinetic Mechanism Generation to Model the Autocatalytic Pyrolysis of Methane. *Industrial & Engineering Chemistry Research* 42, 1000-1010.

He, K., Androulakis, I.P., Ierapetritou, M.G., 2009a. Multi-element Flux Analysis for the Incorporation of Detailed Kinetic Mechanisms in Reactive Simulations. *Energy & Fuels* 24, 309-317.

He, K., Androulakis, I.P., Ierapetritou, M.G., 2010a. Incorporation of Detailed Chemical Mechanisms in Reactive Flow Simulations Using Element-Flux Analysis. *Industrial & Engineering Chemistry Research* 49, 10471-10478.

He, K., Androulakis, I.P., Ierapetritou, M.G., 2010b. On-the-fly reduction of kinetic mechanisms using element flux analysis. *Chemical Engineering Science* 65, 1173-1184.

He, K., Ierapetritou, M.G., Androulakis, I.P., 2008. A graph-based approach to developing adaptive representations of complex reaction mechanisms. *Combustion and Flame* 155, 585-604.

He, K., Ierapetritou, M.G., Androulakis, I.P., 2009b. Integration of on-the-fly kinetic reduction with multidimensional CFD. *AIChE Journal* 56, 1305-1314.

He, K., Ierapetritou, M.G., Androulakis, I.P., 2012. Exploring flux representations of complex kinetics networks. *AIChE Journal* 58, 553-567.

Herbinet, O., Pitz, W.J., Westbrook, C.K., 2008. Detailed chemical kinetic oxidation mechanism for a biodiesel surrogate. *Combustion and Flame* 154, 507-528.

Herbinet, O., Pitz, W.J., Westbrook, C.K., 2010. Detailed chemical kinetic mechanism for the oxidation of biodiesel fuels blend surrogate. *Combustion and Flame* 157, 893-908.

Heywood, J.B., 1988. *Internal combustion engine fundamentals*. McGraw-Hill.

<http://www.nag.co.uk/numeric/fl/FLdescription.asp>.

Hughes, K.J., Fairweather, M., Griffiths, J.F., Porter, R., Tomlin, A.S., 2009. The application of the QSSA via reaction lumping for the reduction of complex hydrocarbon oxidation mechanisms. *Proceedings of the Combustion Institute* 32, 543-551.

Hughes, K.J., Turányi, T., Clague, A.R., Pilling, M.J., 2001. Development and testing of a comprehensive chemical mechanism for the oxidation of methane. *International Journal of Chemical Kinetics* 33, 513-538.

I. Zsély, T.N., J. Simmie, H. Curran, 2009. Reduction of a detailed kinetic model for the ignition of natural gas mixtures at gas turbine conditions, 4th European Combustion Meeting, Vienna, Austria.

Kelly-Zion, P.L., Dec, J.E., 2000. A computational study of the effect of fuel type on ignition time in homogenous charge compression ignition engines. *Proceedings of the Combustion Institute* 28, 1187-1194.

Klinke, D.J., Broadbelt, L.J., 1997. Mechanism reduction during computer generation of compact reaction models. *AIChE Journal* 43, 1828-1837.

Lai, J.Y.W., Lin, K.C., Violi, A., 2011. Biodiesel combustion: Advances in chemical kinetic modeling. *Progress in Energy and Combustion Science* 37, 1-14.

Lam, S.H., Goussis, D.A., 1994. The CSP method for simplifying kinetics. *International Journal of Chemical Kinetics* 26, 461-486.

Lapuerta, M., Armas, O., Rodríguez-Fernández, J., 2008. Effect of biodiesel fuels on diesel engine emissions. *Progress in Energy and Combustion Science* 34, 198-223.

Liang, L., Stevens, J.G., Farrell, J.T., 2009a. A dynamic adaptive chemistry scheme for reactive flow computations. *Proceedings of the Combustion Institute* 32, 527-534.

Liang, L., Stevens, J.G., Raman, S., Farrell, J.T., 2009b. The use of dynamic adaptive chemistry in combustion simulation of gasoline surrogate fuels. *Combustion and Flame* 156, 1493-1502.

Lu, Law, C.K., 2006. Systematic Approach To Obtain Analytic Solutions of Quasi Steady State Species in Reduced Mechanisms. *The Journal of Physical Chemistry A* 110, 13202-13208.

Lu, T., Ju, Y., Law, C.K., 2001. Complex CSP for chemistry reduction and analysis. *Combustion and Flame* 126, 1445-1455.

Lu, T., Law, C.K., 2005. A directed relation graph method for mechanism reduction. *Proceedings of the Combustion Institute* 30, 1333-1341.

Lu, T., Law, C.K., 2008a. A criterion based on computational singular perturbation for the identification of quasi steady state species: A reduced mechanism for methane oxidation with NO chemistry. *Combustion and Flame* 154, 761-774.

Lu, T., Law, C.K., 2008b. Strategies for mechanism reduction for large hydrocarbons: n-heptane. *Combustion and Flame* 154, 153-163.

Lu, T., Law, C.K., 2009. Toward accommodating realistic fuel chemistry in large-scale computations. *Progress in Energy and Combustion Science* 35, 192-215.

Lü, X., Ji, L., Zu, L., Hou, Y., Huang, C., Huang, Z., 2007. Experimental study and chemical analysis of n-heptane homogeneous charge compression ignition combustion with port injection of reaction inhibitors. *Combustion and Flame* 149, 261-270.

Marinov, N.M., Pitz, W.J., Westbrook, C.K., Vincitore, A.M., Castaldi, M.J., Senkan, S.M., Melius, C.F., 1998. Aromatic and Polycyclic Aromatic Hydrocarbon Formation in a Laminar Premixed n-Butane Flame. *Combustion and Flame* 114, 192-213.

Montgomery, C.J., Yang, C., Parkinson, A.R., Chen, J.Y., 2006. Selecting the optimum quasi-steady-state species for reduced chemical kinetic mechanisms using a genetic algorithm. *Combustion and Flame* 144, 37-52.

Nagy, T., Turányi, T., 2009. Reduction of very large reaction mechanisms using methods based on simulation error minimization. *Combustion and Flame* 156, 417-428.

Naik C., W.C.K., Herbinet O., Pitz W. J., Mehl M. , 2010. Detailed Chemical Kinetic Reaction Mechanism for Biodiesel Components Methyl Stearate and Methyl Oleate, *Proceedings of The 33rd International Symposium on Combustion*, Beijing, China.

Niemeyer, K.E., Sung, C.-J., Raju, M.P., 2010. Skeletal mechanism generation for surrogate fuels using directed relation graph with error propagation and sensitivity analysis. *Combustion and Flame* 157, 1760-1770.

Pepiot-Desjardins, P., Pitsch, H., 2008. An efficient error-propagation-based reduction method for large chemical kinetic mechanisms. *Combustion and Flame* 154, 67-81.

Perini, F., Brakora, J.L., Reitz, R.D., Cantore, G., 2012. Development of reduced and optimized reaction mechanisms based on genetic algorithms and element flux analysis. *Combustion and Flame* 159, 103-119.

Pitz, W.J., Mueller, C.J., 2011. Recent progress in the development of diesel surrogate fuels. *Progress in Energy and Combustion Science* 37, 330-350.

Pope, S.B., 1997. Computationally efficient implementation of combustion chemistry using in situ adaptive tabulation. *Combustion Theory and Modelling* 1, 41-63.

Prickett, S.E., Mavrovouniotis, M.L., 1997a. Construction of complex reaction systems—I. Reaction description language. *Computers & Chemical Engineering* 21, 1219-1235.

Prickett, S.E., Mavrovouniotis, M.L., 1997b. Construction of complex reaction systems—II. Molecule manipulation and reaction application algorithms. *Computers & Chemical Engineering* 21, 1237-1254.

Prickett, S.E., Mavrovouniotis, M.L., 1997c. Construction of complex reaction systems—III. An example: alkylation of olefins. *Computers & Chemical Engineering* 21, 1325-1337.

R.J. Kee, F.M.R., E. Meeks, J.A. Miller, 1996. CHEMKIN-III: A FORTRAN chemical kinetics package for the analysis of gas-phase chemical and plasma kinetics. Sandia National Labs, Livermore, CA.

Rabitz, H., Kramer, M., Dacol, D., 1983. Sensitivity Analysis in Chemical Kinetics. *Annual Review of Physical Chemistry* 34, 419-461.

Revel J., B.J.C., Cathonnet M., Bachman J. S., 1994. Derivation of a global chemical kinetic mechanism for methane ignition and combustion. *Journal De Chimie Physique Et De Physico-Chimie Biologique* 91, 365-382.

Smith, G.P., Golden, D.M., Frenklach, M., Moriarty, N.W., Eiteneer, B., Goldenberg, M., Bowman, C.T., Hanson, R.K., Song, S., William C. Gardiner, J., Lissianski, V.V., Qin, Z., [http://www.me.berkeley.edu/gri\\_mech/](http://www.me.berkeley.edu/gri_mech/).

Sun, W., Chen, Z., Gou, X., Ju, Y., 2010. A path flux analysis method for the reduction of detailed chemical kinetic mechanisms. *Combustion and Flame* 157, 1298-1307.

Sung, C.J., Law, C.K., Chen, J.Y., 2001. Augmented reduced mechanisms for NO emission in methane oxidation. *Combustion and Flame* 125, 906-919.

Susnow, R.G., Dean, A.M., Green, W.H., Peczak, P., Broadbelt, L.J., 1997. Rate-Based Construction of Kinetic Models for Complex Systems. *The Journal of Physical Chemistry A* 101, 3731-3740.

Tosatto, L., Bennett, B.A.V., Smooke, M.D., 2011. A transport-flux-based directed relation graph method for the spatially inhomogeneous instantaneous reduction of chemical kinetic mechanisms. *Combustion and Flame* 158, 820-835.

Tran, L.S., Sirjean, B., Glaude, P.-A., Fournet, R., Battin-Leclerc, F., 2012. Progress in detailed kinetic modeling of the combustion of oxygenated components of biofuels. *Energy* 43, 4-18.

Turanyi, T., Tomlin, A.S., Pilling, M.J., 1993. On the error of the quasi-steady-state approximation. *The Journal of Physical Chemistry* 97, 163-172.

Turanyi T., 1990. Reduction of large reaction mechanisms. *New journal of chemistry* 14, 795-803.

Um, S., Park, S.W., 2010a. Modeling effect of the biodiesel mixing ratio on combustion and emission characteristics using a reduced mechanism of methyl butanoate. *Fuel* 89, 1415-1421.

Um, S., Park, S.W., 2010b. Numerical Study on Combustion and Emission Characteristics of Homogeneous Charge Compression Ignition Engines Fueled with Biodiesel. *Energy & Fuels* 24, 916-927.

Van Geem, K.M., Reyniers, M.-F., Marin, G.B., Song, J., Green, W.H., Matheu, D.M., 2006. Automatic reaction network generation using RMG for steam cracking of n-hexane. *AIChE Journal* 52, 718-730.

Wei, J., Kuo, J.C.W., 1969. Lumping Analysis in Monomolecular Reaction Systems. Analysis of the Exactly Lumpable System. *Industrial & Engineering Chemistry Fundamentals* 8, 114-123.

Westbrook, C.K., Pitz, W.J., Herbinet, O., Curran, H.J., Silke, E.J., 2009. A comprehensive detailed chemical kinetic reaction mechanism for combustion of n-alkane hydrocarbons from n-octane to n-hexadecane. *Combustion and Flame* 156, 181-199.

Zhang, S., Broadbelt, L.J., Androulakis, I.P., Ierapetritou, M.G., 2012. Comparison of Biodiesel Performance Based on HCCI Engine Simulation Using Detailed Mechanism with On-the-fly Reduction. *Energy & Fuels* 26, 976-983.

Zheng, X.L., Lu, T.F., Law, C.K., 2007. Experimental counterflow ignition temperatures and reaction mechanisms of 1,3-butadiene. *Proceedings of the Combustion Institute* 31, 367-375.

Zhu, L., Cheung, C.S., Zhang, W.G., Huang, Z., 2011. Combustion, performance and emission characteristics of a DI diesel engine fueled with ethanol–biodiesel blends. *Fuel* 90, 1743-1750.

Zsély, I.G., Nagy, T., Simmie, J.M., Curran, H.J., 2011. Reduction of a detailed kinetic model for the ignition of methane/propane mixtures at gas turbine conditions using simulation error minimization methods. *Combustion and Flame* 158, 1469-1479.